RÉPUBLIQUE ALGÉRIENNE DÉMOCRATIQUE ET POPULAIRE MINISTÈRE DE L'ENSEIGNEMENT SUPÉRIEUR ET DE LA RECHERCHE SCIENTIFIQUE

UNIVERSITÉ FERHAT ABBAS - SETIF1
FACULTÉ DE TECHNOLOGIE

THÈSE

PRÉSENTÉE AU DÉPARTEMENT D'ELECTROTECHNIQUE
POUR L'OBTENTION DU DIPLÔME DE
DOCTORAT

Option : Commande électrique

Par : DJARAF Nourelhouda

THÈME

Contribution à la modélisation et à la commande d'un micro-réseau AC; intégrant des sources d'énergies renouvelables décentralisées.

Soutenue le xx /xx /2025 devant le Jury :

CHAOUI Abdelmadjid	Professeur	Univ. Ferhat Abbas Sétif 1	Président
DAILI Yacine	M.C.A	Univ. Ferhat Abbas Sétif 1	Directeur de thèse
HARRAG Abdelghani	Professeur	Univ. Ferhat Abbas Sétif 1	Co-Directeur
SARI Bila1	Professeur	Univ. Ferhat Abbas Sétif 1	Examinateur
CHOUDER Aissa	Professeur	Univ. Mohamed Boudiaf M'sila	Examinateur
LAYADI Toufik Madani	M.C.A	Univ. Mohamed El Bachir El Ibrahimi BBA	Examinateur
ZEMMIT Abderrahim	M.C.A	Univ. Mohamed Boudiaf M'sila	Invite

PEOPLE'S DEMOCRATIC REPUBLIC OF ALGERIA
MINISTRY OF HIGHER EDUCATION AND SCIENTIFIC RESEARCH
FERHAT ABBAS UNIVERSITY SETIF 1

Faculty of Technologies
Department of Electrical Engineering

Doctoral thesis

IN VIEW OF OBTAINING THE DOCTORAL DEGREE IN ELECTRICAL ENGINEERING

Option : Electrical Control

Theme

Contribution to the modelling and control of an AC micro grid integrating decentralised renewable energy

Presented by :
Miss. DJARAF Nourelhouda

Defended on xx/xx/2025, Before the jury composed of:

CHAOUI Abdelmadjid	Professor	Univ. Ferhat Abbas Setif 1	President
DAILI Yacine	M.C.A	Univ. Ferhat Abbas Setif 1	Thesis Director
HARRAG Abdelghani	Professor	Univ. Ferhat Abbas Sétif 1	Co-Director
SARI Bila1	Professor	Univ. Ferhat Abbas Setif 1	Examiner
CHOUDER Aissa	Professor	Univ. Mohamed Boudiaf M'sila	Examiner
LAYADI Toufik Madani	M.C.A	Univ. Mohamed El Bachir El Ibrahimi BBA	Examiner
ZEMMIT Abderrahim	M.C.A	Univ. Mohamed Boudiaf M'sila	Guest

Declaration

I hereby declare that the work presented in this thesis has not been submitted for any other degree or professional qualification and that it is the result of my independent work.

DJARAF Nourelhouda
01/02/2025

Publications associated with this research

SCIENTIFIC COMMUNICATIONS

- Djaraf Nourelhouda, Daili Yacine, Harrag Abdelghani. (October 2022) "Microgrid-based Virtual Synchronous Generator Control Strategy for inverters". In *The 1st National Conference on Thermal Engineering - Renewable and Conventional Processes (NCTE'22)* Batna, Algeria.
- Djaraf Nourelhouda, Daili Yacine, and Harrag Abdelgani. (2022, November). "A Multiple-Areas Based on PID-Virtual Inertia Control Strategy for Inverters". In *The 5th International Conference on Electrical Engineering and Control Applications* (pp. 151-162). Singapore: Springer Nature Singapore. https://doi.org/10.1007/978-981-97-4776-4-16
- Djaraf Nourelhouda, Daili Yacine, and Harrag Abdelgani. (2023, November). "Virtual Inertia Control Based Adaptive Neuro Fuzzy Interference System for a Connected-Area System". In *The 1st International Conference on Renewable Energies and Power Systems (ICREPS'2024)* University Centre of Naama, Algeria.

PUBLICATIONS

- Djaraf Nourelhouda., Dail, Yacine., and Harrag Abdelgani. "A Review of Recent Control Techniques of Virtual Synchronous Machine for Renewable Energy". The Scientific Bulletin of Electrical Engineering Faculty, 23(2), 20-32.https://doi.org/10.2478/sbeef-2023-0016
- Djaraf Nourelhouda., Daili Yacine., Abderrahim Zemmit., and Harrag Abdelgani. "Fuzzy-Virtual inertia control to improve the frequency response of multi-area power systems". Turkish Journal of Electrical Engineering and Computer Sciences, 33(2),(2025) 145-166.https://doi.org/10.55730/1300-0632.4119

Paper Accepted

- Djaraf Nourelhouda, Daili Yacine, Zdiri Mohamed Ali , Abdelghani Harrag. "Parameter Tuning of Virtual Inertia Control and Load Frequency Controller in Modern Renewable Energy Integrated Power System". A Book Chapter in the Edited book "Microgrid Technology and Microgrid Cluster Development." Elsevier U.S.A (May 2025).

Paper under review

- Djaraf Nourelhouda., Daili Yacine., Zdiri Mohamed Ali., Baseem Khan., Josep M. Guerrero., and Harrag Abdelgani. "Adaptive Virtual Inertia and Damping Control for Frequency Regulation in an Interconnected Power System with High Renewable Energy Integration". The scientific reports journal.

Dedication

I would first like to bow down, thanking Allah Almighty, who granted me the courage and patience to complete this work.

I dedicate this modest work:

To my dear parents for their support and encouragement throughout all my years of study.

To my beloved sisters: Nasrine and Nadjet.

To my brothers: Aymen and Hicham.

To the memory of my teacher, Tourkia Sakri.

To all my teachers during my years of study, from whom I have learned a lot.

To all my dear friends.

To you.

DJARAF Nourelhouda

Acknowledgments

First and foremost, I would like to express my sincerest and deepest gratitude to God for granting me the strength and perseverance to complete this modest work. My faith in Him sustained me during the most challenging moments of this journey.

I extend my profound respect and heartfelt thanks to **Dr. Yacine DAILI** and **Prof. Abdelghani HARRAG** for their unwavering support, valuable guidance, and constant encouragement throughout my PhD studies. I am especially grateful for their human qualities and the insightful advice they provided during every phase of this work.

My sincere thanks and appreciation go to **Prof. Abdelmadjid CHAOUI** from the University of Setif 1, for kindly accepting to chair the jury and evaluate this dissertation.

I am equally thankful to **Prof. Bilal SARI**, from the University of Setif 1, for accepting to review my work and serve as a member of the jury.

I would also like to express my deep gratitude to **Prof. Aissa CHOUDER** from the University of Mohamed Boudiaf – M'Sila, for agreeing to review this dissertation and contribute his expertise as a jury member.

My sincere appreciation goes to **Mr. Toufik Madani LAYADI**, *Maître de Conférences A* at the University of Mohamed El Bachir El Ibrahimi – Bordj Bou Arréridj, for his trust and for accepting to participate in the discussion of this work.

I also thank **Mr. Abderrahim ZEMMIT** from the University of Mohamed Boudiaf – M'Sila, for kindly accepting the invitation to contribute to the discussion of this dissertation.

Finally, I would like to express my sincere gratitude to **Dr. Ali AILANE**, **Dr. Mohamed Ali ZDIRI**, **Dr. Ammar CHOUCHANE**, **Dr. Ilyas BENNIA**, and to all those who supported and assisted me—whether directly or indirectly, from near or far—throughout this academic journey.

Contents

List of Figures

List of Tables

Nomenclature

Nomenclature

Abbreviations

AC Alternative Current

ATS Automatic Transfer Switches

AVR Automatic Voltage Regulator

CIF Climate Investment Funds

DC Direct Current

DER Distributed Energy Resources

DG Distributed Generator

DSP Digital Signal Processor

EMF Electromotive Force

ENTSO European Network of Transmission System Operator

ESS Energy Storage System

ETSO European Transmission System Operator

EV Electric Vehicle

FVIC Fuzzy virtual inertia control

FVIDC Fuzzy virtual inertia and damping control

GA Genetic algorithm

HVDC High Voltage Direct Current

IEA International Energy Agency

IEC International Electrotechnical Commission

IEPE Institute of Electrical Power Engineering

ISE Information Systems Engineering

KHI Kawasaki Heavy Industries

LFC Load frequency control

MG Microgrid

MPC Model predictive control

PCC Point of Common Coupling

PLC Power Loop Controller

PLL Phased Looked Loop

PMW Pulse Width Modulation

PSO Particle swarm optimization.

PV Photovoltaic

RES Renewable Energy Sources

RoCoF Rate of Change of Frequency

RPG Renewable Power Generator

RS Renewable Sources

SG Synchronous Generator

SI Synthetic Inertia

SOC State of charge of battery

SPC Synchronous Power Controller

VIC Virtual Inertia Control

VIDC Virtual inertia and damping control

VISMA Virtual Synchronous Machine

VOC Voltage Oscillation Controller

VSG Virtual Synchronous Generator

Symbols

α_i Activation strength

β Frequency bias factor

Δf Frequency deviation

ΔP_g Power generated by the turbine system

ΔP_L Change in load power

ΔP_m Generated power change from the thermal power plant

ΔP_{RES} Generated power change from RES

ΔP_{Tie} Change in tie-line power

ΔP_{VI} Virtual inertia power changes

$\mu_{\Delta f}$ Membership degrees of frequency deviation

$\mu_{\Delta P_{RES}}$ Membership degrees of renewable power changes

$\mu_{\Delta RoCoF}$ Membership degrees of rate of change of frequency

μ_D Membership degrees of damping factor

μ_J Membership degrees of virtual inertia

ω_m Rotational speed of the rotor

ω_s Synchronous Angular Velocity

θ Phase Angle

D Damping factor

D_{Sys} System load damping

D_{sys} Load damping coefficient

e Terminal Voltage

E_K Kinetic energy

f Frequency

f_n Nominal Frequency

H System inertia

I_d^* Current axe d

i_f Rotor Excitation Current

I_V Virtual Current

I_g Grid Current

J Virtual inertia

K_i Integral controller gain

m Mass of the rotor

M_f Magnitude of Mutual Inductance

n_r Speed of the rotor

p Number of poles

P_D Damping Power

P_g Power Generation

P_L Load Power

P_{in} Active Power Input

P_n Nominal Active Power

P_{out} Active Power Output

P_{Tie} Tie-Line Power

P_{VI} Virtual Inertia Power

Q Reactive Power

Q_{in} Reactive Power Input

Q_n Nominal Reactive Power

Q_{out} Reactive Power Output

R Governor droop constant

r Radial distance from the axis of rotation

R_P Active Power Droop Constant

R_q Reactive Power Droop Constant

R_{droop} Droop Constant

R_{vi} Virtual inertia droop constant

S Apparent Power

T Tie-line Power

T_e Electrical Torque

T_f Time delay

T_g Governor time constant

$T_{i;j}$ Synchronizing coefficient

T_{inv} Inverter's time constant

T_{RES} Renewable energy source's time constant

T_t Turbine time constant

u Control input signal

V_0 Nominal voltage

V_d Voltage axe d

V_g Grid Voltage

V_q Voltage axe q

w Disturbance signal

x State variable

Chapter I

Introduction

I.1 Context

Recently, global energy production has undergone a radical transformation due to an increase in electricity demand. This shift has led to a reliance on renewable energy sources (*RES*) as an effective solution to cope with environmental and economic constraints, paving the way for sustainable developments. For instance, due to the significant transition towards *RESs*, these cities and regions produce almost 90% to 100% of their proper energy from renewable sources, such as Albania, Costa Rica, and Norway [1].

In addition, many countries and organisations have launched programs and investments in the context of the integration of *RESs* to completely dispense with non-renewable sources. The Climate Investment Funds Program (CIF's renewable energy integration program) launched approximately 373 projects and programs in 81 countries, where the main target is to shift from fossil-based to zero-carbon through the smooth integration of intermittent renewable energy generators into power systems [2]. The International Energy Agency (*IEA*) report for 2024 highlights the current investments and strategies major economies are implementing to boost clean energy manufacturing and support incentives for renewable energy. On the other hand, many countries aim to triple renewable energy generator capacity by 2030, according to *IEA* and achieve 100% production based solely on *RESs* in 2050 [3, 4, 5].

Furthermore, the centralised generators present challenges in terms of transmission and distribution of electrical energy from the large centralised power plants to end-users via a complex network of transmission and distributions where relying on distributed generator units located close to the point consumption is considered as one of the most critical solutions for providing energy, especially in rural and isolated regions. The concept of distributed generator (*DG*) mainly depends on small-scale power generator units such as solar photovoltaic, wind turbines, and geothermal power generators, which present the friendly impact of *DGs* on the environmental aspect. It allows the power to be supplied for consumption, bypassing the transmission network issues.

Incorporating renewable sources (*RS*) as a source of electrical production has many benefits. However, it has several drawbacks that impact the quality of energy and system stability. The individual and the direct integration of *RS* into the grid present a major challenge due to the intermittency of generation. Additionally, most *RESs* and *DGs* mainly depend on power electronic devices in the transformation phase, which is offset with many problems such as low inertia propriety, connection and disconnection of *DGs*, energy storage issues, and the intermittency of generation due to the weather conditions.[6, 7, 8].

I.2 Background on Micro-grid Concept

The concept of microgrid (*MG*) is introduced as a potential solution to cope with the problems associated with the integration of individual distributed energy resources (*DER*) into the grid. It is paramount for modern power systems to deal with power quality challenges. *MG* can be described as"*A network of low voltage power generating units, storage devices and loads capable of supplying a local area such as suburban area, industry or any commercial area with electric power and heat*"[9, 10]. From the *IEEE*2030.7 standard and international standard *IEC*62898 – 2 "*a microgrid is a group of interconnected loads and distributed energy resources within clearly defined electrical boundaries that acts as a single controllable entity with respect to the grid. A microgrid can connect and disconnect from the grid to enable it to operate in both grid-connected or island-mode*"[11, 12].

According to the previous definitions and those provided in [13, 14, 15, 16], the *MG* is a small-scale power grid (low voltage system) including hybrid energy sources and energy storage system (*ESS*) for supplying power to consumers with the ability to operate in grid-connected or islanded modes as shown in figure I.1.

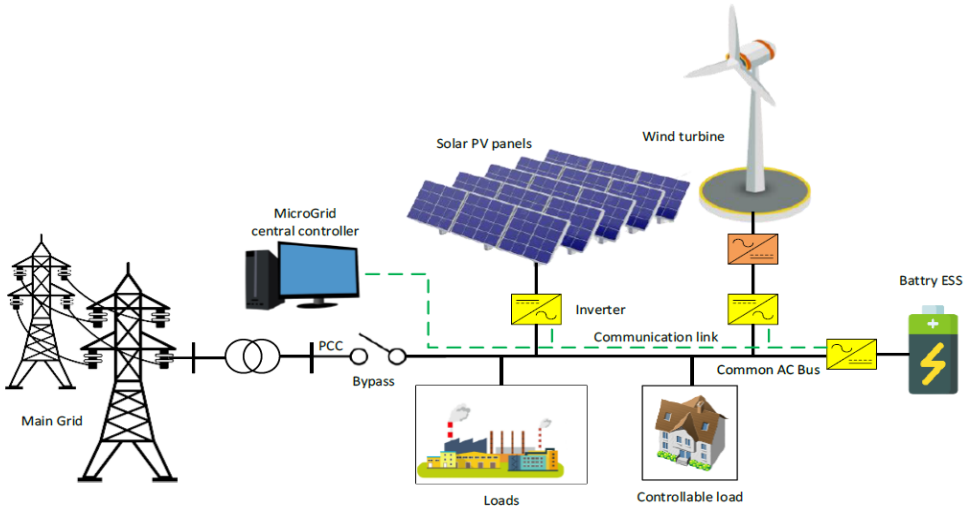

Figure I.1: Microgrid configuration.

I.2.1 Microgrid applications and research interest

Recently, the shift towards green energy has led to an increase in the number of *MGs*. Globally, the major countries have moved towards investing in the field of the *MGs* [17, 18]. It is applicable in several areas, such as educational institutes, approximately equal to 33% of the total number of the existing *MGs*, remote areas, military bases, commercial and industries, and others [17].

In terms of investment, the precedence researcher, the global MG market, was evaluated at USD 36.30 billion in 2023, and it is approximately USD 43.19 billion in

(a) (b)

Figure I.2: (a) Microgrid project location in Algeria, (b) Kabartin renewable energy station in Adrar.

2024; this value is expected to reach USD 206.69 billion by 2033, with a compound annual growth rate of 19%, where the United State is the leader market followed by a fast-growing of Asia Pacific [19, 20]. According to the 2023 statistics, *MGs* are particularly prevalent in North America, Europe, Asia Pacific, Latin America, and the Middle East and Africa, where the number of *MGs* in the United States is approximately equal to 3700 *MGs* in operations, and 692 *MGs* are concentrated in Alaska (Kodiak Island powered by wind and hydro-power), California (Stone Edge Farm *MG* based PV system, wind turbines, and *ESS*), New York (Brooklyn *MG* based *PV* system), Georgia, Maryland, Oklahoma, and Texas [20, 21].

While other countries are endeavouring to incorporate *MG* technologies by developing investment plans and programs in green energies, Algeria is increasingly using *MGs* as a means to improve energy accessibility and include *RESs* into its overall energy plan (see Figure I.2a)[22, 23]. An exemplary initiative is the pilot Ghardaia *MG*, which integrates the *PV* system, *ESS*, and cutting-edge grid control technologies. The purpose of this *MG* is to provide a consistent provision of electricity in an area that experiences sporadic connection to the main power grid [24].

Additionally, as shown in Figure I.2b, the Adrar *MG* project relies on *PV* systems and wind turbines with battery storage systems to power the local community to cope with the challenges of sustaining a stable grid connection in the desert. Furthermore, the Timimoun hybrid *MG* combines *PV* systems and diesel generators to supply power for remote areas [25]. The Touat *MG* project aims to combine solar energy with battery storage to meet the energy requirements of the local community. Another notable endeavour is the Hassi R'Mel *MG* project, which investigates the integration of *PV* systems and *ESS* to decrease dependence on diesel generators and encourage the adoption of sustainable energy practices.

I.2.2 Architecture of micro-grids

Figure I.3 illustrates the architecture of *MG* [26]. Each component plays a crucial role in ensuring the optimal operation of the *MG*. Typically, *MG* consists of localised power generation units designed to supply electricity to loads using either *RESs* such as solar photovoltaic panels (PV panels) and wind turbines, which are non-dispatchable (meaning their output depends on external conditions like sunlight and wind and cannot be easily controlled to match demand), or non-renewable sources like diesel generators, which are dispatchable (able to be turned on or off, or adjusted to deliver a specific amount of power as needed). Often, these sources are combined in what is known as hybrid generations, which are the most commonly used configuration [27, 28, 29]. Additionally, *ESS* are essential for balancing supply and demand, controlling power, maintaining quality, and providing rapid response times. [16, 29, 30].

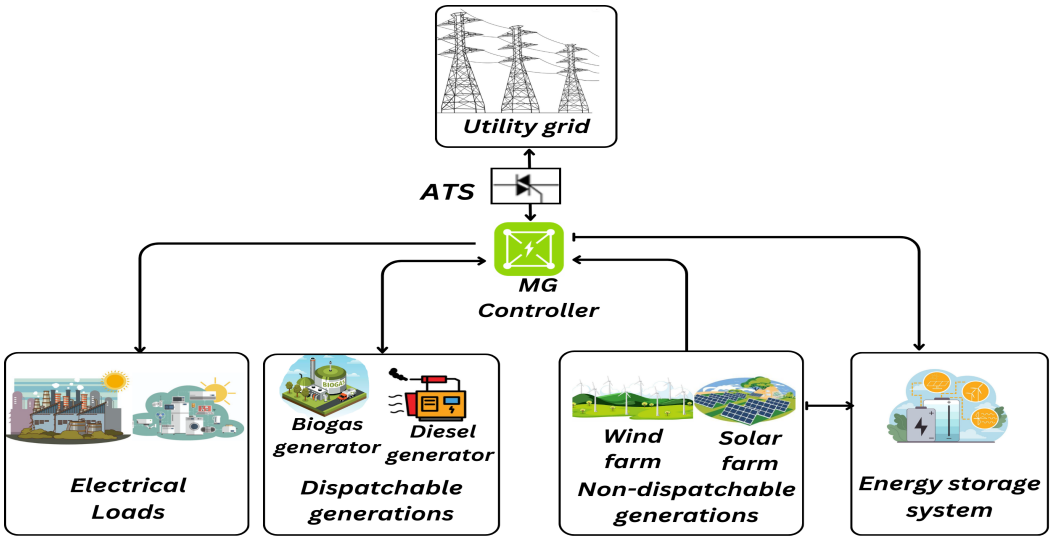

Figure I.3: Conceptual diagram of a microgrid.

Electrical loads within *MGs* can be categorized into linear and non-linear types, with critical loads, such as hospitals, requiring constant power supply, while deferrable loads that are adjustable for *MG* load balancing [16, 31]. The control system serves as the central management unit of the *MG*, overseeing power distribution, load management, and the connection and disconnection from the main grid. It coordinates the various components of the *MG* under all conditions, ensuring both power quality and the dynamic stability of the system [32]. Additionally, automatic transfer switches (*ATS*) are vital for their reliability in facilitating seamless transitions between grid-connected and island modes, ensuring uninterrupted power supply.

I.2.3 Micro-grid coupling architecture

The diversity of power sources in the *MG* has been demonstrated to be a crucial factor in enhancing the system's reliability. Since all power sources possess distinct

operational characteristics, it is essential to select an appropriate connection architecture for these resources utilizing converters and buses to supply the load. Multiple topologies exist to integrate diverse energy sources into a working hybrid system. Energy storage units are interconnected via a bidirectional converter, which is employed to store energy and can fulfill the load's requirements during periods of inadequate supply. The primary purpose of these structures is to provide optimal energy flow to end users, minimize complexity, eliminate conversion losses, and enhance system reliability and cost-effectiveness. In this context, *MGs* are divided into three main categories: direct current *MG* ($DC-MG$), alternative current *MG* ($AC-MG$), and AC/DC hybrid *MG*. Each type offers several advantages to power systems and comes with specific challenges for different operational conditions [33, 34, 35, 36].

I.2.3.1 Direct current microgrid

Typically, $DC-MGs$ are linked to the grid utility through DC/AC converters. However, the different *MG* components are connected to the *MG* via a common *DC* bus, as illustrated in FigureI.4 [37]. It can power *AC* and *DC* loads with varying levels of voltage using power electronic converters such as DC/AC and DC/DC converters. This type of *MG* offers better stability to the power system (no reactive power) with lower power conversion losses, providing high efficiency, which makes it preferable for the integration of *RESs* [36, 38, 39, 40].

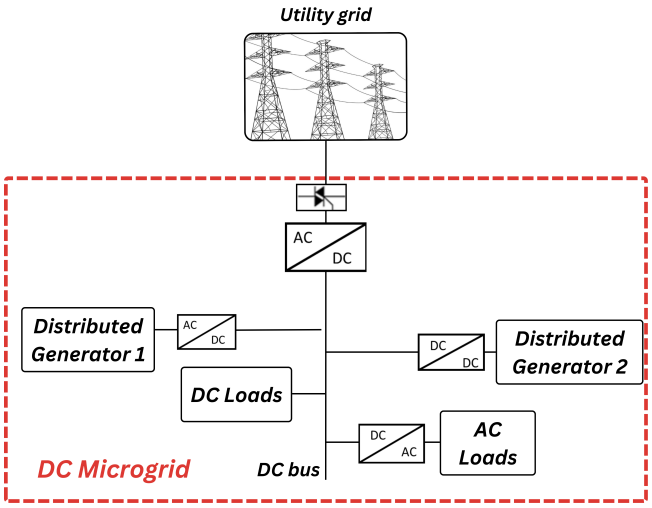

Figure I.4: *DC* microgrid architecture.

I.2.3.2 Alternative current microgrid

The $AC-MG$ is most architecture compatible with the present power systems, which enhances the controllability and flexibility of the system. The different $AC-MGs$ components are connected to the MG via a common *AC* bus as illustrated in Figure I.5 [37], which facilitates the transitions between islanded and grid-connected modes,

respecting the synchronising conditions by maintaining voltage magnitude, phase angle, and frequency. Additionally, the *DC* components as *DC* loads and PV systems are interfaced to the *AC* bus through DC/AC converters, which influence the system efficiency [36, 38, 40].

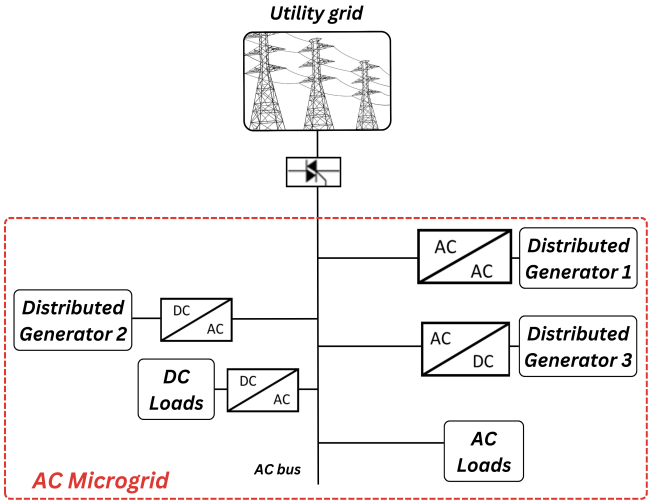

Figure I.5: *AC* microgrid architecture.

I.2.3.3 AC/DC hybrid microgrid

The AC/DC microgrid combined both $DC-MG$ and $AC-MG$ to benefit from the advantages of each one, as shown in Figure I.6 [37]. It includes a DC bus and *AC* bus to supply power to *AC* and *DC* loads where the MG components can easily connected to *DC* and *AC* sides without synchronisation for the generation and storage system. It aims to improve the reliability and efficiency of the whole system by minimising the number of conversion stage and interface devices [36, 38, 40].

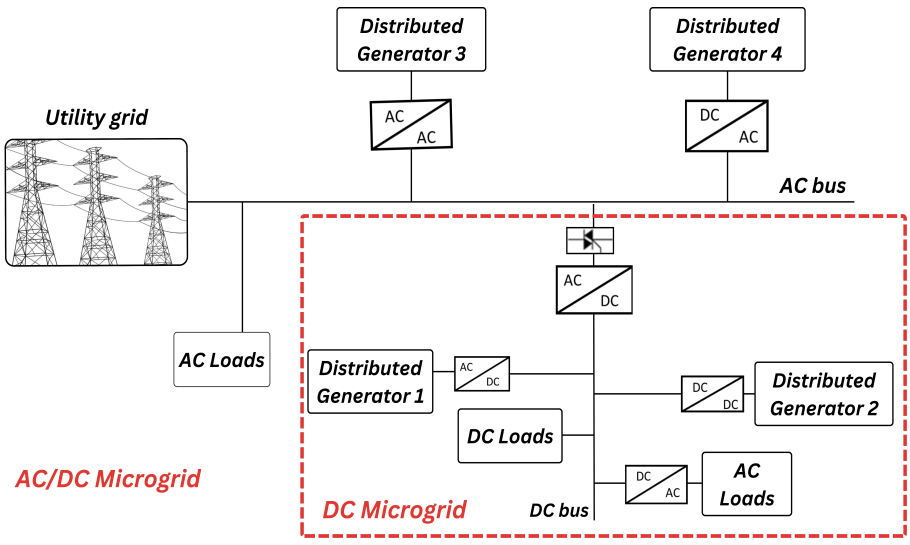

Figure I.6: AC/DC microgrid architecture.

I.2.4 Operating modes of microgrid

Both stand-alone and grid-connected operations are possible with *MG*, as shown in Figure I.7. It depends on various criteria, such as load demand, weather conditions, the capacity of storage, and grid contingency. The subsequent section will provide a concise overview of the two operational modes.

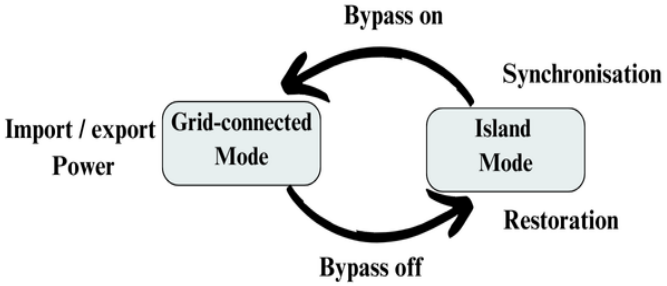

Figure I.7: Operating modes of microgrid.

I.2.4.1 Islanded Mode

Islanded *MG*, also referred to as stand-alone *MG*, operates independently of the main grid where usually the local power generation relies on *DGs*-based *RESs* and integrates *ESSs* such as batteries to ensure power supply to local loads such as rural regions. However, this mode necessitates a control system with high performance to meet the dynamic stability (voltage and frequency) and ensure efficient power system management with fewer power losses. It is designed with the ability to connect to the main grid in case of high demand and less power generation [27].

I.2.4.2 Grid-connected Mode

This mode allows the bidirectional power flow between the MG and the main grid by importing the energy when there is a defect in the MG and exporting it in case of excess to support the main grid. In this mode of operation, the voltage amplitude, frequency, and phase are determined by the main grid; these parameters can easily be obtained at the point of common coupling (*PCC*). The *PCC* is a connection point between the MG and the main grid. Distributed energy resources usually work under grid-feeding control strategy also they able to work in grid-forming if it is necessary. The synchronization between the main grid and the MG, in this case, is carried out by a phase-locked loop (*PLL*).[27].

I.3 Microgrid control criteria

MGs differ from conventional power systems in terms of generation sources, scale, distribution and transmission. It also differs in the control system in terms of com-

plexity, objectives and scope. The control in the conventional system focuses mainly on controlling the traditional generation units and dealing with the large distribution and transmission of energy to ensure the stable operation of a large and interconnected system [38, 41, 42].

However, *MG* depends on *DGs* and *RESs*, which are intermittent generation units due to weather conditions such as wind speed and sunlight. Unlike the traditional system, *ESSs* represent an important component in *MGs*, especially for the control systems to ensure power management. In addition, it should deal with the connection and disconnection of loads and generation units to meet the stability of the whole system, resulting in specific needs in terms of power quality to handle different scenarios[43, 44].

Consequently, the *MG* control system plays a critical role in accommodating its reliable operation in both operation modes. The key recommendations for the *MG* control system are shown in FigureI.8. It should meet the power balance, synchronisation and power exchange with the main grid, smooth transition between operation modes, coordination of *DGs*, ensuring power quality, voltage and frequency regulations with consideration of the sensitivity of system components [43, 45, 46].

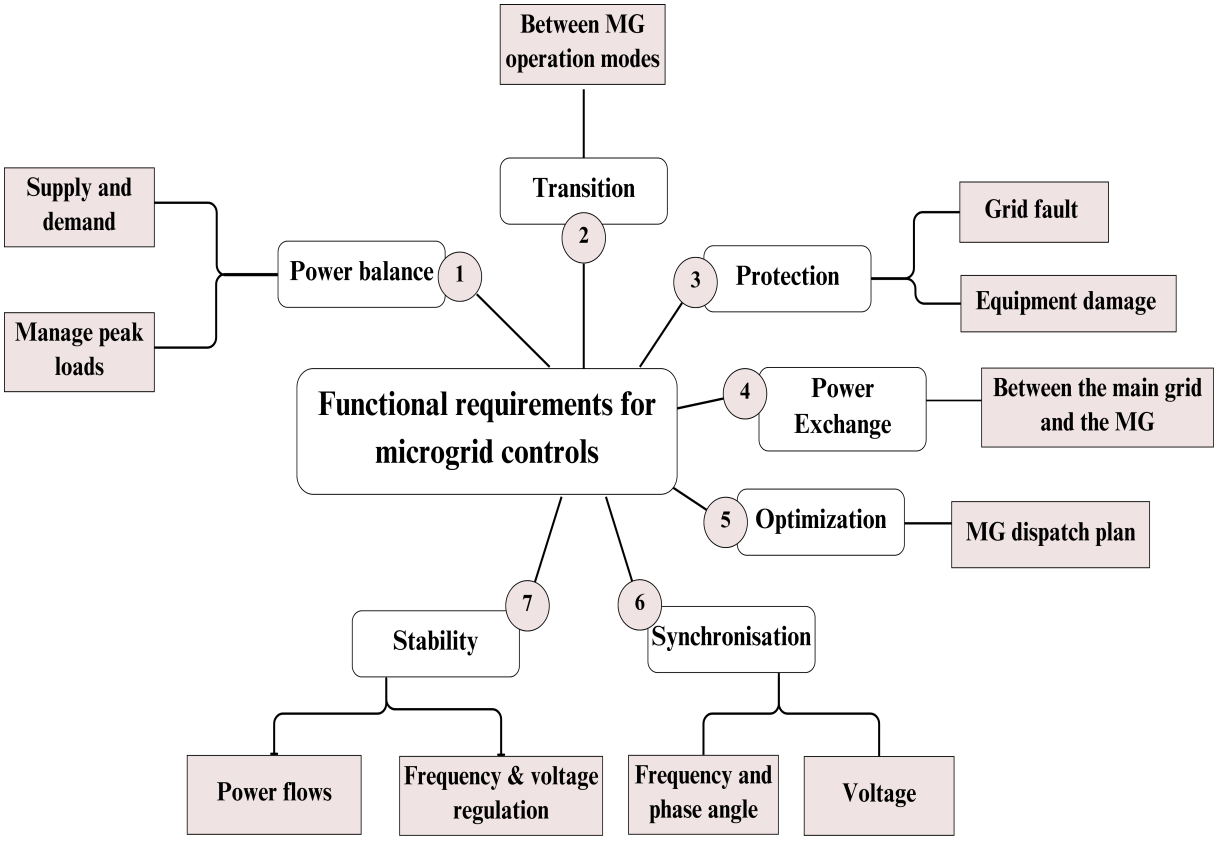

Figure I.8: Functional requirements for *MG* controls.

I.3.1 Hierarchical control for microgrid

Managing the operation of *MG* presents significant challenges, particularly in maintaining stability and efficiency under varying conditions. To address these challenges, a hierarchical control structure is commonly employed, offering a robust framework to coordinate the operation of MGs effectively. This structured approach is a hybrid strategy consisting of three levels: primary, secondary and tertiary controllers, and it can only be in two levels (primary and secondary), which is bi-level control, serves for monitoring and supervising *MG* [39, 47, 48]. Each level is designed with specific objectives and methods to ensure particular tasks, such as commanding and overseeing lower-level systems. It is designed to improve operating efficiency and offers flexibility with less communication pressure, minimising operating costs and performing better load and current sharing. Each level should generate reference signals to the lower levels without impacting the system stability, resulting in a decrease in bandwidth with the increase in control levels. This control strategy improves the power quality, and it offers reliability and stability of *MG* in different modes [41, 49, 50]. Additionally, it ensures proper power flow and management, a synchronisation process with smooth transitions between mods, and accurate power sharing between *DGs*, which provide more expandability to the system with more integration of *RESs*. Power management within an *MG* and power exchanges with the main utility grid have been implemented using hierarchical control structures via a "multi-agent system" for two European *MGs*: one on the Greek island of Kythnos and another in the German 'Am Steinweg project.

The architecture of the hierarchical control is illustrated in Figure I.9. The primary control is the basic level designed as decentralised control to ensure power sharing between *DG* units. It is a local frequency and voltage control implemented for each *DG*, generally based on a droop controller; it operates at the millisecond scale to control the common bus voltage, frequency, and current. However, in case of severe disturbances and malfunctions, it presents the drawbacks of frequency and voltage deviations and less efficient reactive power sharing. Hence, the secondary control is introduced as centralised or distributed control to restore the frequency and voltage to their set points, eliminate the deviations, ensure the synchronisation of *MG* with the main utility grid and improve the power quality. It operates from milliseconds to minutes. Finally, the tertiary control (slowest control), which is centralised control, operates on timelines of hours to days for the detection of islanded mode, and it is activated during the transition from the islanded to grid-connected mode to managing the bi-directional power flow between *MG* and the main grid. In addition, it focuses on managing the battery storage, *DGs* scheduling, and dispatch. The following sub-sections will provide detailed descriptions of the fundamental structures of each control level.(see Figure I.10).

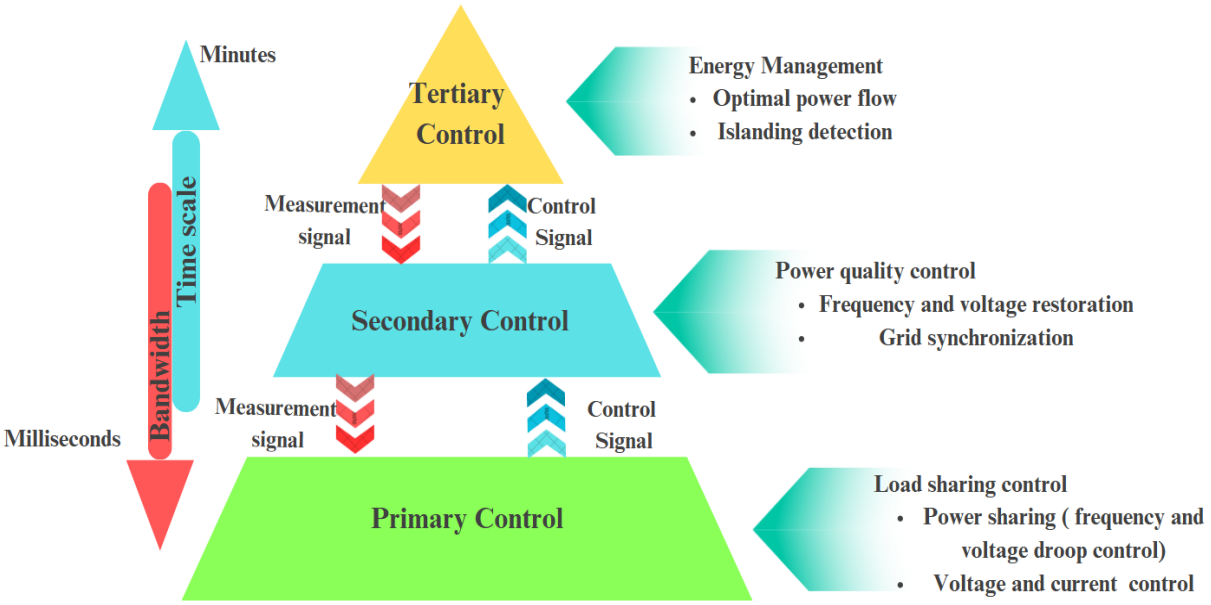

Figure I.9: Hierarchical control architecture for *MG*.

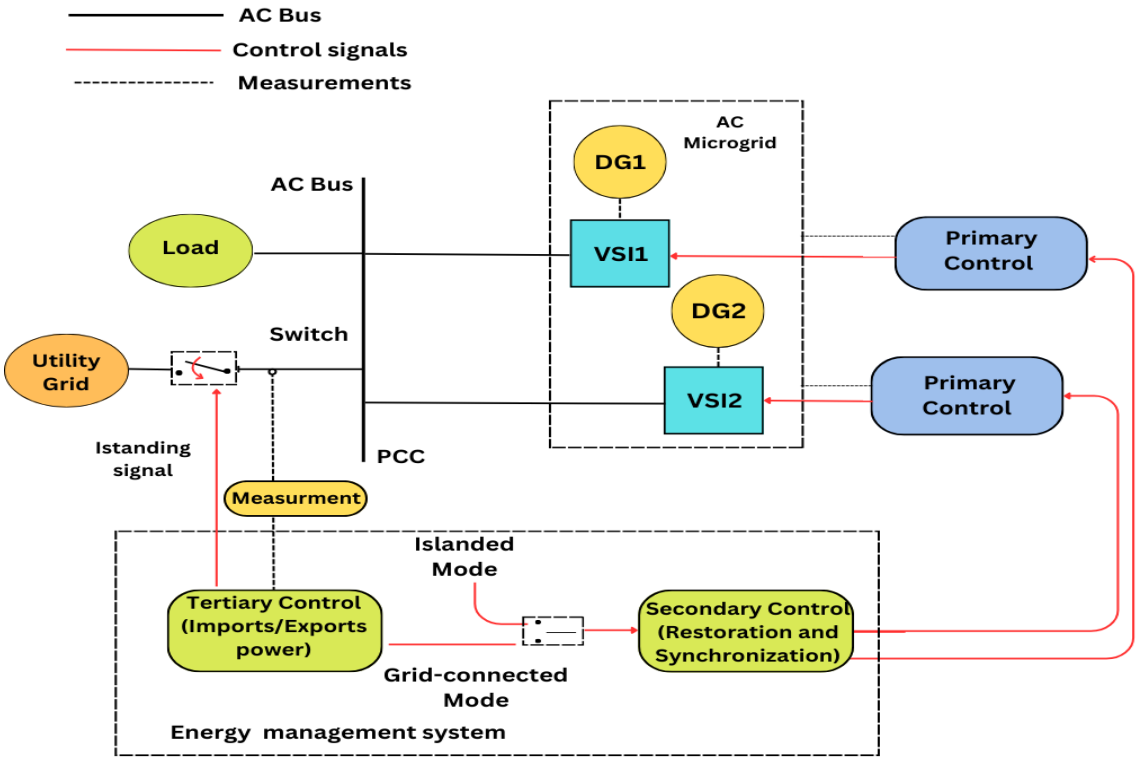

Figure I.10: Hierarchical control implementation for AC-MG.

I.3.1.1 Primary control

In the*MG* system, adequate power sharing between the units is crucial. The primary layer of the hierarchical control is designed to ensure this specific task is based on local measurements such as voltage, current, and active and reactive power to generate and send the control signal at milliseconds directly towards the power converter to realise the power-sharing among different *DGs*, addressing some power issues to contribute in the stabilisation of *MG*. Each *DG* unit operates autonomously to con-

trol load disturbances, ensuring the local frequency and amplitude regulation with less fluctuation [38, 49].

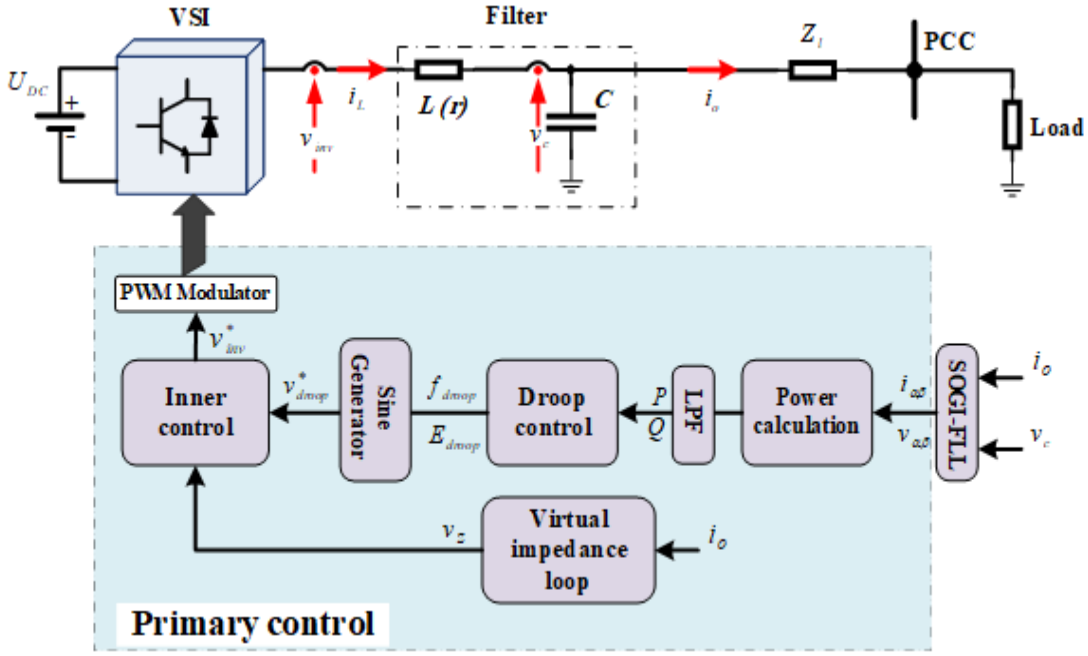

Figure I.11: Primary control architecture.

Mainly, the primary control for voltage source inverters ($VSIs$) based on frequency and voltage droop controllers for active and reactive power sharing, respectively, between DGs to deal with load changes where the idea comes from the conventional primary control of synchronous generators realised by turbine-governors and voltage regulation. The droop controller is based mainly on the implementation of two main properties the mechanical power compensation from the rotating machine in the case of increasing in power damned and voltage drops in the case of increasing reactive power sharing, which is the basic idea of the exciter control of synchronous generator [49].

The primary control loops are droop control, inner loop, virtual impedance loop, and power calculation block, as illustrated in FigureI.11. Firstly, the phased locked loop (PLL) is used to measure the output current and voltage (i_o, v_o) for the power calculation block to calculate the average value of active and reactive power (P, Q). Then, the calculated values are used from the droop controller to adjust the frequency and voltage (f_{droop}, v_{droop}) proportionally to active and reactive power deviations, respectively. Besides, the current and voltage control loop unit serves to achieve the inverter voltage (V^*_{inv}), frequency, and amplitude stabilisation. On the other hand, the virtual impedance loop is integrated to improve power-sharing accuracy, compensate for line impedance differences, and address harmonic distortion [38, 49].

I.3.1.2 Secondary control

During islanded mode operation, the secondary control is the highest control layer; it serves to suppress the frequency and amplitude deviations produced by the primary control layer. On the other hand, during the transition from island to grid-connected mode, the synchronisation of the *MG* with the main grid is ensured from this control layer. Additionally, it can suppress circulating currents and eliminate harmonics within the *MG*, allowing the energy management system (*EMS*) to proceed by considering the power flow and power quality [38, 47].

The structure of the secondary layer can be implemented as centralised or distributed control as illustrated in Figures I.12a and I.12b In the centralised secondary control structure, the frequency and voltage of each *DG* are transmitted to a central control unit that coordinates the *DGs* via a high data rate communication bus to restore the *MG* frequency and voltages. However, it is suffering from a single point of failure. On the other hand, the distributed structure is based on a local measurement of frequency and voltage that is communicated to the other *DG* units. The exchange of information between *DGs* is ensured via a peer-to-peer communication network. For both strategies, the voltage, frequency, and amplitude are estimated through PLL and compared with their reference values; then, the errors $\delta\omega$ and δE are sent to all the units to restore the output voltage. In addition, to synchronise the *MG* phase with the main grid, the phase between the grid and the *MG* is measured and sent to all the modules [38, 49].

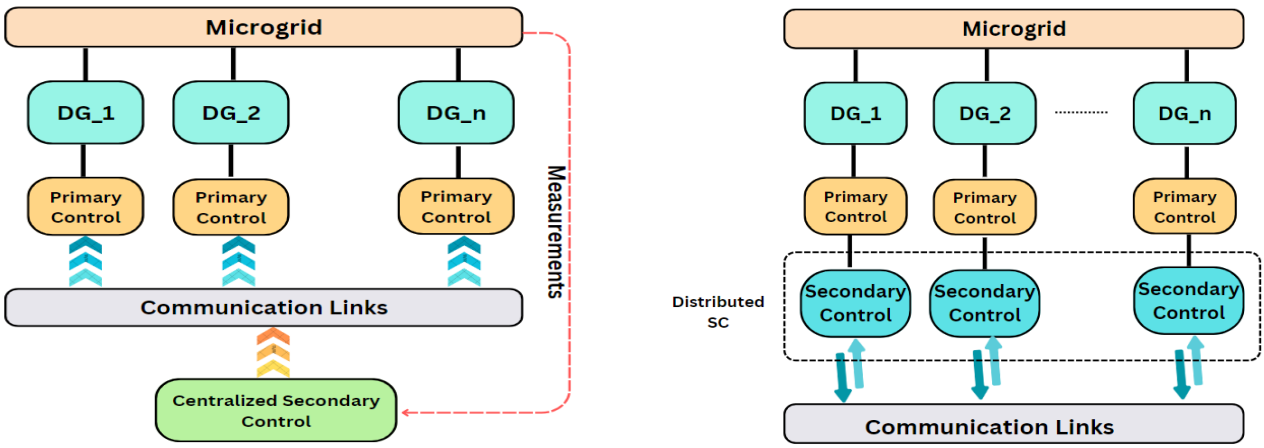

Figure I.12: (a) Centralised secondary control architecture. (b) Distributed secondary control architecture.

I.3.1.3 Tertiary control

In gird-connected mode, the tertiary control level is introduced as a global central controller to ensure load balance and control of active and reactive power flow be-

tween the *MG* and the main grid at the point of common coupling (PCC), and it is deactivated when islanding mode is detected. It is used for optimal bidirectional control of the active and reactive power flow, power management, and coordination of DG units at optimal set points. In grid-connected mode, the primary objective of tertiary control is to manage power flow by enabling any energy deficit in the *MG* to be supplied by the utility grid and by sending any excess energy in the *MG* to the main grid.

According to the structure of the tertiary control for multiple *DGs* formed *MG* connected to the main AC grid shown in Figure I.12b, it defines the desired active and reactive power values by providing the voltage amplitude and frequency set points to the lower control levels to control the bidirectional power flow, where the active and reactive power (P_g, Q_g) can be computed from the measured grid current and voltage (i_g, v_g). These quantities are compared with their corresponding desired values P_g and Q_g. Then, the new amplitude and frequency set points are calculated using PI compensators and sent to the secondary control layer for power flow control at the inverter level [38, 49].

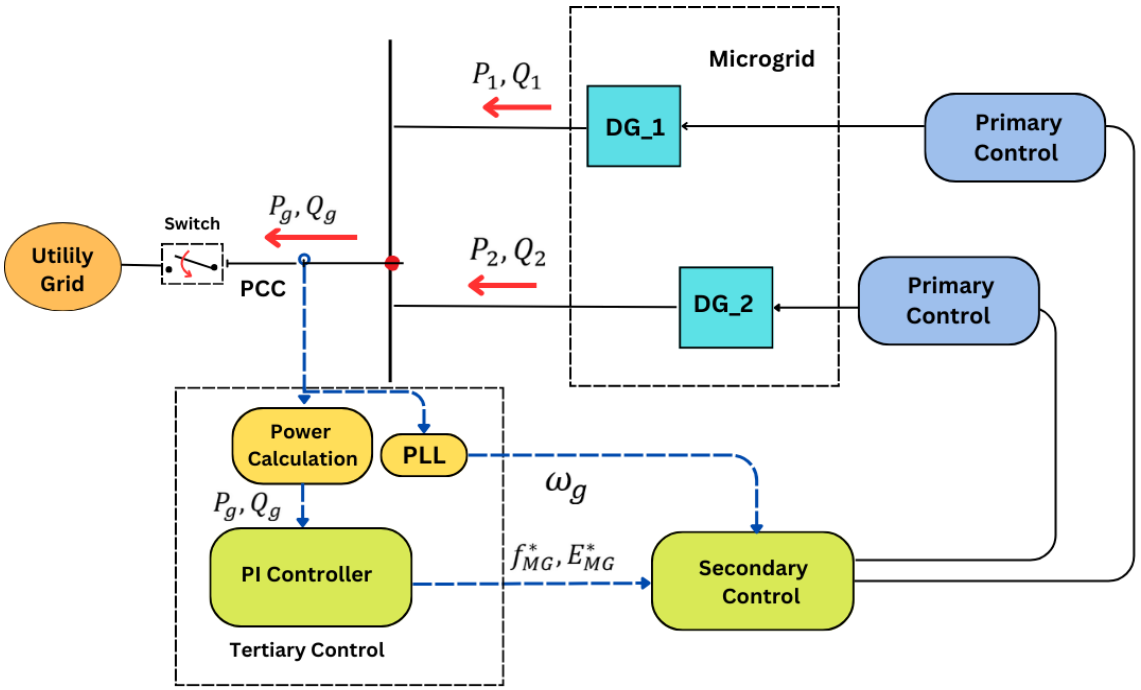

Figure I.13: Tertiary control architecture.

I.4 Research and motivation

In *MG*, power transmission from *DG* units to consumers mainly depends on power electronic devices; on the other hand, the prolific integration of *RESs* is matched by a significant reliance on power electronic devices; in this way, the rotating machines are constantly decreasing, which present challenges for frequency control of modern

power systems. Conventionally, system frequency is controlled within a specified range by inertial response and frequency regulation from a synchronous generator (*SG*). While a generator trips offline or the load increases, the frequency deviates from its set point. Hence, the kinetic energy stored in rotating mass, which refers to the physical inertia from the *SGs*, resists these changes; it helps to absorb or release the imbalance, which highlights the significant impact of inertia response in frequency regulation. It directly contributes to the initial response and reserve power for primary and secondary frequency control. As illustrated in Figure I.14, the high inertia system provides a buffer against fast frequency changes with the slowest rate of change of frequency (*RoCoF*) and less frequency nadir, which ensures great system stability [51, 52].

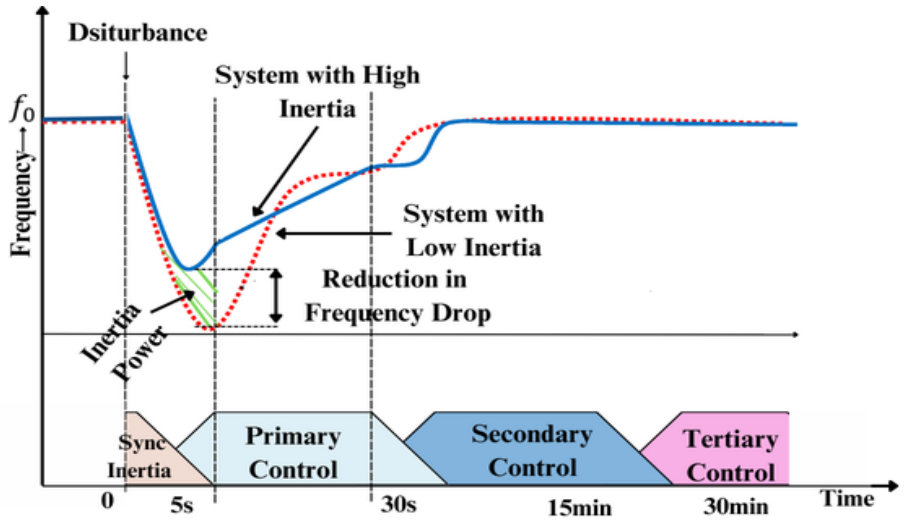

Figure I.14: The correlation between inertia and frequency response.

However, the increase of *DGs* interfaced with power electronic devices resulted in a consistent decrease in the total inertia of the whole system. Consequently, sudden load or generation disturbance causes degradation of frequency performance for low or no-inertia systems, such as large frequency deviation and high *RoCoF*, faulty protection action, or even system split and blackout. Furthermore, the inherent dampening effect of inertia is reduced in systems with low inertia. This decrease in damping results in more prominent and persistent oscillations after disturbances, which might strain system components and diminish the overall reliability of the power system. This lack of inertia and damping results in the high *RoCoF*, leading to abrupt frequency variations with larger amplitudes and load-shedding, even at a small disturbance [53]. Additionally, due to the intermittency of generator-based *RESs*, ensuring a balance between power supply and demand becomes increasingly challenging in low-inertia systems. It requires faster and more dynamic frequency regulation services (see FigureI.15).

Consequently, in normal operation, the *DGs* and *RESs* have a low capacity to engage in frequency regulation processes. Hence, integrating them into the power

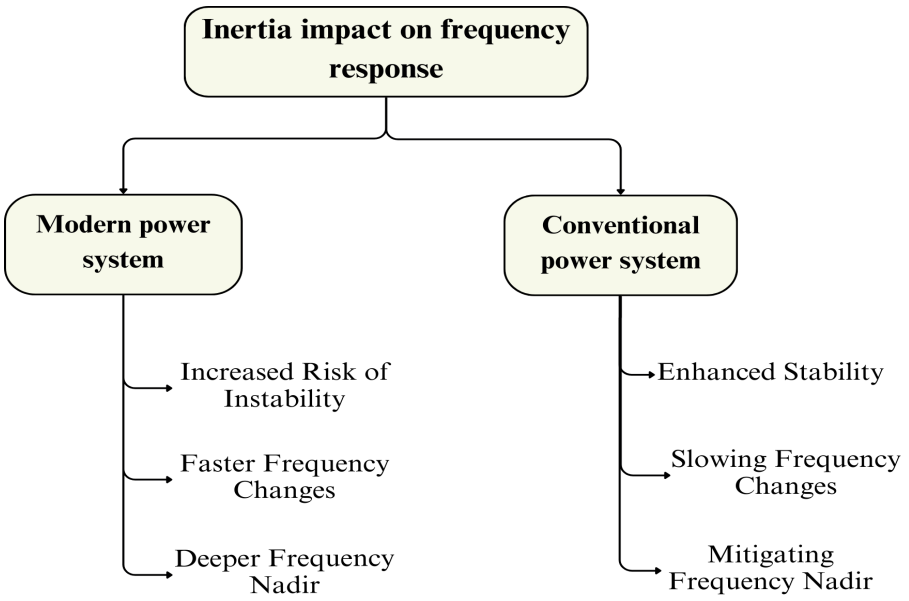

Figure I.15: Impact of inertia on frequency response.

system will inevitably result in a decrease in the overall system inertia and damping. This might have adverse effects on power system dynamics, frequency and voltage regulation, and other operational and control concerns. During severe scenarios, these issues have the potential to result in system instability and cascading failures and may lead to blackout [52].

I.5 Thesis objectives

To address the stability issues previously mentioned regarding the low inertia system, this thesis addresses the following objectives:

- To elaborate on the concept of active power-based inertia compensation regarding frequency control to give a clear understanding of inertia compensation and frequency control.
- To review existing literature on inertia compensation techniques for *MG* to provide a comprehensive overview of current knowledge and understanding.
- To produce a frequency response model of an islanded and interconnected *MGs*-based load frequency control using hierarchical control topology to study and analyse the system responses and controllers' performance regarding the rate of integration of *RESs*.
- To design virtual inertia control *VIC*-based *ESS* to ensure inertia compensation for low inertia systems and enhance the dynamic stability and power quality of *MGs* operating in an islanded or interconnected mode.

- To examine the impact of *VIC* parameters on system stability. Assess the performance of the *MG* under various scenarios through simulations.
- To develop advanced *VIC* techniques tailored specifically for interconnected *MGs* integrated with *RESs* to manage power fluctuations and frequency changes adaptively.

I.6 Thesis Outline

The rest of this thesis is organized as follows:

- **Chapter 2**: provides a comprehensive overview of virtual inertia, a fundamental principle emulation of physical inertia from *SG* behaviour, and its significant impact on modern power systems. It emphasizes their importance in maintaining system stability and presents a literature review of virtual inertia control strategies implemented in artificial inertia for modern power systems.
- **Chapter 3**: introduces the frequency response model for islanded and interconnected *MGs*-based *VIC*. It analyses *MG* dynamics, highlighting the role of virtual inertia in frequency stability. This chapter develops a state-space model that accurately captures *MG* components' dynamics, justifying its simplified version for efficient control design and simulations. It also discusses the design and implementation of *VIC* strategies for stabilizing *MG* frequency under dynamic operating conditions. It examines the impact of control parameters on system stability.
- **Chapter 4**: Presents the development of fuzzy-virtual inertia control to improve the frequency response of interconnected *MGs*. Also, the validity of the proposed controller is verified based on several tests.
- **Chapter 5**: Presents the advancement of adaptive virtual inertia and damping control utilizing artificial neural networks for frequency regulation in an interconnected power system with significant renewable energy integration. The control system observes critical indicators such as frequency deviation, *RoCoF*, and renewable energy source power fluctuations to enhance precision and flexibility, intelligently adjusting virtual inertia and damping for each region, even amidst disturbances. The approach improved coordination between multiple virtual inertia across interconnected regions. The obtained results are presented and discussed, and these performances are compared to conventional methods.

Finally, the thesis concludes with a section summarising the main contributions of this research and outlining potential directions for future work

Chapter II

Overview of virtual inertia control

II.1 Introduction

Recently, power generation infrastructures based on fossil fuels shifted toward integrating *RESs* to fulfill the load dammed and cope with the economic and environmental criteria. Unlike the classical power system based on high inertia, the design of modern power systems is based mainly on power electronic devices to convert the power from renewable power generators (*RPG*) to consumers with low or no inertia, such as the PV system. Generally, reducing inertia in modern power systems brings challenges for maintaining the stability of the system [54, 55].

From this point, virtual inertia is introduced to cope with the impact of reduced inertia from modern power systems. This concept aims to provide additional inertia to the system by controlling power electronic devices via control algorithms to emulate the inertia response of conventional power systems. This artificial inertia stabilises the system and improves the integration of *RESs* while maintaining the system reliability [54, 56, 53].

This chapter aims to provide a comprehensive understanding of virtual inertia, a fundamental principle based on the emulation of physical inertia from synchronous generator behaviour, and its significant impact on modern power systems. It aims to highlight its importance in maintaining system stability. Additionally, it offers an overview of control strategies for virtual inertia implemented through artificial inertia in modern power systems.

II.2 Fundamentals of inertia in power systems

II.2.1 Traditional inertia response

Generally, coal, natural gas, and nuclear fission reactions are the main sources used in the conventional power system, which is based on *SGs* to transform the mechanical power to electrical power [57]. The stator and rotor are the main parts of *SGs* where the rotational speed of the rotor (n_r in rpm) is expressed by equation II.1.

$$n_r = \left(\frac{60f}{p}\right) \tag{II.1}$$

Where f is the system frequency (in Hz), and p is the number of poles.

From the equation II.1, the speed of the rotor is directly proportional to the frequency of the host power system with which the governor is connected. Besides, the rotor's mass (m in Kg) offers inertia to the system; as a result, it resists rotational speed changes and opposes the frequency shift. The significant inertia represents a buffer against grid collapse, as it contributes substantial kinetic energy [54, 57, 58] where the inertia (J) of SG and the kinetic energy (E_K) are expressed by equations II.2, and II.3 and the rotational speed of the rotor ω_m (in rad/s) is giving by equation

II.4.

$$J = \int r^2 dm = r^2 m \tag{II.2}$$

$$E_K = \frac{1}{2} J \omega_m^2 \tag{II.3}$$

$$\omega_m = \frac{n_r}{60} 2\pi \tag{II.4}$$

Where r is the radius of the rotor (in m).

The load or generation disturbances cause the imbalance between the power supply and dammed; as a result, the rate of change of kinetic energy stored in the rotating mass of *SGs* is equivalent to change in generation (ΔP_g) and load (ΔP_L) [58]. It is given as:

$$\frac{dE_K}{dt} = \Delta P_g - \Delta P_L - D(\omega_m - \omega_s) \tag{II.5}$$

Where D is the damping factor, ω_s refers to the rotational speed of the stator (in rad/s).

Considering the apparent power (S) rating of the generator and total kinetic energy stored in the rotor, the inertia constant (H) can be expressed by equations II.6.

$$H = \frac{E_K}{S} = \frac{J \omega_m^2}{2S} \tag{II.6}$$

Hence, in the case of several *SGs* connected to the power system, the total inertia constant can be represented as the resistance caused by the exchange of kinetic energy between rotating machines. This exchange helps compensate for the frequency deviations during the power imbalances, representing the inertial response during a few seconds [59]. The total inertia constant (H_{Total}) is dictated by the following equationII.7

$$H_{Total} = \frac{E_{K_{Total}}}{S_{Total}} = \frac{\sum_{i=1}^{n} S_i H_i}{\sum_{i=1}^{n} S_i} \tag{II.7}$$

Typically, the *RoCoF* of the power system is used to adjust active power and the system frequency in response to power imbalance. Besides, it is used to assess power system inertia. Therefore, the system inertia constant is determined by the *RoCoF* as follows:

$$RoCoF = \frac{d\omega_m}{dt} = \frac{\omega_m}{2HS} [\Delta P_g - \Delta P_L - D(\omega_m - \omega_s)] \tag{II.8}$$

On the other hand, small disturbances lead to deviation of rotor speed due to mechanical loss; the damping effect of the rotor generated from the damper or armature winding in *SGs* plays a significant role in restoring the synchronous speed of the rotor. During the deviation in the speed of the rotor, the air-gap flux rotates with the synchronous speed. It penetrates the damper armature, causing an electromagnetic force and current to be induced in it, which produces a damping torque severs to

restore the synchronous speed of the rotor. When $\Delta\omega < 0$, then the damping power (P_D) rejects the deceleration of the rotor's speed and vice versa; afterwards, the rotor will follow its usual path and attain synchronism without continuous oscillations[54].

Consequently, the inertia response refers to the ability of rotating masses to resist changes in rotational speed, resulting in maintaining the stability and frequency of the power system.

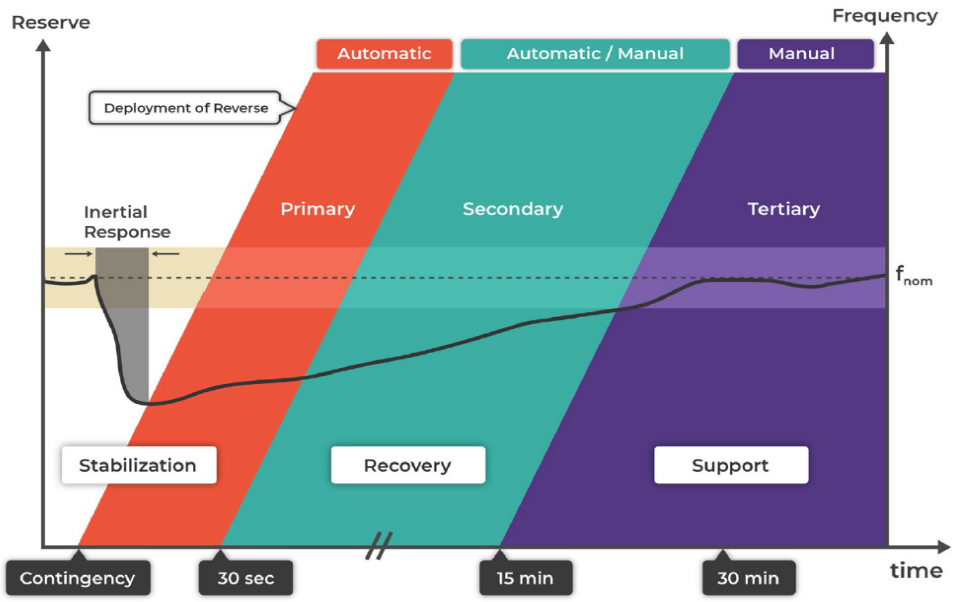

Figure II.1: Stage of frequency response in traditional power system.

Additionally, as illustrated in Figure II.1, after a few seconds from the disturbances, the governor of the traditional generators acts to supply or absorb real power based on its droop characteristics via primary regulation (i.e. primary control) for $10s$ to $30s$, where the total power generated or absorbed from governor action is directly related on the frequency deviation (Δf), it can be expressed by equation II.9[57].

$$P_{g_{total}} = \sum_{j=1}^{n_g} \frac{\Delta f}{R_{droop}} \tag{II.9}$$

Where R_{droop} is the droop constant and $P_{g_{total}}$ is the generator power.

However, it introduces a frequency nadir resulting in study state error; hence, the secondary control is operated to reset the frequency to its set point. It can persist for around $30s - 15min$. When the tertiary control is activated power, it adjusts the frequency through the re-dispatching of the committed generators [57].

II.2.2 Impact of reduced inertia

With the increasing integration of *RESs*, the inertia response of power systems significantly decreases with the retirement of traditional power systems. Furthermore, weather conditions such as sunlight, wind speed, temperature, and humidity in-

fluence modern power generation, where most *MG* components, such as solar *PV* plants, are associated with more uncertainty. On the other hand, the nature of loads connected to *MG*, such as electric vehicles (*EVs*) and non-linear light loads, may introduce harmonic distortions into the host grid. Most *MG* components are also matched with power electronic devices with no rotating masses. As a result, they do not contribute to inertia response [59].

Figure II.2 presents the impact of the integration rate of *RESs* on frequency responses and the *RoCoF*. Where the high integration of *RESs* introduces power stability issues, and where reduced inertia and damping responses cause frequency stability issues, increasing the risk of system instability. While the conventional power system benefits from the inertia response by providing inertia and damping power to slow down the frequency changes, it limits the *RoCoF* and frequency nadir during grid contingency, which gives more stability to the system, the modern power system relies on power converters with low or no rotating masses suffering from the reduced or the absence of inertia response which impacts the system stability where the increased *RoCoF* indicated the rapid changes of frequency under load or generation disturbance, the frequency response is faster with deeper frequency nadir compared with the conventional sources[58, 57, 60].

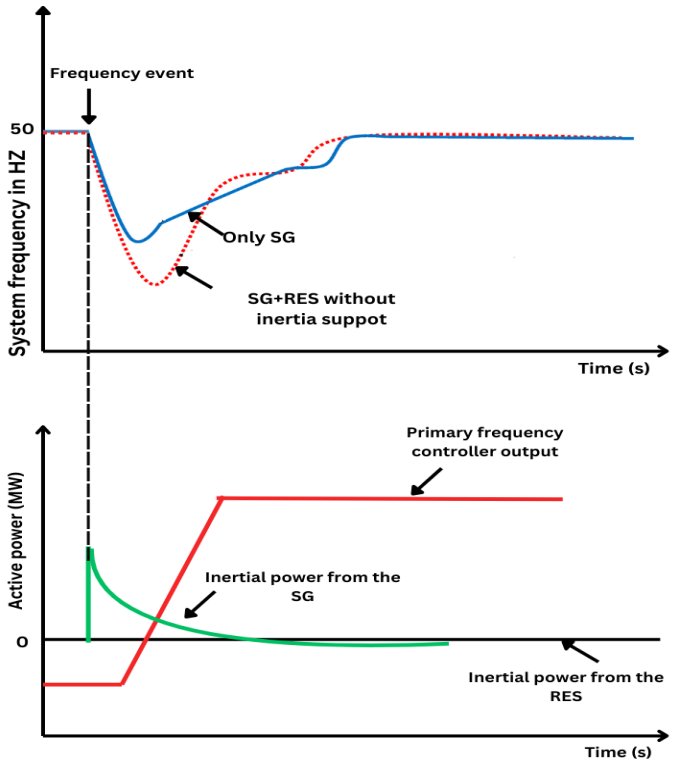

Figure II.2: Impact of inertia on frequency response.

This variation may exceed the frequency limits and standards and lead to cascading failures of the whole system, resulting in blackouts and collapses, which was the case in 2016 in South Australia, where the grid equipped with a wind generator collapsed. It led to catastrophic incidents and losses in the distribution and trans-

mission network. After the analyses carried out by the experts, they concluded that the collapse of the network was due to the reduced inertia from the wind generators, which allowed the increase of *RoCoF* and frequency deviations and led to cascading failure of the system. This event approximates the one in Taxes Winter Storm 2021, where the power grid suffered from significant stability issues. The decrease in generation capacity and the limited inertia from renewable sources (PV systems) led to widespread outages and frequency instability. This event highlights the susceptibilities of low-inertia systems during extreme conditions [52].

Table II.1 presents the top five power system stability problems identified and classified by European transmission system operators (European TSOs) as published by the European Network of Transmission System Operators (ENTSO-E) [59, 61] where the decreased inertia of power system has the highest score of 17.35 which demonstrates the real impact of reduced inertia in power system and highlights the importance of developing strategies and mechanisms to provide additional inertia such as virtual inertia to deal with stability issues and enhance the dynamic performance of modern system [61].

Table II.1: Power stability issues classified by European TSOs.

Classification	Score	Issue
1	17.35	Low inertia
2	10.16	Resonance caused by power electronics and cables
3	9.84	Reduced transient stability margins
4	8.91	Power electronics-connected generators participation in frequency containment is either absent or incorrect
5	8.19	Interactions between power electronics controllers and passive AC components

II.3 Concept of virtual inertia

In a low inertia power system, the most important target is to achieve a suitable integration of *RESs* for stable operation. This necessitates coping with the frequency issues by increasing the system inertia to ensure frequency support in the first milliseconds from the contingency. From this point of view, the virtual inertia concept was first introduced in [62] via power converters for modern power systems to provide inertia response (inertia and damping properties) in the frequency regulation process. It is defined in [63] as "*A facility provided by a Power park module or HVDC system to replace the effect of the inertia of a synchronous power generating module to a prescribed level of performance*.

This concept is based on emulating the inertia response of conventional *SGs*, which is possible based on sophisticated control techniques for power electronic devices. Unlike the physical inertia in *SGs*, which is derived from the kinetic energy of rotating masses, the virtual inertia is generated by controlling power electronic converters that connect *RESs* and *DGs* units to the power system. It is introduced in literature under various typologies and labels such as virtual synchronous generator (*VSG*), virtual synchronous machine (*VSM*), virtual inertia control (*VIC*), and synthetic inertia (*SI*) where all strategies aim to control the power converters to behave as real *SGs* to improve system stability by providing a faster and adaptive response to frequency, equivalent to the conventional inertia response [64, 65]

II.3.1 Principal of virtual inertia

The basic operation of virtual inertia mimics or emulates the mechanical behaviour of *SGs* by absorbing or releasing power from converters to cope with the frequency deviations as illustrated in Figure II.3 [52]. The virtual inertia is created by modulating the active power via an inverter similar to the speed of the *SG* rotor based on control algorithms inspired by the concept of *SGs*, where the most proposed algorithm is based on the mathematical model of *SGs*. The main parameters, i.e. virtual inertia and virtual damping, are chosen according to the power size of the system, the rate of integration of *RESs*, and the available power reserve [53, 52].

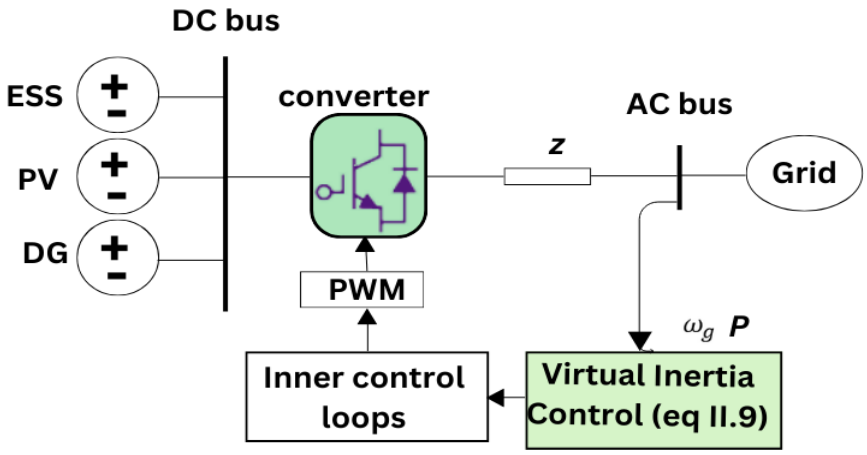

Figure II.3: Conceptual diagram of virtual inertia.

The frequency measurement is essential for virtual inertia emulation to continuously monitor the power system's frequency. Where the measured frequency is processed through a control algorithm which is designed to deal with the concept of virtual inertia to adjust the output power of the connected *DGs* or *ESSs* via a power converter, it rapidly injects or absorbs power, enabling virtual inertia to react almost instantaneously to frequency changes[64].

II.4 Overview of virtual inertia control topologies

In the past year, this concept has received much attention and has seen significant applications to reproduce the mechanical property of real *SG* in power converters based on the swing equation, *SG* modelling, and *SG* phasor-diagram to benefit as much as possible from the *SG* to support the low-inertia system in maintaining stability [52, 62, 66]. It is introduced in [67] for a grid-connected voltage source converter (*VSC*) controlled as a Virtual Synchronous Machine (*VSM*) based on the swing equation of *SG* to provide a power-balance-based synchronisation of the converter control system to the grid. In [68], the concept of virtual inertia used the *SG* modelling to control inverter-based *RESs* to stabilise the frequency similarly to the *SG* behaviour during contingency. One other study presented in [51] for signal area power system presents the impact of virtual inertia and damping factor of system-based *RESs* where the frequency response is improved with the increase of virtual inertia and damping parameters. The authors in [69] aim to prove the efficiency of virtual inertia in frequency regulation for low inertia power systems where the proposed strategy is implemented in parallel inverters based on the swing equation of *SG* and compared with real *SG* behaviour. Reference [70] used this concept for wind turbines to ensure fast frequency support. The virtual inertia emerged for the *PV* systems via a power electronic converter based on the *SG* phasor-diagram in [71] to compensate for the lack of inertia as a result of improving the dynamic performance of the power system. In [72], the VSG based on the mathematical model of *SG* is introduced for a single-phase inverter based on *RESs* to support the frequency and voltage stability. The experimental results presented in[73] show the efficiency of virtual inertia compensation for modern power systems. Germans applied the virtual inertia concept in MG to overcome the frequency issues. All these studies highlight the significant impact of virtual inertia in compensation for the lack of inertia in modern power systems by enhancing the regulation process of frequency, resulting in better dynamic performances.

The fundamental principles of virtual inertia in the literature are mainly identical because its definition is based on its effect rather than the implemented strategy. Therefore, multiple topologies can be distinguished based on their specific model and application strategy as shown in Figure II.4 [51, 64]. One approach to replicating the behaviour of an *SG* in topology is to use its mathematical model. Another approach is to directly use the swing equation of synchronous machines to simplify the implementation of power converters. Additionally, some approaches incorporate responsive *DGs* to react to frequency changes. The following sub-sections will present the basic structures of main virtual inertia topologies and their detailed description.

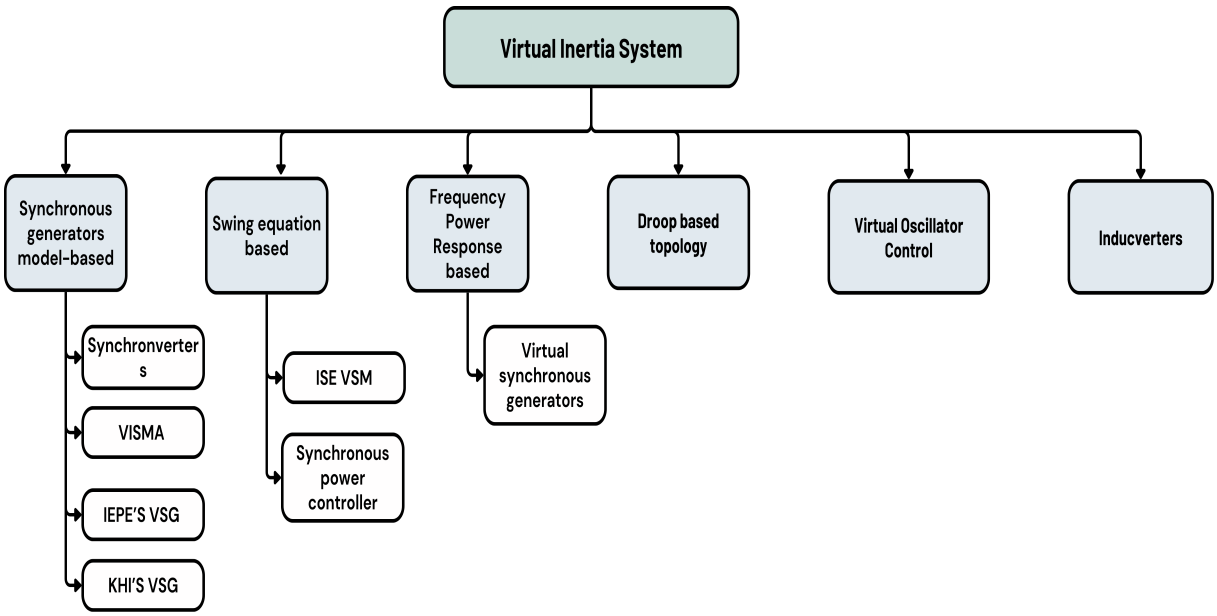

Figure II.4: Virtual inertia classifications.

II.4.1 Synchronous generators model-based topology

II.4.1.1 Synchronverters

Synchronverters is a developed topology in [68]; it aims to allow inverters-based *RESs* to behave as real *SGs* by replacing the mechanical power exchange with the *DC* bus; it can have all properties of an *SG*. Unlike the *SG* model, this technique can choose system parameters such as inertia, friction coefficient, field inductance, and mutual inductances, as well as the values of parameters that are impossible in a real *SG* with no magnetic saturation and no eddy current.

Furthermore, the synchronverter can be operated with connection to the main power system as a generator with the conventional control algorithm in the same way as *SG* or as a synchronous motor, deciding the direction of energy flow between the *DC* bus and *AC* bus automatically according to the system frequency. This concept consists of filter inductors and capacitors associated with a control algorithm based on the dynamic equations of *SG* (the electrical torque (T_e), terminal voltage (e) and reactive power (Q)) additionally to the regulation of active power via frequency droop control [64, 68]. The main control equations are expressed as follows:

$$T_e = M_f i_f \langle i, \widetilde{\sin\theta} \rangle \tag{II.10}$$

$$e = \dot{\theta} M_f i_f \widetilde{\sin\theta} \tag{II.11}$$

$$Q = -\dot{\theta} M_f i_f \langle i, \widetilde{\cos\theta} \rangle \tag{II.12}$$

Where M_f is the magnitude of the mutual inductance between the field coil and the stator coil, θ is the angle between the rotor axis and one of the phases of the

stator winding, and i_f is the rotor excitation current. Denote

$$i = \begin{bmatrix} i_a \\ i_b \\ i_c \end{bmatrix} ; \widetilde{\sin\theta} = \begin{bmatrix} \sin\theta \\ \sin\left(\theta - \frac{2\pi}{3}\right) \\ \sin\left(\theta - \frac{4\pi}{3}\right) \end{bmatrix} ; \widetilde{\cos\theta} = \begin{bmatrix} \cos\theta \\ \cos\left(\theta - \frac{2\pi}{3}\right) \\ \cos\left(\theta - \frac{4\pi}{3}\right) \end{bmatrix} \tag{II.13}$$

The configuration of this strategy is depicted in Figure II.5. It consists of two main parts: the power part is represented by a red dashed box, acting as an *SG* connected in parallel with three capacitors to ignore the ripple (small oscillations in voltage and current).

On the other hand, the inductors L_g help in synchronisation and power control, ensuring that the output of the synchronverter aligns correctly with the grid; the energy storage system on the *DC* bus is essential to absorb the power from the virtual prime mover which represents the mechanical power input in a real *SG* and the inertia power of the virtual rotating part of the *SG*. The capacitor voltage represents the terminal voltage of virtual *SG*, and the L_s;R_S depicts the stator windings of virtual *SG*. Additionally, the average of $e(e_a, e_b e_c)$ is the back *EMF* due to the movement of the virtual rotor. On the other hand, the *DC* source i_f is adjusted to feed the virtual field (rotor) windings.

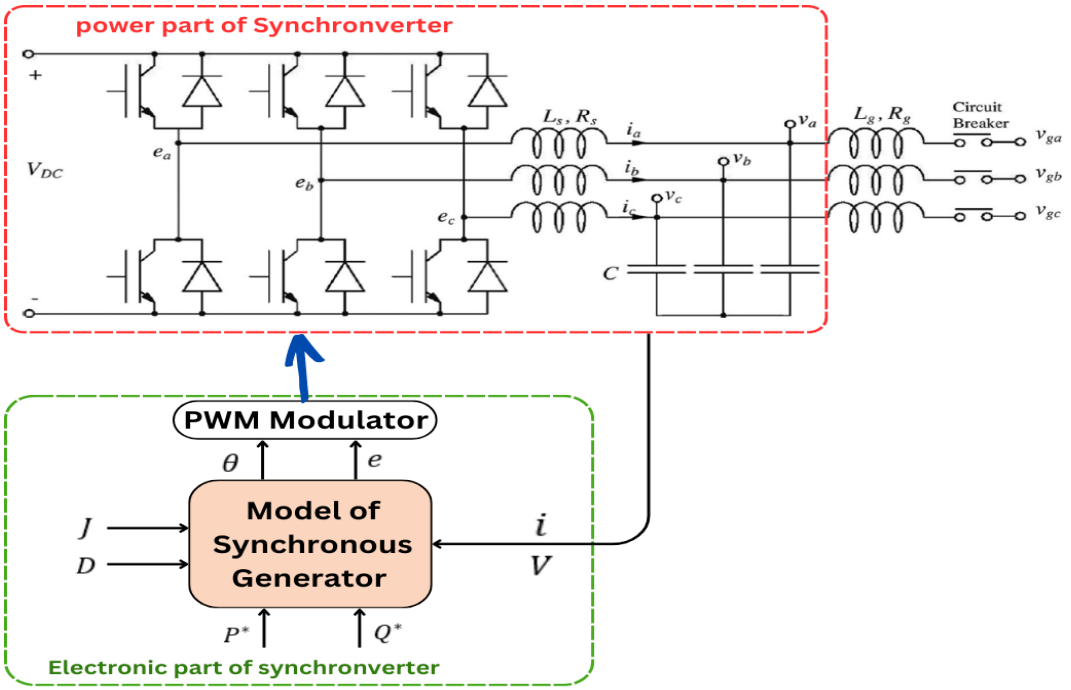

Figure II.5: The conceptual diagram of the synchronverter.

The digital signal processor (*DSP*) and associated circuits control switch under a special program represent the electronic part of the synchronverter, including voltage and current sensors, signal conditioning circuits, and analogue/digital converters. Where the equations II.10, II.11, and II.12 with the frequency and voltage droop loops

are the core part for implementing the electronic part of synchronverter as shown in II.6 [64, 68].

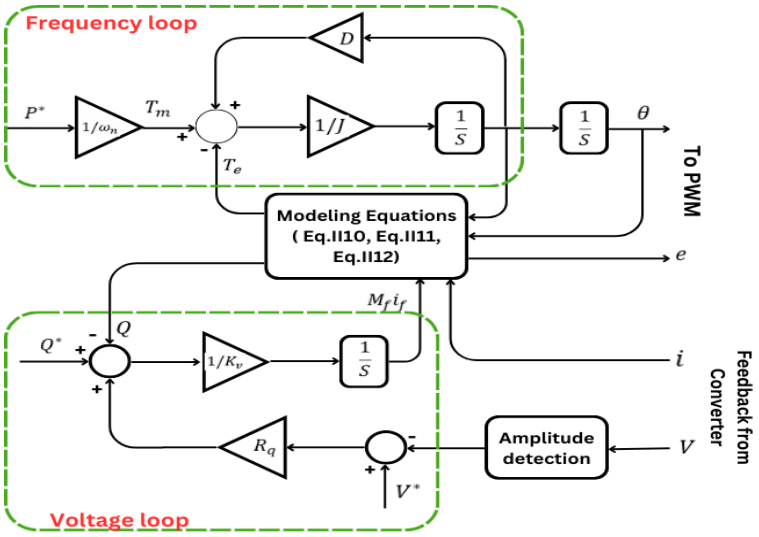

Figure II.6: Detailed control diagram of the electronic part of synchronverter.

Where P^*, Q^* are active and reactive power references, ω_n is the nominal pulsation, and T_m is the mechanical torque.

To enhance the transient response, the controller part of the synchronverter is modified in [74] by adding a damping correction loop to act only during the transients. In [75], two major changes in the electronic part of the synchronverter to develop a self-synchronisation strategy to overcome the *PLL* drawbacks; first, a virtual impedance is introduced to calculate the virtual current (I_v) for initial synchronisation which offers a sluggish synchronisation process, second, a *PI* controller is added to the frequency control loop to allows for the generation of an incremental phase angle, which effectively eliminates the steady-state inaccuracy in torque. The concept of synchronverter is adopted to single-phase systems with a low pass filter for active and reactive power in [76]. The authors in [77] proposed a modified synchronverter for three-phase *PWM* rectifiers to operate a rectifier to mimic a synchronous motor to directly control the real power extracted from the source and the output voltage.

II.4.1.2 VISMA and IEPE'S VSG topologies

The ideal-linear model of *SG* is the main concept proposed by the Institute of Electrical Power Engineering (*IEPE*) to emulate the inertia response for modern power systems, which is called virtual synchronous machine (*VISMA*) [78]. It emulates the stator circuit of *SM* and the mechanical subsystem to introduce the virtual rotor and damping effect based on the electro-mechanical power balance. Furthermore, this topology was implemented via two types: $VISMA - Method - 1$, where the measured grid voltage is used to feed the *VISMA* algorithm, and then the inverter is controlled via hysteresis control by the calculated stator current in real-time from the

VISMA (voltage-to-current model) as shown in Figure II.7a [79].

However, the $VISMA - Method - 2$ used the voltage reference for *PWM* to control the inverter (current-to-voltage model) as shown in Figure II.7b [80]. The second technique achieves better power quality compared to the voltage-to-current model[79, 81].

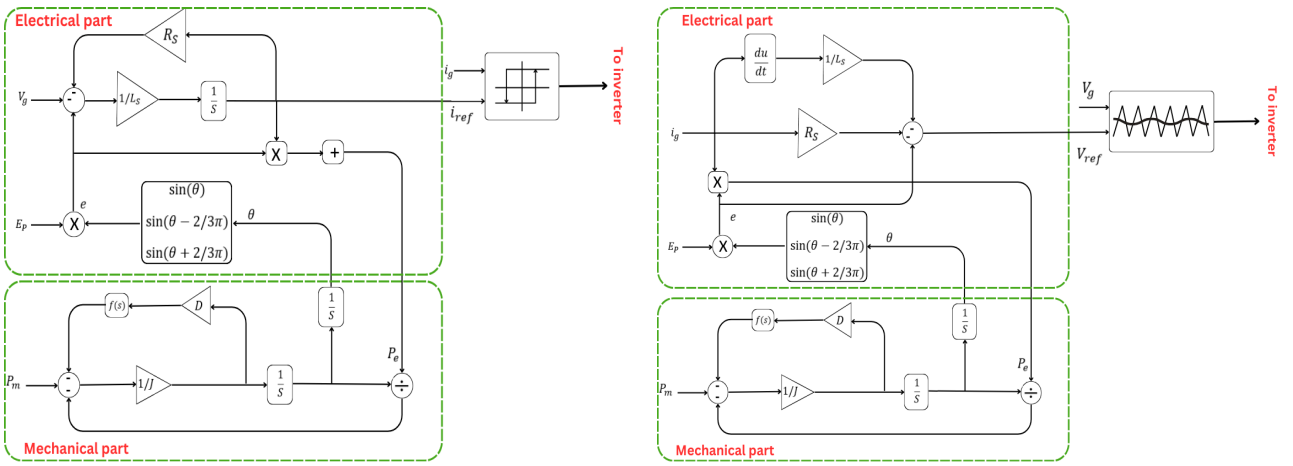

(a) (b)

Figure II.7: Block diagram of : (a) the VISMA-Method 1. (b): the VISMA-Method 2.

II.4.1.3 KHI'S VSG topology

The phasor diagram of *SG* is considered by Kawasaki Heavy Industries (*KHI*) [78, 82] to reproduce the inertia response for the grid-connected inverter without crossing over the electrical dynamic of the generator. This topology is called *virtual generator model of the algebraic type*, where the control system is configured to emulate the inertia response with the automatic voltage regulator (*AVR*), and the frequency, voltage, power factor controllers are performed similarly to the traditional *SG*. The designed control is based on the algebraic relation between the current and voltage phasor, as illustrated in Figure II.8 [82]. Additionally, the active power deviation with a droop represents the governor model to provide the rotor angular speed of the virtual generator; on the other hand, the voltage reference is produced via the *AVR* based on reactive power deviation with a droop.

II.4.2 Swing equation-based topology

II.4.2.1 ISE VSM topology

In [83], the Information Systems Engineering (*ISE*) laboratory proposed the concept of virtual inertia through a virtual synchronous machine (*VSM*) based on the swing equation of *SG* to emulate the kinetic energy stored in the rotor. The main idea is to ensure power-frequency regulation by providing the virtual inertia response via *ESS*.

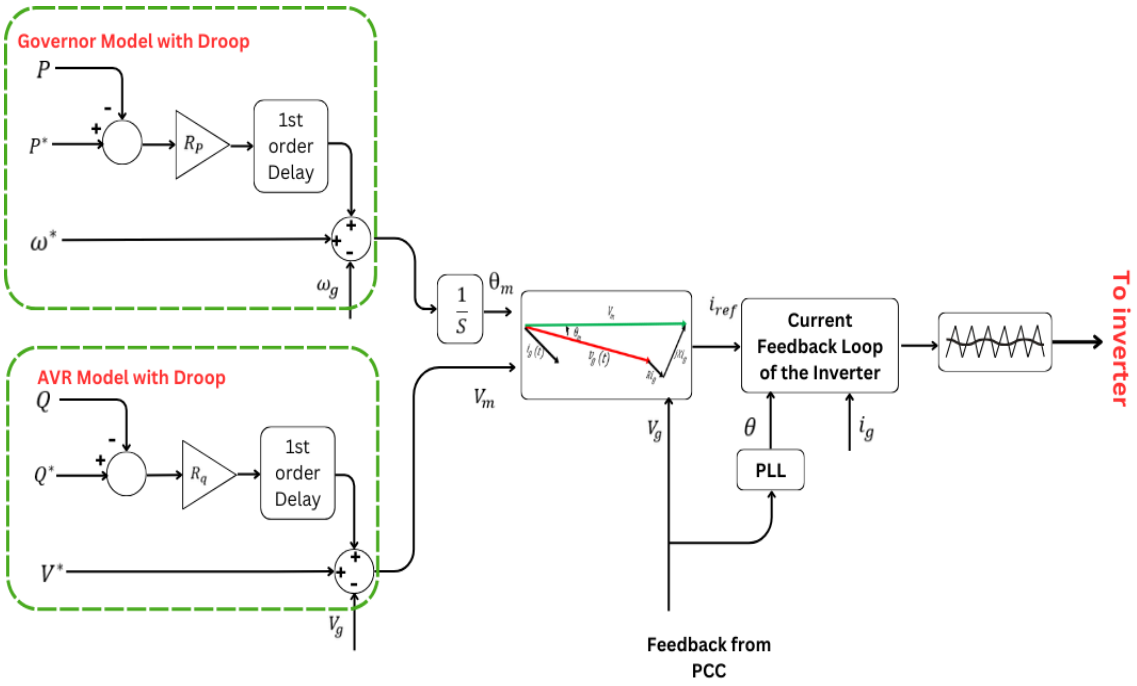

Figure II.8: Block diagram of KHI'S VSG topology .

The *PLL* and power meter used the measured voltage V_g and current i_g in the output of the inverter to calculate the frequency of grid ω_g and the active power output P_{out} respectively for the virtual inertia loop to generate the appropriate phase angle θ_m used fro *PWM* also a governor model shown in II.9 is used to give the active power input P_{in}, where the main control equations are formulated as:

$$\begin{cases} P_{in} - P_{out} = J\omega_m \frac{d\omega_m}{dt} + D(\omega_m - \omega_g) \\ P_{in}(s) = P_0 + \frac{K}{1+T_d s}(\omega^*(s) - \omega_g(s)) \end{cases} \tag{II.14}$$

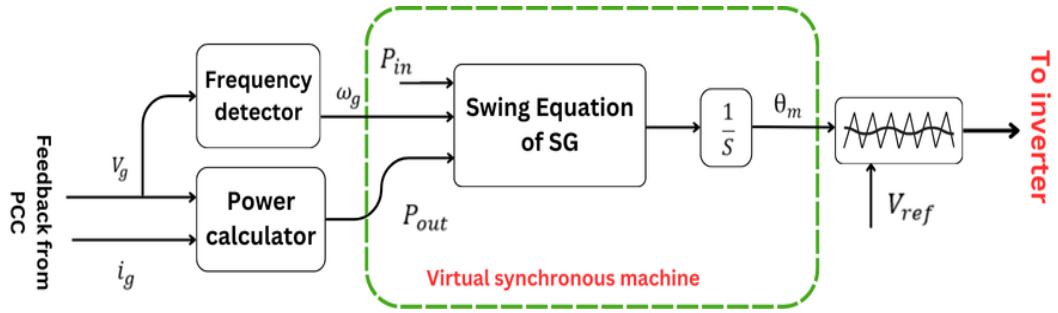

Figure II.9: Control diagram of ISE VSM topology.

According to [84], the voltage amplitude reference V_{ref} is generated according to the voltage-reactive droop control, and the frequency-active power droop controller can be used to provide the reference power P_{in} rather than the governor model given by equation II.15. Additionally, a virtual resistance control loop is added to the

designed control to get a short time constant of the current imbalance.

$$\begin{cases} \Delta\omega = \omega_g - \omega_0 = -R_P(P_{in} - P_n) \\ \Delta V = V_m - V_0 = -R_q(Q_{out} - Q_n) \end{cases} \tag{II.15}$$

Where Rp is the active power droop constant, Rq is the reactive power droop constant, and V_m and V_0 are the measured and nominal voltage, respectively. P_n and Q_n are the nominal active and reactive power, respectively.

II.4.2.2 Synchronous power controller topology

The synchronous power controller (SPC) is introduced for inverters-based DGs to ensure better interaction between converters and power system [85, 86]. The SPC control scheme mainly consists of two blocks, the electro-mechanical and virtual admittance blocks, as shown in Figure II.10. Depending on the grid requirements and the DC side configuration, outer loops can be added. Additionally, $Q-V$ droop controller is used for weak grid support and island grid forming, while an outer $P-V_{dc}$ droop control is associated with $P-F$ droop for limiting the power reserve. The inertia propriety can be integrated into the electro-mechanical control loop through the appropriate design of the power loop controller [85].

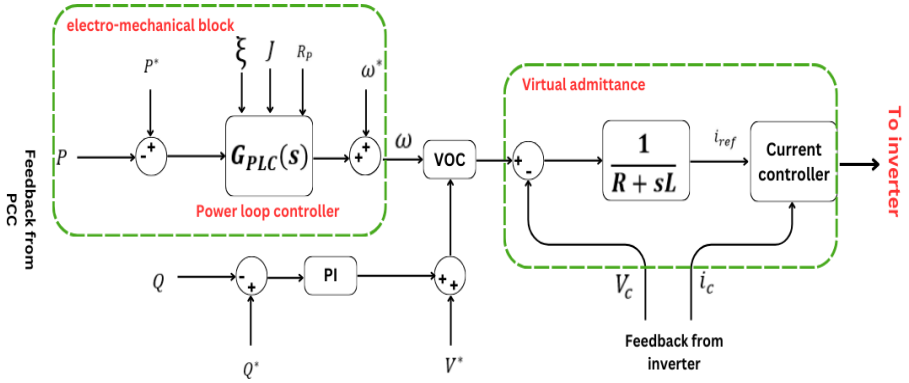

Figure II.10: Detailed diagram of the synchronous power controller.

According to the control schema presented II.10, the electro-mechanical block is based on the power loop controller (G_{PLC}) characterised by equation II.16, which is designed according to the swing equation of SG where the calculated power deviation is used for the G_{PLC} to generate the phase signal θ. The voltage reference is generated from the reactive droop control and used from the voltage oscillation control (VOC) to determine the virtual EMF. On the other hand, the virtual admittance impedance emulates the output impedance of the SG; it is used as an inner control loop to generate the current reference for the current controller of inverters. It is crucial in load sharing and provides a natural voltage magnitude droop feature for grid

voltage support [85].

$$G_{PLC} = \frac{1}{\omega_m(Js+\xi)} \tag{II.16}$$

The *SPC* is introduced in [87] for the *PV* system to operate seamlessly in grid-connected and island mode. The authors of [88] offered new *SPC* to decrease the cost of the power converter by removing the synchronous control from the internal controller and substituting a central synchronous controller; it regroups the different power converters united into a unique virtual synchronous generator.

II.4.3 Frequency power response-based topology

II.4.3.1 Virtual synchronous generators

The virtual synchronous generator (*VSG*) is proposed to cope with modern power system challenges. The concept of *VSG* topology is based mainly on frequency-power response associated with a basic droop controller to emulate the inertia and damping proprieties of real *SG*; this approach considers both the dynamic and steady-state performances without incorporating the detailed equation of *SG*, which makes this typology easy for implementation [78, 51]. It used the *RoCoF* ($\frac{d\Delta\omega}{dt}$) and frequency deviation ($\Delta\omega$) to determine the virtual inertia power (P_{VI}) needs during power disturbances according to equation II.17.

$$P_{VI} = D\Delta\omega + J\frac{d\Delta\omega}{dt} \tag{II.17}$$

In island *MG*, the *RoCoF* may rapidly increase and introduce system instability; however, the impact of virtual inertia on the *RoCoF* and the effect of the damping factor enhances the frequency dynamics. The conceptual schema of *VSG* topology is illustrated in Figure II.11, the *PLL* is used to measure the frequency deviation, and the *RoCoF* is to be used in the calculation of active power reference according to equation II.17. The current reference (I_d^*)is generated for the current inverter control loop according to equation II.18.

$$I_d^* = \frac{2}{3}\frac{V_d P_{VI} - V_q Q}{V_d^2 + V_q^2} \tag{II.18}$$

Where V_d, V_q are the voltages representing the $d-q$ frame.

II.4.4 Droop based topology

To ensure effective power-sharing for *MG*, the droop controller is the most recognised approach, which includes $P-F$ and $Q-V$ droop controllers as outlined in equation II.15. However, to improve the inertia response for inverters-based DGs, the $P-F$ droop controller is modified as depicted in Figure II.12 where a low pass

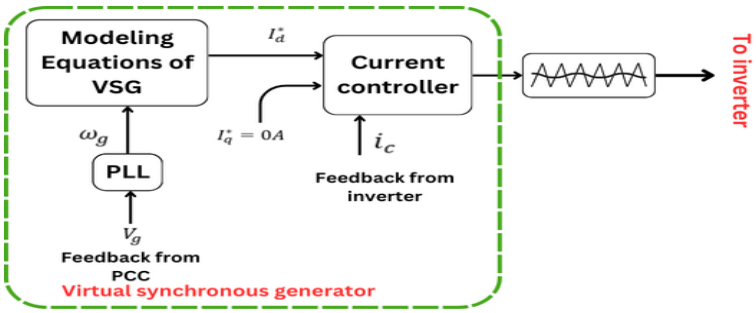

Figure II.11: Control diagram of the virtual synchronous generators.

filter is introduced for the measured active power output P_{out} to filter out the noise and the high-frequency components from inverter [89, 90]. Where T_f is the filter's

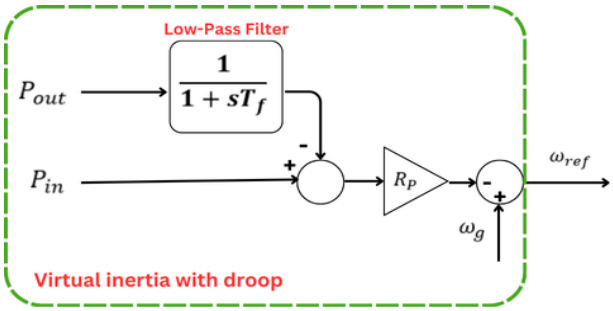

Figure II.12: Basic diagram of virtual inertia-based droop controller.

time constant.

Consequently, the droop controller associated with a well-designed filter can behave as real *SG*, which can be expressed in equation II.19 similarly to the virtual synchronous topology:

$$P_{in} - P_{out} = \frac{1}{R_p}(\omega_m - \omega_g) + T_f \frac{1}{R_p} s\omega_m \tag{II.19}$$

Where mathematically, the virtual inertia is introduced from this topology as time delay and virtual damping can be written as droop gain as follows:

$$\begin{cases} J = T_f \frac{1}{R_p} \\ D = \frac{1}{R_p} \end{cases} \tag{II.20}$$

II.4.5 Virtual oscillator control

The virtual oscillator controller (*VOC*) is an additional *VSM* topology that synchronises *DG* units without communication. Instead of simulating *SG* or induction generators, the controller incorporates a non-linear oscillator to ensure the inertia response to the power system. In the case of *DGs*, managing the grid, making this approach is particularly advantageous as the controller can share the system load and maintain synchronisation [91, 92].

II.4.6 Inducverters

The principle of the inducverter is mostly based on the inertial characteristics of an induction machine [93]. An induction machine possesses both self-start and soft-start capabilities. The system can detect changes in the grid and automatically synchronise itself with the grid. The inducverter employs these identical principles to imitate inertia. An inducverter is a device that controls the active power and frequency by utilising the virtual rotor inertia of a power electronic inverter.

The inducverter consists of two main components: a) an electrical component, which is an inverter with a filter, and b) a control component, which generates voltage signals to make the inverter function like an induction machine. Figure II.13 depicts the control diagram of the inducverter. The control section of the inducverter comprises two main components: a power damping/synchronisation unit and a core controller unit [58, 93].

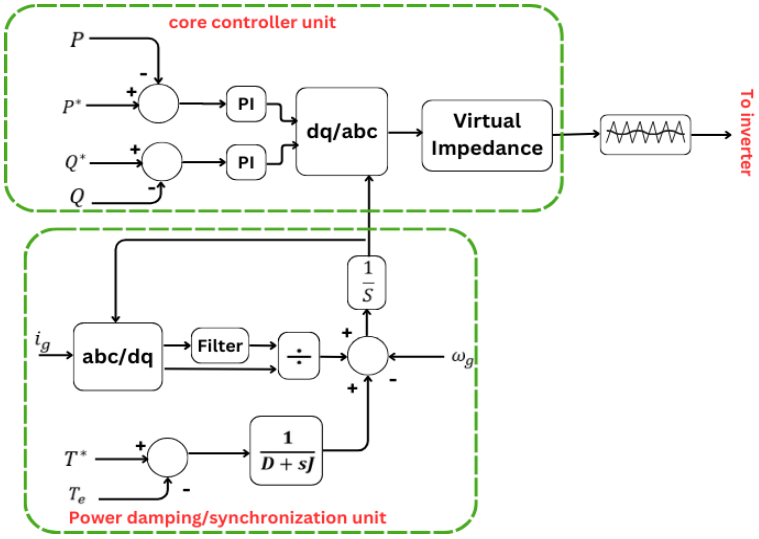

Figure II.13: Detailed control diagram of inducverters.

The power damping/synchronisation device generates the reference frequency and is designed to achieve grid stability and automatic synchronisation. The inverter reduces the need for a synchronisation device and a phase-lock loop. Additionally, it has self-start or soft-start capabilities. The central controller unit modifies the voltage references for three-phase power to provide the predetermined real and reactive power values. The system is composed of two separate channels: the first channel of the core controller governs the actual power using a proportional-integral controller, and the second channel enforces the management of reactive power. The virtual impedance block transformed the reference currents produced by the core controller into voltage references and then applied them to the pulse width modulation generator. Therefore, the power electronic inverter, controlled by the inducverter, can contribute to an inertial response in the event of a power imbalance. The inducverter regulates the inertial response and can control the voltage amplitude through the re-

active power control loop. A grid can benefit from increased inertia by incorporating a power electronic inverter and an inducverter, especially when a significant presence of *RES* [58].

II.4.7 Summary of virtual inertia control topologies

The summary of major Key features and drawbacks of the main topologies used to emulate the inertia and damping properties of real SG for low-inertia systems is outlined in Table II.2.

Table II.2: Summary of Virtual Inertia Control Topologies.

Type	Topology	Features	Drawbacks	Ref
Based on Synchronous generator model	Synchronverters	*Emulation of the precise dynamics of real SG without need for the frequency derivative. **PLL* employed only for synchronization. *Ensure power-sharing with high controllability of voltage and frequency. *Adjustable control parameters (inertia and damping).	*Possibility of numerical instability due to the complexity of the differential equation involved. *Needs an external protection system.	[68, 74, 75, 76, 77]
	VISMA and IEPES VSG	*Emulation of the ideal-linear model of SG. *VISMA-Method 1 based voltage to current and VISMA-Method 2 based voltage to current for the inverter. *Automated power sharing. * Conceptually straightforward. *Suitable for use in stand-alone mode.	* Possibility of numerical instability. *Managing transient currents during the synchronisation period in a grid-connected mode might be challenging.	[79, 81]
	KHI'S VSG	*Inertia emulation based on the phasor diagram of SG with the automatic voltage regulator. *Effective in handling imbalanced loads and sudden changes in the power system.	*Complex differential equations cause oscillatory behaviour. *Lack of safety mechanisms for over-current complicates design.	[82]

Continuation of Table II.2

Type	Topology	Features	Drawbacks	Ref
Swing equation-based topology	ISE VSM	*Simpler model compared to SG based model **PLL* employed only for synchronization		[83, 84]
	Synchronous power controller topology	* Implementing a cascaded control system involves using a virtual admittance, including an inner control loop for current and an outer control loop for voltage. *Provide intrinsic over-current protection *More resistance to numerical instability	*Setting control system parameters is more challenging due to the nested loop structure.	[85, 86, 87, 88]
Frequency Power Response-based topology	Virtual synchronous generators	*It is based on the derivative of frequency measurement. *Mimics inertial response to frequency deviation. *Provide load sharing amongst parallel-connected devices. *Fast reaction in the monitoring of steady-state frequency	*Necessitate sophisticated PLL *Sensitive to noise which may affect the system operation	[51, 78]
Droop based topology		*Communication-less Concepts similar to traditional droop control in SGs	*Slow transient response Improper transient active power sharing	[89, 90]

Continuation of Table II.2				
Type	Topology	Features	Drawbacks	Ref
Virtual Oscillator Control		*The controller uses a non-linear oscillator to synchronise DG units without communication. * Ensure better voltage regulation.	*High sensitivity to parameter variations can lead to instability. *Can introduce harmonic distortion, impacting power quality. * tuning and stability analysis challenges often require iterative simulations.	[91, 92]
Inducverters		*It relies on the inertial features of the induction machine. *Provide automatic synchronisation without the PLL. *Ensure the total system load sharing.	*Inducverters are sensitive to synchronisation, risking instability during grid transitions. *Performance relies on accurate parameter settings; inaccuracies can cause instability.	[58, 93]

II.5 Conclusion

The transition to modern power systems, characterised by the integration of *RESs* and reduced reliance on traditional *SGs*, has necessitated innovative approaches to maintaining system stability and frequency regulation. This chapter explored virtual inertia as a critical solution to diminishing physical inertia in power grids.

We began by examining the fundamentals of inertia in power systems and the adverse impacts of reduced inertia on system dynamics. Then, we introduced the concept of virtual inertia, highlighting its ability to emulate the inertial response of conventional generators using advanced control strategies and power electronics.

Various virtual inertia control (VIC) topologies were discussed in detail, including synchronverter-based models, swing equation-based designs, and frequency-power response-based approaches. These topologies offer diverse methods to achieve frequency stability, each with distinct advantages and limitations tailored to specific grid conditions. Emerging strategies such as virtual oscillator control and inducverters demonstrate the ongoing innovation in this field.

Virtual inertia is a transformative concept that bridges the gap between traditional and modern power systems. By emulating the inertial characteristics of SGs, virtual inertia enables grid operators to enhance stability, support renewable integration, and maintain reliable power system operation. The diversity of control topologies discussed in this chapter underscores the importance of continued research and development to refine these technologies and adapt them to the evolving needs of power systems worldwide.

Chapter III

Modelling and design of interconnected MGs-based virtual inertia control

III.1 Introduction

The increasing penetration of *RESs* into *MG* presents significant challenges for maintaining grid stability, particularly regarding frequency regulation. Unlike traditional power systems, where large *SGs* provide inherent inertia, the decentralised and intermittent nature of *RESs* reduces the effective system inertia, leading to rapid frequency fluctuations. To mitigate these issues, *VIC* has emerged as a crucial solution that mimics the behaviour of physical inertia through advanced control strategies.

This chapter focuses on developing and implementing a *VIC* strategy for interconnected *MGs*, with the primary aim of mitigating reduced inertia in modern power systems, particularly with the increasing penetration of *RES*. It delves into the design of *VIC* based on *ESS* and the state-space modelling technique to capture isolated and interconnected *MGs* dynamics. The analysis highlights the critical role of *VIC* in enhancing frequency stability by exploring the frequency response model of *MGs*. Furthermore, it examines the impact of reduced inertia on system stability and evaluates the effectiveness of *VIC* under different scenarios. The chapter also provides a detailed analysis of the impact of *VIC* parameters on system response to highlight the importance of *VIC* in ensuring the stable and resilient operation of interconnected *MGs* with significant *RESs*.

III.2 Frequency response modelling

The balance between real power generation and demand directly influences the frequency of a power system. A shift in real power demand at any location within the network affects the entire system by causing a frequency change. As a result, system frequency serves as a reliable indicator of imbalances between supply and demand. Any short-term energy imbalance leads to an immediate frequency variation, with the kinetic energy stored in rotating machinery initially compensating for the disturbance. However, if a substantial generation loss occurs and the system cannot respond appropriately, this can lead to severe frequency deviations beyond the plant's operational limits [94, 95, 96].

The real power output of a generator is governed by the mechanical power supplied by its prime mover, which can include devices such as steam turbines, gas turbines, hydro turbines, or diesel engines. In steam and hydro turbines, control valves regulate the flow of steam or water to adjust the mechanical input. Continuous regulation of this mechanical input is essential to ensure the generator's real power output aligns with the system's demand. Maintaining near-constant system frequency is critical for stable power system operation, as frequency deviations can indicate imbalances between generation and load. Proper control mechanisms are therefore necessary to ensure frequency stability and efficient system performance

[94, 95].

In addition to primary frequency control, most large *SGs* are equipped with a secondary frequency control loop. This secondary control plays a vital role in stabilising system frequency by correcting any remaining deviations after primary control actions. A schematic block diagram illustrating a synchronous generator equipped with both primary and secondary frequency control loops is presented in Figure III.1

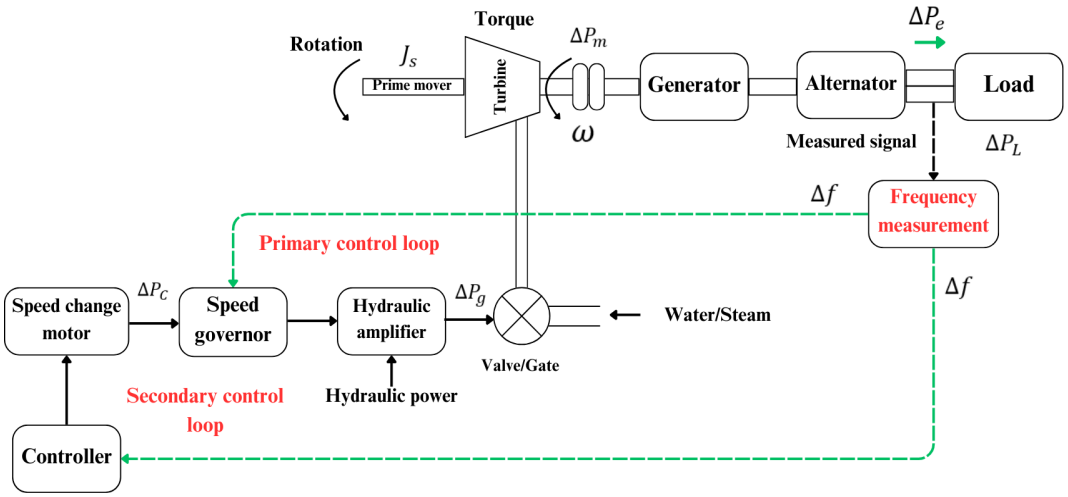

Figure III.1: A schematic block diagram of synchronous generator-based primary and secondary control

Where J_s is the moment of inertia of the prime mover, ΔP_C the ACE action change (signal) from secondary control, ΔP_L is the Load power variation, ΔP_m is the mechanical power the turbine provides to the generator, ΔP_g is the change in valve/gate position for controlling the turbine's power output, and ΔP_e is the electrical power output of the generator.

III.2.1 Structure of frequency response

Power systems' dynamic behaviour is often characterised by time-varying and nonlinear attributes. Nevertheless, a simplified linear low-order model is utilised to implement frequency control synthesis in response to fluctuations in load or the output power from *RESs*. It is crucial to recognise that the frequency response dynamics occur slower than the rotor angle and voltage dynamics, typically spanning seconds to minutes [51].

Furthermore, analysing both slow and fast dynamics in power systems requires an in-depth investigation of generation and load behaviours, often demanding complex numerical techniques. These techniques enable adjustments to the simulation time step in response to variations in system parameters. By disregarding the rapid dynamics associated with rotor angle and voltage, the overall complexity of computation, data requirements, and modelling processes can be significantly reduced, leading to more straightforward results and analyses.

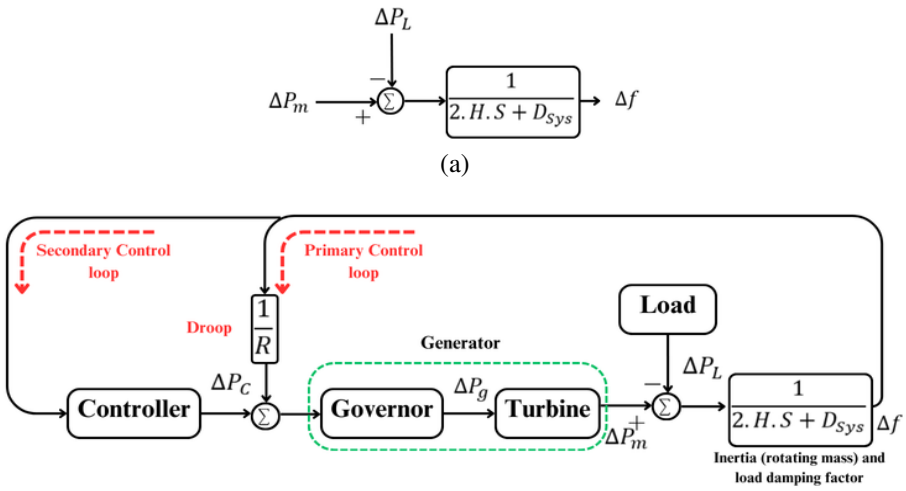

Figure III.2: Schematic block diagram of the load-generator model for frequency control (b) Reduced block diagram of a synchronous generator with primary and secondary frequency control.

This section elaborates on a frequency response structure based on the schematic diagram in Figure III.1. The overall dynamic relationship between the incremental power mismatch ($\Delta P_m - \Delta P_L$) and the frequency deviation (Δf) can be described using the swing equationIII.1.

$$\Delta P_m(t) - \Delta P_L(t) = 2H\frac{d\Delta f(t)}{dt} + D_{sys}\Delta f(t) \tag{III.1}$$

where H is the inertia constant and D_{sys} is the load damping coefficient, which represents the percentage change in load corresponding to a 1% shift in frequency.

Using Laplace transform, the equation III.1 can be written as:

$$\Delta P_m(s) - \Delta P_L(s) = 2H_{sys}s\Delta f(s) + D_{sys}\Delta f(s) \tag{III.2}$$

According to the equation III.2, Figure III.2-a represents the block diagram of the load-generator model for frequency control. This model reduces the complexity of the closed-loop SG block diagram from Figure III.1, with the final simplified diagram shown in Figure III.2-b.

The non-reheat steam generator proposed in Figure III.3 is the most useful in *MGs* that integrate *RESs*. It can complement these intermittent sources by providing a steady backup power supply. Their ability to operate effectively in variable conditions helps enhance the overall stability and reliability of the *MG*. The governor-turbine system in Figure III.3 is represented using first-order transfer functions to accurately capture its dynamic response. It is utilised to analyse power system frequency dynamics and develop control strategies.

where T_g and T_t are the time constants of governor and turbine, respectively.

The primary function of the turbine-governor control is to regulate the system's frequency by modulating the turbine's mechanical power output (ΔP_m), ensuring that

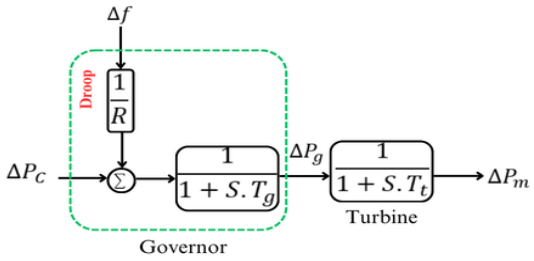

Figure III.3: Block diagram of non-reheat steam generator.

the system frequency remains within the desired range. The relationship between the frequency deviation (Δf) and the change in generator output power is depicted in Figure III.4.

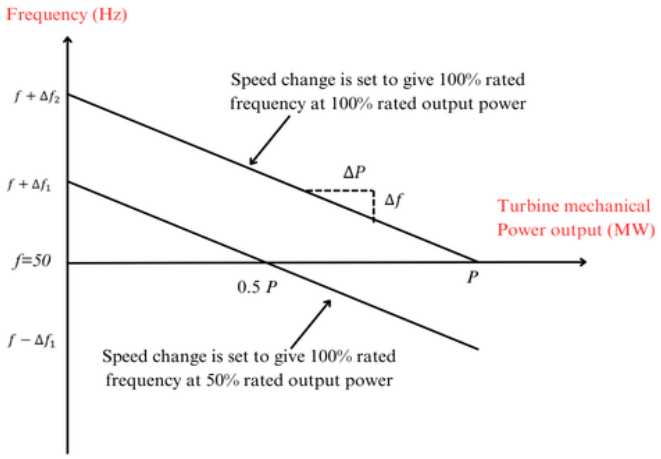

Figure III.4: Characteristic of the frequency -power relationship.

According to Figure III.4, the droop gains (R) characterise the frequency-power relationship of the turbine-governor can be expressed by equation III.3 as:

$$R = \frac{\Delta f}{\Delta P} \tag{III.3}$$

When power demand increases or generation decreases, causing a drop in frequency ($\Delta f < 0$), the governors automatically increase mechanical power output ($\Delta P > 0$) to restore frequency stability. Conversely, when demand decreases, resulting in a frequency rise ($\Delta f > 0$), the governors reduce power output ($\Delta P < 0$) to prevent overproduction.

III.2.1.1 Physical constraints for frequency control

The governor dead band is a critical physical constraint in frequency control. It refers to a small range of frequency deviations around the nominal system frequency (typically 50 Hz or 60 Hz) where the governor remains inactive. This dead band prevents unnecessary turbine adjustments in response to minor fluctuations caused by transient or short-term events, thereby reducing wear on the turbine and improv-

ing overall efficiency. The typical dead band is set between $0.03Hz$ and $0.05Hz$, depending on the system's design. Once the frequency deviation exceeds this range, the governor adjusts the turbine's output to restore the system's frequency [51].

Another key physical constraint is the generation rate, also known as the generation rate of change (*GRC*). It defines how quickly a non-reheat unit can modify its power output in response to frequency deviations or set-point commands. Since non-reheat units lack a reheat cycle, they can respond faster than reheat units, as they do not undergo the intermediate steam reheating process. This faster response time is crucial in managing sudden frequency changes, with typical generation rates ranging from 3% to 10% of the unit's rated capacity per minute [51, 97, 98].

When the system frequency surpasses the governor dead band's limits, the turbine's steam flow is adjusted to correct the deviation. The generation rate governs the speed of these adjustments, with non-reheat units offering faster responses than their reheat counterparts. These physical constraintsgovernor dead band and generation rateare essential in maintaining frequency stability and ensuring effective control within the power system.

The *GRC* and governor dead band can be analysed by incorporating hysteresis patterns and limiters into the turbine-governor model, as illustrated for a non-reheat steam turbine in Figure III.5. The variables V_L and V_U represent the lower and upper constraints that regulate the valve or gate's opening and closing speeds.

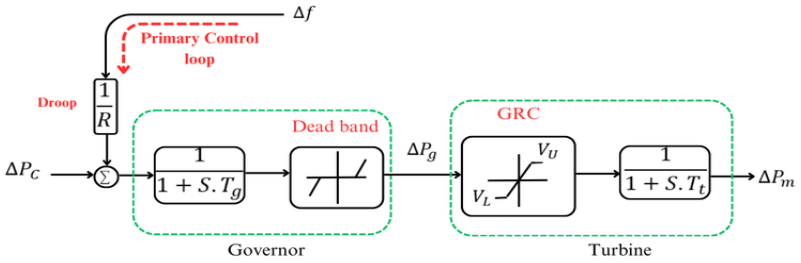

Figure III.5: Dynamic structure of the GRC and governor dead band for on-reheat steam generator.

III.2.1.2 Considering RESs effect in modern power system

In power system operations, *DGs* and *RESs* are classified as uncertainties or disturbances due to their unreliable nature in maintaining power system stability. Specifically, the variable output from *RESs*, which is difficult to forecast accurately, complicates power system management and requires additional measures to handle these fluctuations. Furthermore, *RESs* can trigger rapid frequency changes when their output suddenly decreases, such as during unexpected changes in weather. As these sources cannot provide inertia, the power system becomes more vulnerable to frequency deviations. Additionally, with greater integration of *RESs*, the system's overall inertia declines, making it more susceptible to disturbances and requiring faster responses from conventional generators or alternative balancing mechanisms.

The simplified model of wind and solar systems, as depicted in Figure III.6, is deemed adequate for frequency stability studies and analysis. Consequently, the model employed in this work is sufficiently accurate for studying frequency stability [99, 100, 101, 102, 103]. It is important to note that the simplified model incorporates the effects of external inputs, control or manipulated signals, and uncontrollable disturbances, all of which are accounted for in the mathematical models of *RESs*/*DGs* and loads.

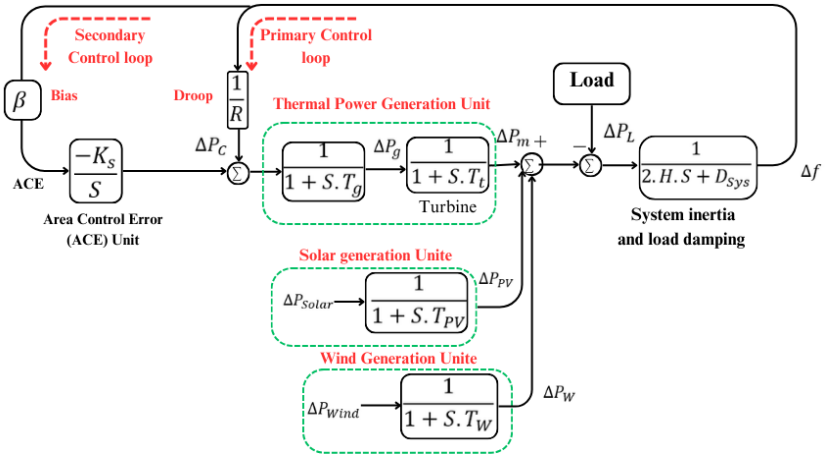

Figure III.6: Dynamic frequency response model of the modern power system.

III.3 Interconnected power system

A multi-area power system is composed of numerous regions that are connected by high-voltage transmission lines or tie lines. The aggregate power mismatch across the interconnected system is reflected in the frequency trends observed within each control area rather than just within an individual control area. Load Frequency Control (LFC), also known as secondary frequency control, regulates the local frequency and power exchange with other regions within the interconnected network in each control area. In this context, Figure III.7 illustrates a power system comprised of N control areas.

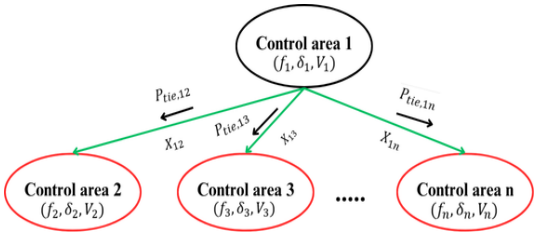

Figure III.7: Dynamic frequency response model of the modern power system.

The power transfer via the tie-line from region 1 to area 2 is defined in Equation III.4.

$$P_{\text{tie},12} = \frac{V_1 V_2}{X_{12}} \sin(\delta_1 - \delta_2) \tag{III.4}$$

Where V_1, V_2 are the voltages (in p.u.) at equivalent machine's terminals of areas 1 and 2; δ_1, δ_2 are the power angles of equivalent machines of the areas 1 and 2; and X_{12} is the tie-line reactance between area 1 and 2.

By linearizing III.4 about an equilibrium point $\left(\delta_1^0, \delta_2^0\right)$:

$$\Delta P_{\text{tie},12} = T_{12}\left(\Delta\delta_1 - \Delta\delta_2\right) \tag{III.5}$$

where T_{12} represents the synchronizing torque coefficient presented by

$$T_{12} = \frac{|V_1||V_2|}{X_{12}}\cos\left(\delta_1^0 - \delta_2^0\right) \tag{III.6}$$

By considering the relationship between the area power angle and frequency, Equation III.5 is rewritten as follows:

$$\Delta P_{\text{tie},12} = 2\pi T_{12}\left(\int \Delta f_1 - \int \Delta f_2\right) \tag{III.7}$$

where Δf_1 and Δf_2 are frequency changes in areas 1 and 2, respectively.

The Laplace transform of III.7 results in Equation III.8:

$$\Delta P_{\text{tie},12}(s) = \frac{2\pi}{s} T_{12}\left(\Delta f_1(s) - \Delta f_2(s)\right) \tag{III.8}$$

Similarly, the net power interchange between A1 and A3 is given in Equation III.9:

$$\Delta P_{\text{tie},13}(s) = \frac{2\pi}{s} T_{13}\left(\Delta f_1(s) - \Delta f_3(s)\right) \tag{III.9}$$

Considering equations III.8 and III.9, the total tie-line power change between area 1 and the other areas can be calculated as expressed in III.10:

$$\Delta P_{\text{tie},1} = \Delta P_{\text{tie},12} + \Delta P_{\text{tie},13} = \frac{2\pi}{s}\left[\sum_{j=2,3} T_{1j}\Delta f_1 - \sum_{j=2,3} T_{1j}\Delta f_j\right] \tag{III.10}$$

Similarly, for N-control areas (Figure III.7), the total tie-line power change between area 1 and other areas is

$$\Delta P_{\text{tie},i} = \sum_{j\neq i}^{N} \Delta P_{\text{tie},ij} = \frac{2\pi}{s}\left[\sum_{j\neq i}^{N} T_{ij}\Delta f_i - \sum_{j\neq i}^{N} T_{ij}\Delta f_j\right] \tag{III.11}$$

Equation III.11 can be represented by a block diagram, which can be added to the mechanical power mismatch $(\Delta P_m - \Delta P_L)$ that was described in Figure III.8.

Hence, the simplified block diagram of the interconnected power system is shown in Figure III.8. It represents the secondary control loop in the presence of a tie-

line. The tie-line power flow change ($\Delta P_{\text{tie},i}$) is added to the frequency change (Δf_i) through a secondary feedback loop. The area control error (ACE_i) signal is then computed as shown in Equation III.12 and applied to the controller $K(s)$:

$$\text{ACE}_i = \Delta P_{\text{tie},i} + \beta_i \Delta f_i \tag{III.12}$$

Where β_i is a bias factor, which can be obtained according to Equation III.13 [3]:

$$\beta_i = \frac{1}{R_i} + D_i \tag{III.13}$$

In response to a frequency drop within the area, the Load Frequency Control (LFC) controller, $K(s)$, will act to bring the Area Control Error (ACE_i) back to zero. It achieves this by sending corrective signals to the governor, thereby adjusting generation to restore the area's frequency and ensuring the net interchange power aligns with the scheduled level.

The control system (see Figure III.8) of each region is based on primary control which dependent on the governor unit of the thermal generator to limit frequency deviation, and load frequency control uses the area control error to return the frequency to its nominal range[104]. [105], [106]. The frequency response of each region is obtained from the frequency deviation based on changes in power generation from thermal generation (ΔP_m), the generated power change from RESs (ΔP_{RESS}), the total load change (ΔP_L), and the change in tie-line power transfer between areas (ΔP_{Tie}). As expressed in the following equations [51]:

$$\Delta P_{m,i}(s) = \frac{1}{1+sT_{t,i}} \Delta P_{g,i}(s) \tag{III.14}$$

$$\Delta P_{g,i}(s) = \frac{1}{1+sT_{g,i}} \left(\Delta P_{ACE,i}(s) - \frac{1}{R_i} \Delta f_i \right) \tag{III.15}$$

$$\Delta P_{RESS,i}(s) = \frac{1}{1+sT_{RES,i}} \left(\Delta P_{RES,i}(s) \right) \tag{III.16}$$

$$\Delta P_{ACE,i}(s) = \frac{K_i}{s} \left(\beta_i \Delta f_i \right) + \left(\Delta P_{Tie,i}(s) \right) \tag{III.17}$$

$$\Delta P_{Tie,i}(s) = \frac{2\pi}{s} \left(\sum_{\substack{i=1 \\ j \neq i}}^{N} T_{i;j} \Delta f_i - \sum_{\substack{i=1 \\ j \neq i}}^{N} T_{i;j} \Delta f_i \right) \tag{III.18}$$

$$\Delta f_i(s) = \frac{1}{2H_i.s + D_{sys,i}} \left(\Delta P_{m,i}(s) + \Delta P_{RES,i}(s) - \Delta P_{L,i}(s) - \Delta P_{\text{Tie},\,i}(s) \right) \tag{III.19}$$

Where s is the Laplace transform operator, Δf is the frequency deviation, ΔP_g is the power generated by the turbine system, ΔP_{ACE} is the area control error, the

turbine time constant is T_t, the governor time constant is T_g, R is the governor droop constant T_{RES} is the renewable energy source's time constant, β_i is the bias factor, k_i is the integral controller gain, $T_{i;j}$ is the synchronising coefficient, the system inertia is H, and the system load damping is D_{sys} .

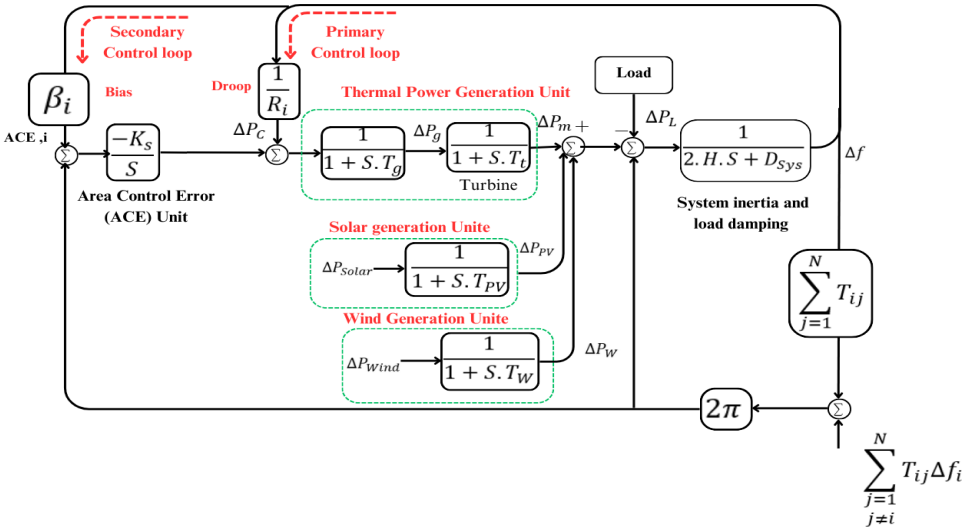

Figure III.8: Synoptic schema of load frequency control (LFC).

III.3.1 Design of virtual inertia control based ESS

As previously mentioned, all areas were blended with primary and secondary controls. However, this approach is still insufficient due to the low inertia characteristics of systems, including RESs, which affect the stability and power quality. Consequently, VIC is added in all areas based on the ESS as a first step to address the inertia issue and improve the frequency response. The reaction of VIC is obtained through virtual inertia power as given by the equation below:

$$P_{VI} = J\frac{d\Delta f}{dt} + D\Delta f \tag{III.20}$$

Where J is the inertia coefficient, D is the damping factor, the frequency deviation is Δf, and the inertia power is P_{VI}.

According to the equations above and the Control diagram of VIC presented in Figure III.9, it is clear that the power system changes lead to a frequency change, which means that the frequency regulation depends on the active power amount. As a result, the control system must be robust and perform well to ensure active power and frequency regulation. As a result, the $P-F$ droop controller is associated with VIC, where the power inertia can be extracted through a dynamic model of the inverter from [106]:

$$\Delta P_{VI} = \left(\frac{1}{R_{VI}}\right)\frac{s.J+D}{1+s\cdot T_{INV}}\Delta f \tag{III.21}$$

R_{VI} is the virtual inertia droop constant, and T_{INV} is the inverters time constant.

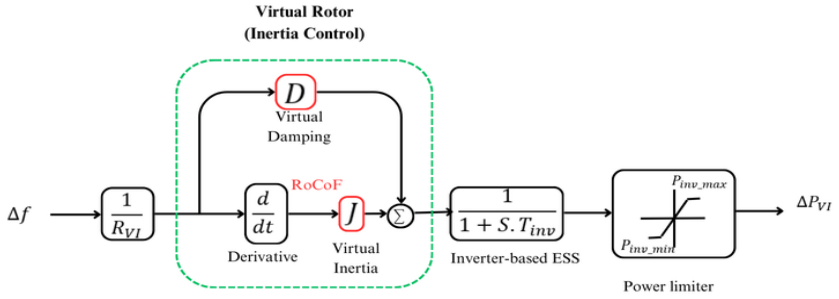

Figure III.9: Control diagram of virtual inertia control.

Consequently, in addition to the virtual inertia power, the frequency deviation expressed in equation (III.19) becomes:

$$\Delta f_i(s) = \frac{1}{2H_iS + D_{sys,i}} \left(\Delta P_{m,i}(s) + \Delta P_{RESs,i}(s) - \Delta P_{VI,i}(s) - \Delta P_{L,i}(s) - \Delta P_{Tie,i}(s)\right) \tag{III.22}$$

III.3.2 State space modelling

To analyse the responses of the interconnected power system and facilitate the study, state-space modelling [51] is used, where the variables (x_1, x_2, x_3, w, u) are based on the power changes of the thermal generators, virtual inertia power, RESs, tie-line power, load frequency control $(\Delta P_{LFC_i}), \Delta f$, and $RoCoF$ from each region. The studied system can be described using the state space model provided below:

$$\dot{x} = Ax + B_1 w + B_2 u \tag{III.23}$$

Where the state variable x, w is the disturbance signal, and u is the control input signal given by:

$x^T = [x_1 x_2 x_3]$

With:

$x_1 = \left[\Delta f_1 \Delta P_{m1} \Delta P_{g1} \Delta P_{LFC1} \Delta P_{VI1} \Delta P_{RES1} \Delta P_{Tie1}\right]$;

$x_2 = \left[\Delta f_2 \Delta P_{m2} \Delta P_{g2} \Delta P_{LFC2} \Delta P_{VI2} \Delta P_{RES2} \Delta P_{Tie2}\right]$;

$x_3 = \left[\Delta f_3 \Delta P_{m3} \Delta P_{g3} \Delta P_{LCF3} \Delta P_{VI3} \Delta P_{RES3} \Delta P_{Tie3}\right]$;

$w^T = [\Delta P_{RES1} \Delta P_{RES2} \Delta P_{RES3} \Delta P_{L1} \Delta P_{L2} \Delta P_{L3}]$;

$u^T = \left[\frac{d\Delta f_1}{dt} \frac{d\Delta f_2}{dt} \frac{d\Delta f_3}{dt}\right]$

The coefficients A, B_1 and B_2 of the state space model of three interconnected

areas are given as :

$$A = \begin{bmatrix} A_{11} & A_{12} & A_{13} \\ A_{21} & A_{22} & A_{23} \\ A_{31} & A_{32} & A_{33} \end{bmatrix}_{(21*21)} \quad ; \quad B_1 = \begin{bmatrix} B_{11} & B_{12} \end{bmatrix}_{(21*6)} ; \quad B_2 = \begin{bmatrix} C_{11} & C_{12} & C_{13} \end{bmatrix}_{(21*3)}$$

$$A_{\substack{(i,j=i) \\ i=1\to 3 \\ j=1\to 3}} = \begin{bmatrix} \frac{-D_{sysi}}{2H_i} & \frac{1}{2H_i} & 0 & 0 & \frac{1}{2H_i} & \frac{1}{2H_i} & \frac{-1}{2H_i} \\ 0 & \frac{-1}{T_{t,i}} & \frac{1}{T_{t,i}} & 0 & 0 & 0 & 0 \\ \frac{-1}{T_{g,i}R_i} & 0 & \frac{-1}{T_{g,i}} & \frac{1}{T_{g,i}} & 0 & 0 & 0 \\ K_S\beta_i - 2\pi T_i & 0 & 0 & 0 & 0 & 0 & 0 \\ \frac{D_i}{R_{VI,i}T_{VI,i}} & 0 & 0 & 0 & \frac{1}{T_{INV,i}} & 0 & 0 \\ 0 & 0 & 0 & 0 & 0 & \frac{1}{T_{RES,i}} & 0 \\ 2\pi T_i & 0 & 0 & 0 & 0 & 0 & 0 \end{bmatrix}$$

$$A_{(i;j)} = \begin{bmatrix} 0 & 0 & 0 & 0 & 0 & 0 & 0 \\ 0 & 0 & 0 & 0 & 0 & 0 & 0 \\ 0 & 0 & 0 & 0 & 0 & 0 & 0 \\ -2\pi T_{i;j} & 0 & 0 & 0 & 0 & 0 & 0 \\ 0 & 0 & 0 & 0 & 0 & 0 & 0 \\ 0 & 0 & 0 & 0 & 0 & 0 & 0 \\ -2\pi T_{i;j} & 0 & 0 & 0 & 0 & 0 & 0 \end{bmatrix}$$

$$B_{11}^T = \begin{bmatrix} 0 & 0 & 0 & 0 & 0 & 0 & 0 & \frac{1}{T_{RES,1}} & 0 & 0 & 0 & 0 & 0 \\ 0 & 0 & 0 & \frac{1}{T_{RES,2}} & 0 & 0 & 0 & 0 & 0 & 0 & 0 & 0 & 0 \\ 0 & 0 & 0 & 0 & 0 & 0 & 0 & 0 & 0 & 0 & 0 & \frac{1}{T_{RES,3}} & 0 \end{bmatrix}_{(3*21)}$$

$$B_{12}^T = \begin{bmatrix} \frac{-1}{2H_1} & 0 & 0 & 0 & 0 & 0 & 0 & 0 & 0 & 0 & 0 & 0 & 0 \\ 0 & 0 & 0 & 0 & \frac{-1}{2H_2} & 0 & 0 & 0 & 0 & 0 & 0 & 0 & 0 \\ 0 & 0 & 0 & 0 & 0 & 0 & 0 & 0 & \frac{-1}{2H_3} & 0 & 0 & 0 & 0 \end{bmatrix}_{(3*21)}$$

$$C_{11}^T = \begin{bmatrix} 0 & 0 & 0 & 0 & \frac{J_1}{R_{VI1}T_{VI1}} & 0 & 0 & 0 & 0 & 0 & 0 & 0 & 0 & 0 & 0 & 0 & 0 & 0 & 0 & 0 & 0 \end{bmatrix}_{(21*6)}$$

$$C_{12}^T = \begin{bmatrix} 0 & 0 & 0 & 0 & 0 & 0 & 0 & 0 & 0 & 0 & 0 & \frac{J_2}{R_{VI2}T_{VI2}} & 0 & 0 & 0 & 0 & 0 & 0 & 0 & 0 & 0 \end{bmatrix}_{(21*6)}$$

$$C_{13}^T = \begin{bmatrix} 0 & 0 & 0 & 0 & 0 & 0 & 0 & 0 & 0 & 0 & 0 & 0 & 0 & 0 & 0 & 0 & 0 & 0 & \frac{J_3}{R_{VI3}T_{VI3}} & 0 & 0 \end{bmatrix}_{(21*6)}$$

III.4 Implemented power system-based virtual inertia control

III.4.1 Isolated system

Figure III.10a shows the configuration of the studied stand-alone *MG* equipped with virtual inertia control-based *ESS*. The MATLAB/Simulink software develops the small-signal/dynamic response model. The simulation parameters are listed in Table III.1 [51], and the simulation model is shown in Figure III.10b.

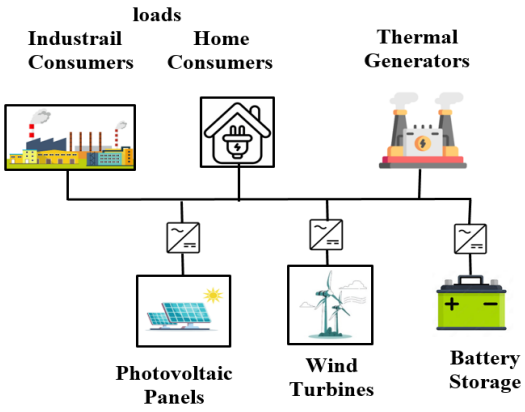

(a)

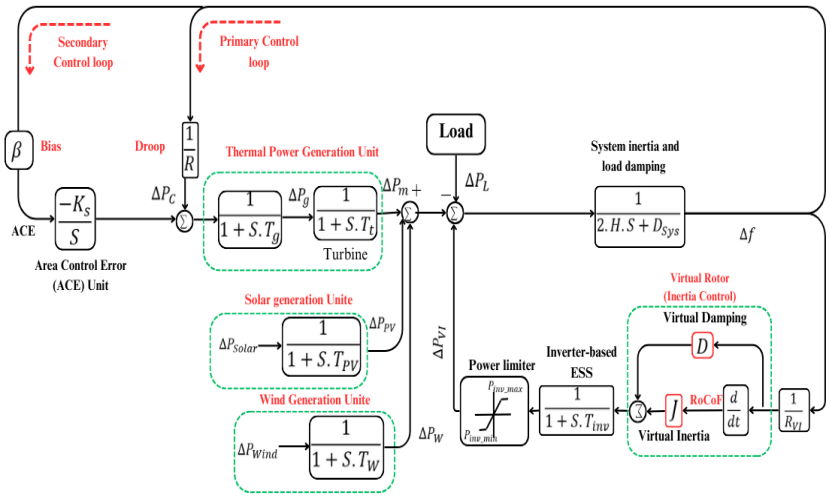

(b)

Figure III.10: (a): Configuration of the studied MG (b): Dynamic model of MG with virtual inertia control.

This section examines the simulation results to investigate the system's dynamic behaviour under various conditions. The analysis focuses on several key aspects,

including the impact of reduced inertia, which highlights the challenges posed by diminishing system inertia on stability, as well as the influence of virtual inertia control parameters on overall performance. Additionally, it examines the role of virtual inertia in enhancing system stability, the contribution of the damping factor in suppressing oscillations, and the effects of the active droop constant on power-sharing and frequency regulation. Each of these aspects is discussed in detail, with supporting data and observations presented in the subsequent subsections.

Table III.1: Simulation Parameters of Island System

Parameters	**Values**
Gain of Integral controller K_s(s)	0.1
Governor time constant T_g(s)	0.07
Turbine time constant T_t(s)	0.37
Governor droop constant R(Hz/p.u)	2.6
Bias factor β (p.u/Hz)	0.98
Virtual inertia constant J (p.u.s)	0.6
Virtual damping constant D (P.u/Hz)	0.3
Virtual inertia control droop R_{vi}(Hz/p.u)	2.7
Time constant of inverter-based ESS T_{inv} (s)	1.0
Time constant of wind turbine T_{wt} (s)	1.4
Time constant of solar system T_{pv} (s)	1.9
System inertia H (p.u.s)	0.0830
System load damping D_{sys} (p.u./Hz)	0.0160

III.4.1.1 Impact of reduced inertia

A test scenario involving sudden changes in system load and generation was simulated to evaluate the impact of reduced system inertia. At $t = 2$ s, a sudden load increase of 0.025 p.u. was applied to the system, followed by a sudden rise in renewable power generation at $t = 20$ s, with solar and wind power contributions of 0.015 p.u. and 0.01 p.u., respectively. The system's response was analysed under conditions where the system inertia (H) and load damping (D_{sys}) were progressively reduced from 100% to 40% of their original values. Figures **??** and III_11 highlight how these reductions affect the system's stability, frequency deviations, and overall dynamic performance with and without virtual inertia control.

Figure III_11 illustrates the frequency response of the system under varying levels of reduced H and D_{sys} without virtual inertia control. Following a sudden load

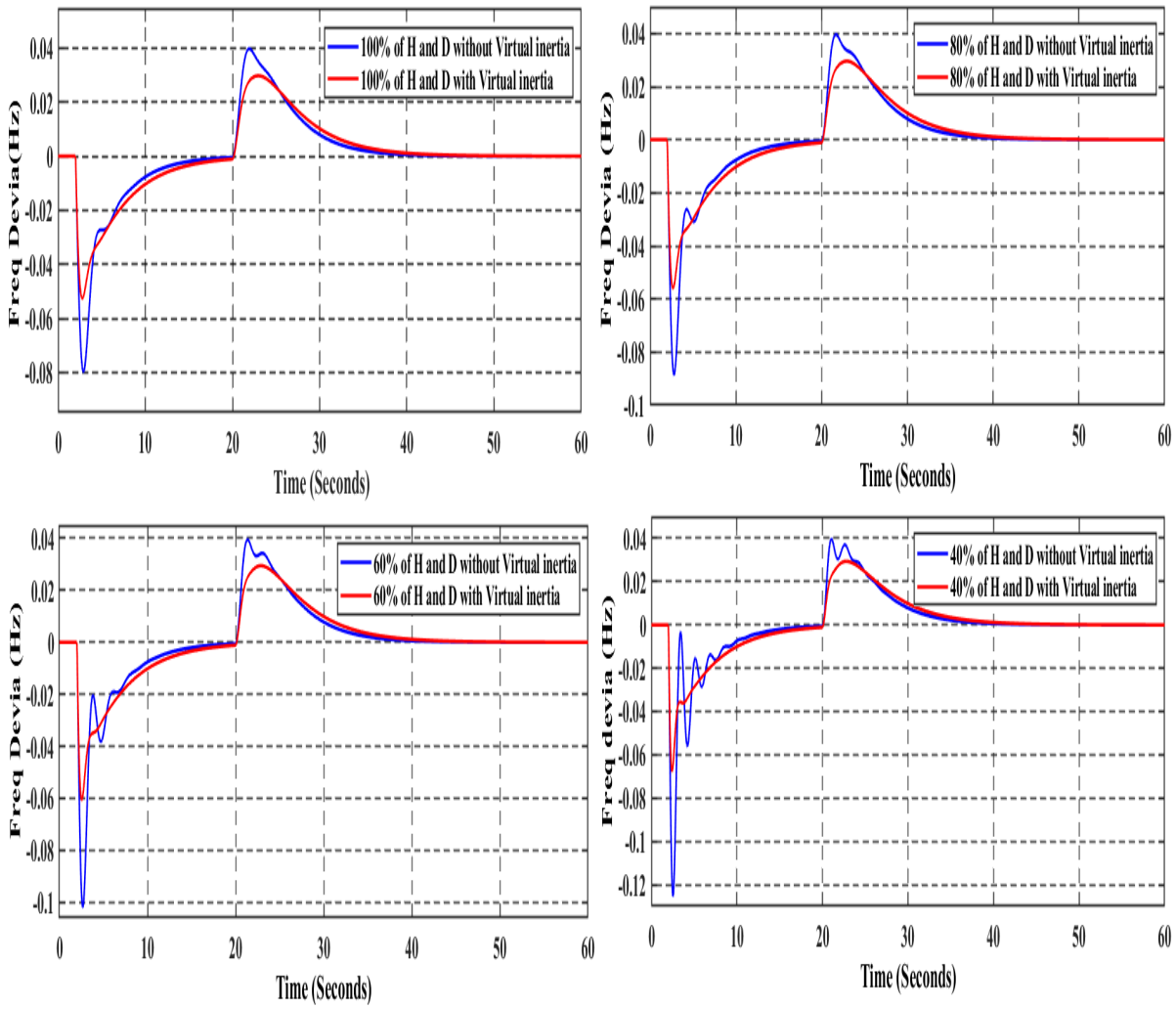

Figure III.11: Frequency response with virtual inertia control and under reduced inertia.

increase at $t = 2$ s, the system experiences a sharp frequency drop, with the magnitude of the deviation increasing as H and D decrease, particularly for lower inertia cases (e.g., 40%), where the frequency deviation reaches approximately -0.12 Hz. The system struggles to recover, exhibiting large oscillations and prolonged settling times, which indicate reduced system stability. Similarly, when renewable energy is introduced at $t = 20$ s, a sudden increase in solar and wind power generation causes a frequency rise. Systems with lower H and D_{sys} show larger overshoots and longer settling times, highlighting their diminished ability to recover quickly from disturbances.

Figure III.11 presents the same scenarios but with virtual inertia control applied. At 2 seconds, the frequency drop due to the load increase is significantly reduced across all cases, with overshoots limited to around 0.03 Hz, even in the 40% inertia case. The frequency stabilises much faster, with less pronounced oscillations and quicker settling times. When renewable energy is introduced at $t = 20$ seconds, the frequency deviation is much smoother, with minimal spikes, and the system rapidly returns to its nominal frequency. Virtual inertia helps absorb the impact of load and

renewable fluctuations, ensuring a stable response across different inertia levels.

A comparison of the overshoot and undershoot across the different inertia levels, both with and without virtual inertia, is summarised in Table III.2. The table provides precise numerical values that further highlight the improvements in system performance with virtual inertia, illustrating how it effectively mitigates the impact of reduced physical inertia by stabilising frequency deviations and ensuring faster recovery.

Table III.2: Performances of virtual inertia control.

Inertia and Damping	Overshoot (Hz)		Undershoot (Hz)	
	Without VIC	With VIC	Without VIC	With VIC
100% H and D	0.04	0.03	-0.08	-0.05
80% H and D	0.04	0.03	-0.085	-0.058
60% H and D	0.04	0.03	-0.1	-0.06
40% H and D	0.04	0.03	-0.12	-0.062

In Figures III.12, the thermal and virtual inertia power responses are shown under reduced system inertia. Figure III.12a shows that the thermal power response without virtual inertia exhibits notable oscillations and a slower recovery time, particularly when inertia is reduced to 40%. However, in Figure III.12b, the application of virtual inertia significantly improves the power response, as seen by reduced oscillations and faster stabilisation across all inertia levels. Where Figure III.12c demonstrates the virtual inertia unit's contribution to the power response. The ESS equipped with virtual inertia generates additional power during the transient state, rapidly absorbing and compensating for disturbances. This additional power helps reduce the deviations, improving overall system stability.

This analysis underscores the critical role of system inertia and damping in maintaining stability, as they effectively reduce frequency deviations, suppress oscillations, and enable faster recovery following disturbances. Ensuring sufficient levels of inertia and damping is therefore essential for the reliable operation of power systems, particularly in scenarios with significant renewable energy integration.

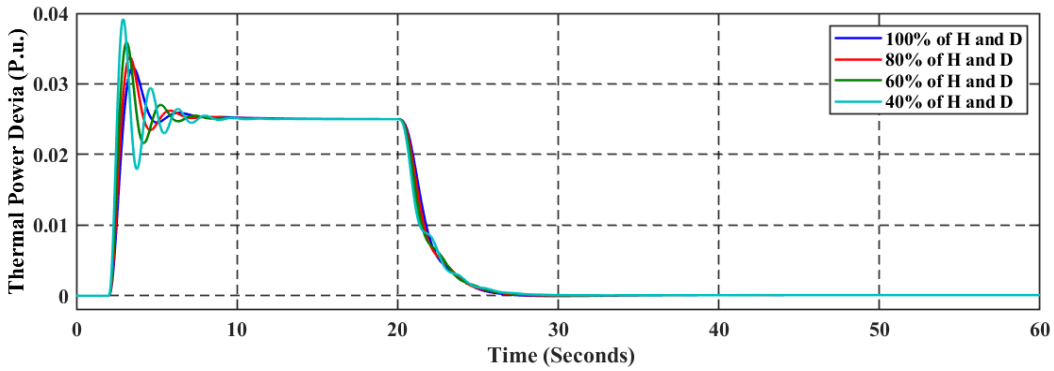

(a)

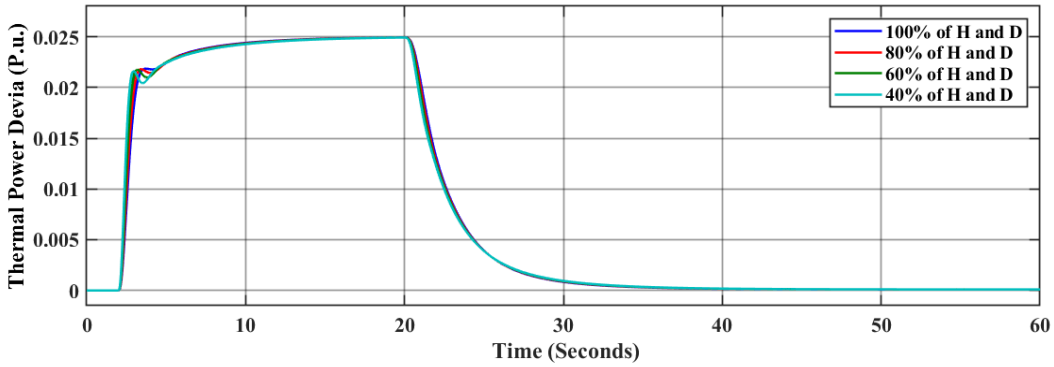

(b)

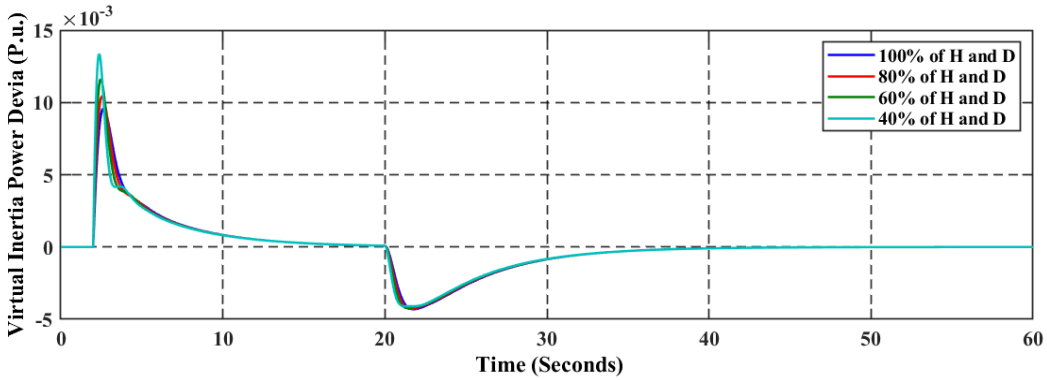

(c)

Figure III.12: Power response under reduced inertia. (a): thermal power without virtual inertia control and (b): with virtual inertia control. (c) Virtual inertia power

III.4.1.2 Impact of virtual inertia control parameters

- **Impact of virtual inertia**

  To evaluate the effectiveness of virtual inertia in enhancing system stability, fixed values of the virtual inertia constant (J) were employed. Simulations were conducted under the degraded situation of 50% of H and D_{sys}. Figures III.13 illustrate the responses of the system subjected to two distinct types of disturbances: abrupt load changes occurring at 2 seconds and fluctuations from *RESs* at 25 seconds.

  Increasing the virtual inertia constant (J) significantly reduces the frequency

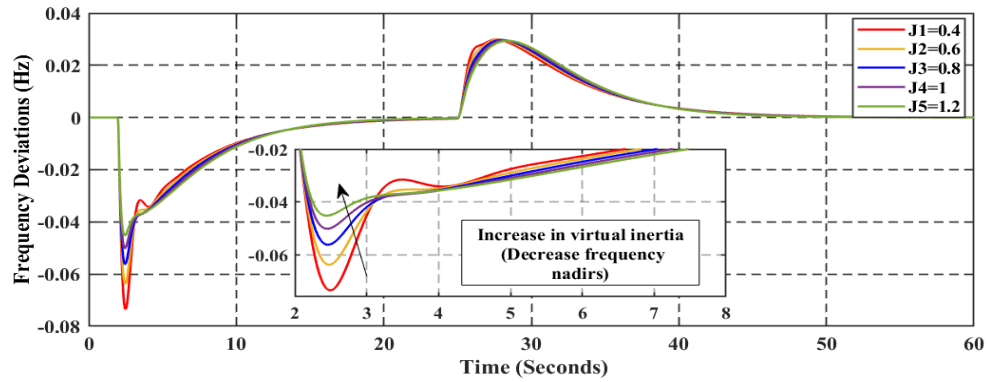

(a)

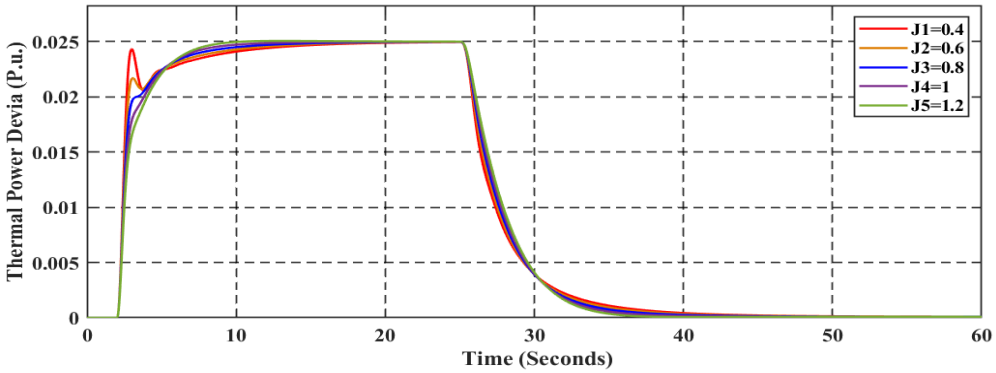

(b)

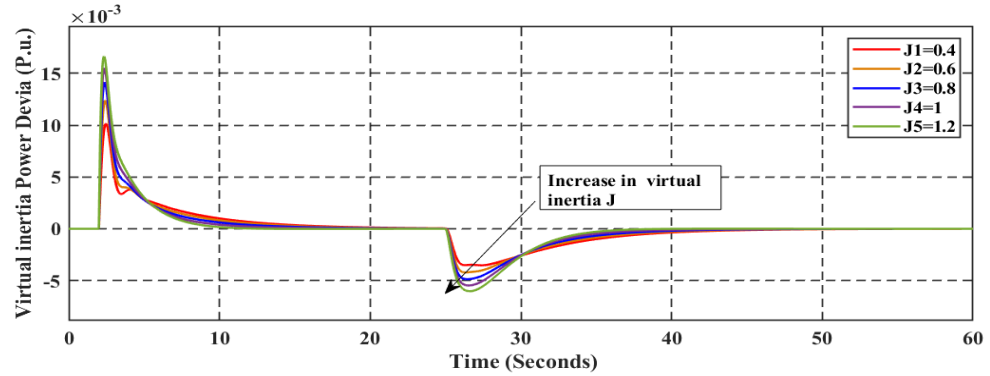

(c)

Figure III.13: (a) Frequency response. (b) Thermal power response. (c) Virtual inertia power response.

of nadir and overshoots, improving the overall performance and stability of the system. However, when J exceeds a certain threshold, the system requires more time to settle, negatively impacting damping performance. To address this issue, an increase in the virtual damping constant can be applied to optimise the damping characteristics and achieve a faster settling time.

- **Impact of damping factor**

  Figure III.14 illustrates the impact of varying the virtual damping constant (D) on the system's frequency deviation, thermal power deviation, and virtual inertia power deviation.

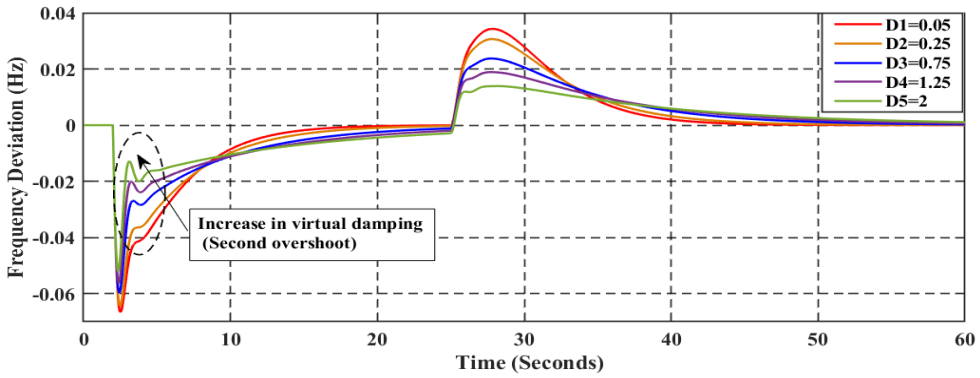

(a)

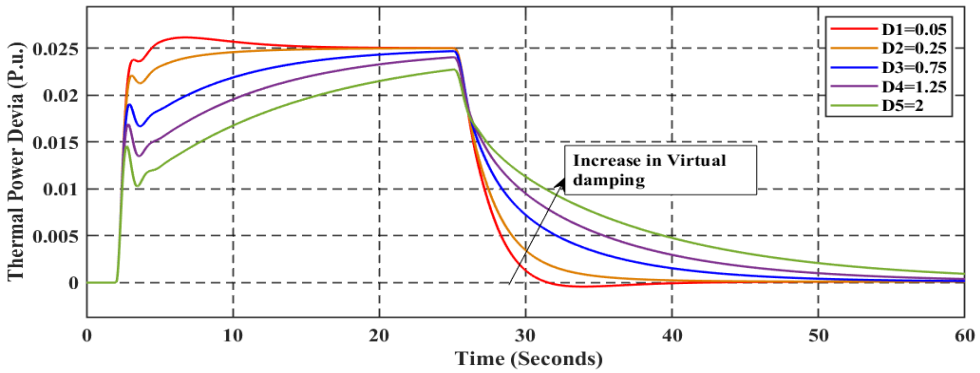

(b)

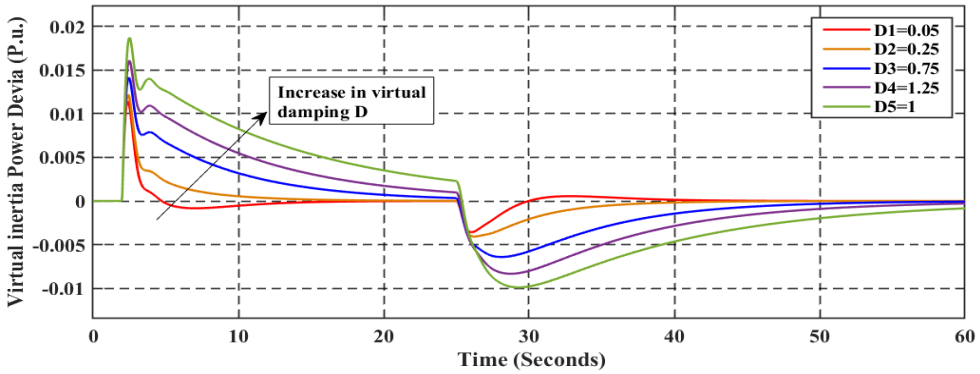

(c)

Figure III.14: (a) Frequency response. (b) Thermal power response. (c) Virtual inertia power response.

From the frequency response shown in figure III.14a, it is evident that an increase in D significantly reduces the magnitude overshoot in frequency deviation, demonstrating enhanced oscillation suppression and improved stabilisation of frequency response, How ever too much virtual damping can introduce second overshoot. Similarly, Figures III.14b and III.14c show that increasing the D clearly indicates that the virtual inertia unit necessitates greater steady power post-disturbance to mitigate the impact of prolonged stabilisation time. This emphasises the critical role of virtual damping in minimising oscillations, ensuring faster system stabilisation, and maintaining the power system's overall performance and reliability.

- **Impact of active droop constant**

Figures III.15 demonstrate the impact of varying the active droop constant (R_{VI}) on system dynamics, particularly frequency deviation, thermal power deviation, and virtual inertia power deviation. In Figure III.15a, reducing the R_{VI}, the system can attain enhanced performance with less frequency nadir/overshoot, although the stabilisation time is prolonged.

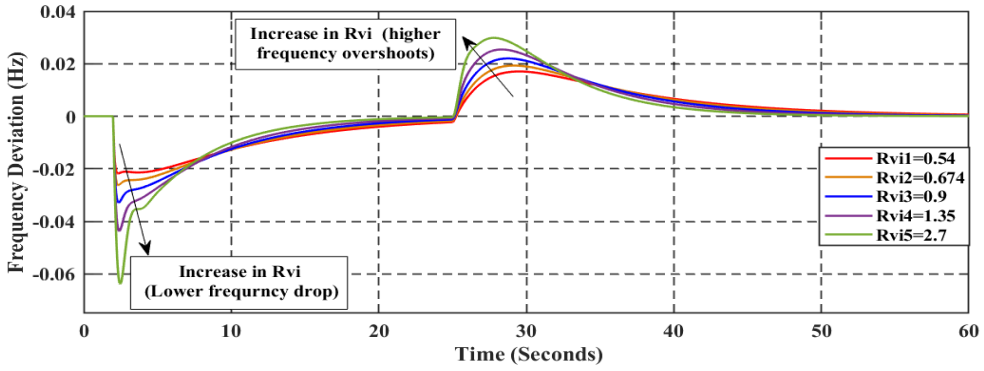

(a)

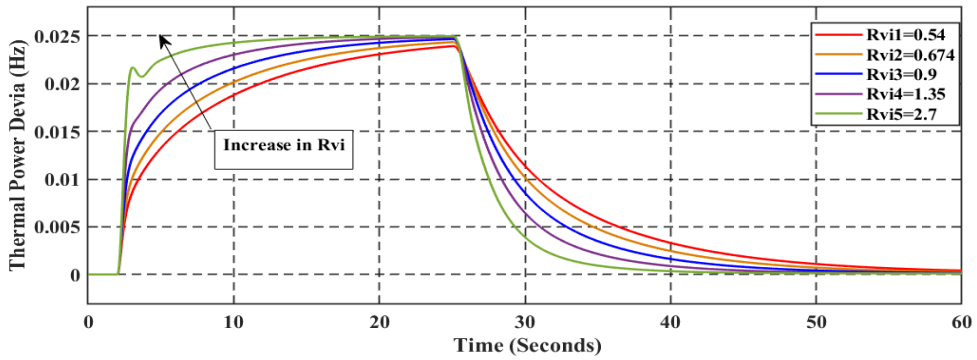

(b)

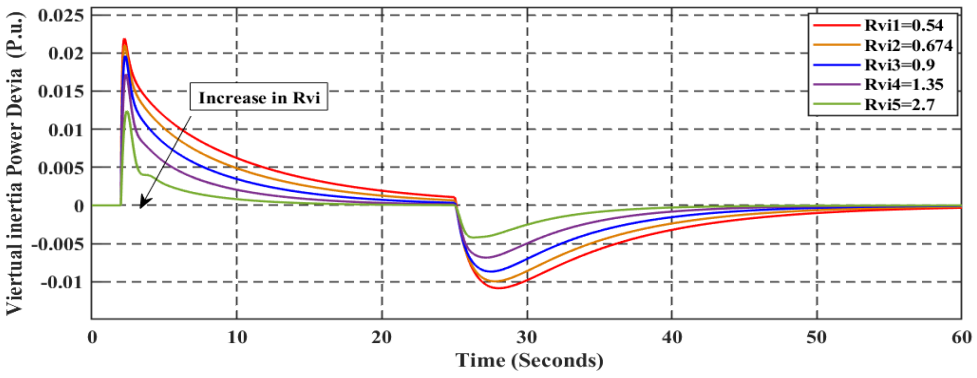

(c)

Figure III.15: (a) Frequency response. (b) Thermal power response. (c) Virtual inertia power response.

In Figure III.15b, reducing R_{VI} results in less stress on the conventional producing unit, leading to diminished power output. Conversely, the inverter-based ESS unit generates greater inertia power with an expedited response time. Nev-

ertheless, as the imitated inertia power increases due to the reduction of R_{VI}, the system's response results in an extended stabilisation time after disturbances.

These results underline the importance of selecting optimal J, D, R_{VI} values to achieve a balance between frequency stability, overshoot mitigation, and efficient power distribution in the system.

III.4.2 Interconnected MGs

The Virtual inertia control system is implemented in an interconnected power system, as shown in Figure III.16. The system contains three control areas (Area 1, Area 2, and Area 3), which are connected by tie-lines to help each other in regulation, exchanging interchange power and improving the dynamic performance of the power system. Each area consists of the thermal generator (conventional sources), *RESs* (non-conventional sources), *ESS*, and loads (see Figure III.16). To verify the efficiency of the virtual inertia control for the interconnected system, the study is based on the frequency response model for stability analysis under continuous disturbances. The state space model of the system developed previously (**section III.3**) is implemented using MATLAB/Simulink based on Figure III.17 and Table III.3.

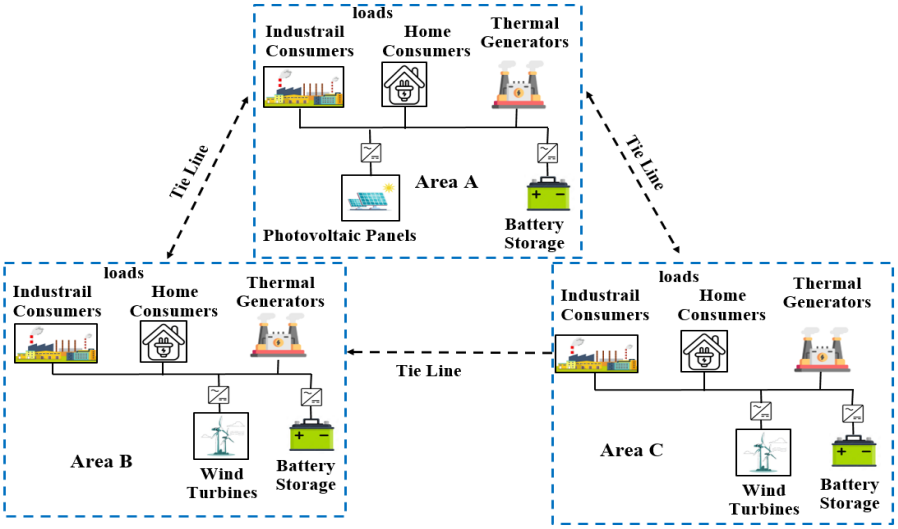

Figure III.16: Configuration of interconnected MG system.

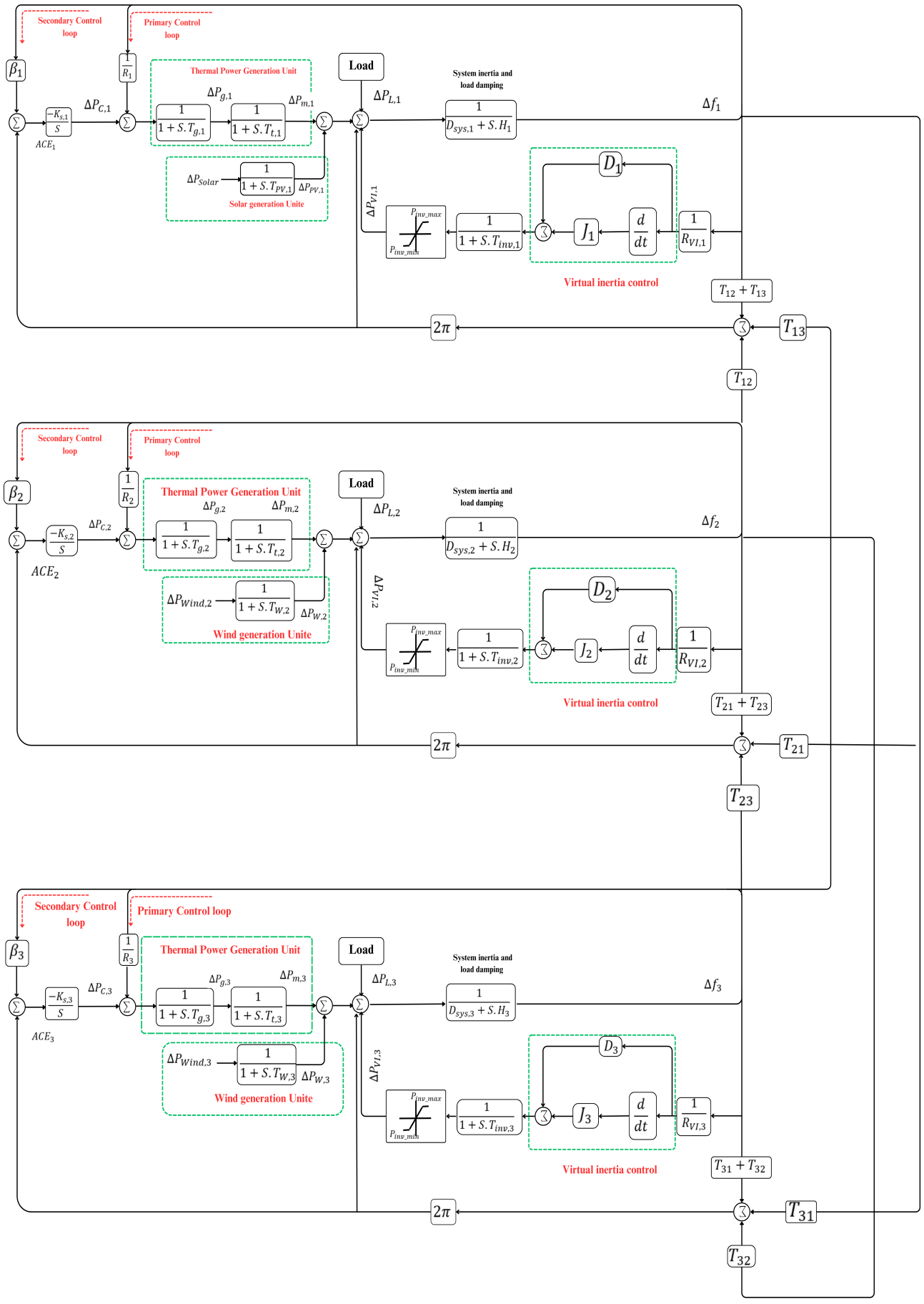

Figure III.17: Simulink model of interconnected MG system .

Table III.3: Simulation parameters of interconnected MGs.

Parameters	Area 1	Area 2	Area 3
Active power of ESS (MW)	4	4	4
The active power of RESs (MW)	6	8	6
Generation active power (MW)	12	15	10
Active power of load (MW)	15	20	13
Integral controller gain (s) K_s	0.3	0.2	0.4
Governor time constant T_g (s)	0.08	0.07	0.06
Turbine time constant T_t (s)	0.39	0.46	0.35
Governor droop constant R (Hz/p.u.)	3.05	2.74	2.81
Bias factor β (p.u./Hz)	0.34	0.37	0.36
Virtual inertia constant J(p.u.s)	1.25	1.5	1.07
Virtual damping constant D(p.u./Hz)	0.5	0.5	0.5
Virtual inertia control droop R_{vi} (Hz/p.u.)	2.5	2.7	2.3
Inverter-based ESS time constant T_{inv} (s)	1	1.2	0.9
Wind turbine time constant $T_{wt}(s)$	-	1.5	1.2
Solar system time constant $T_{pv}(s)$	1.3	-	-
System inertia H (p.u. s)	0.083	0.1010	0.0623
System load damping D_{sys} (p.u/Hz)	0.015	0.016	0.014
Synchronizing coefficient (p.u.MW/Hz)	$T_{12} = 0.2$ $T_{13} = 0.25$	$T_{21} = 0.2$ $T_{23} = 0.12$	$T_{31} = 0.25$ $T_{32} = 0.25$

III.4.2.1 Efficacy of multiple-virtual inertia control under disturbances

- **Load disturbances**

To evaluate the efficiency of multiple virtual inertia controls under disturbances, the power system is subjected to load disturbances, as shown in Figure III.18. Each load experiences a step change in power at different times during the simulation.

Figure III.19a shows the frequency deviation of the power system in all areas without virtual inertia control; it is obvious that the system could not achieve its stability and presents significant deviations in areas 1, 2, and 3 (between -0.18 Hz and +0.05 Hz) with pronounced oscillations and slow recovery to steady-state values where the disturbances in one area affect the frequency stability in all areas of the

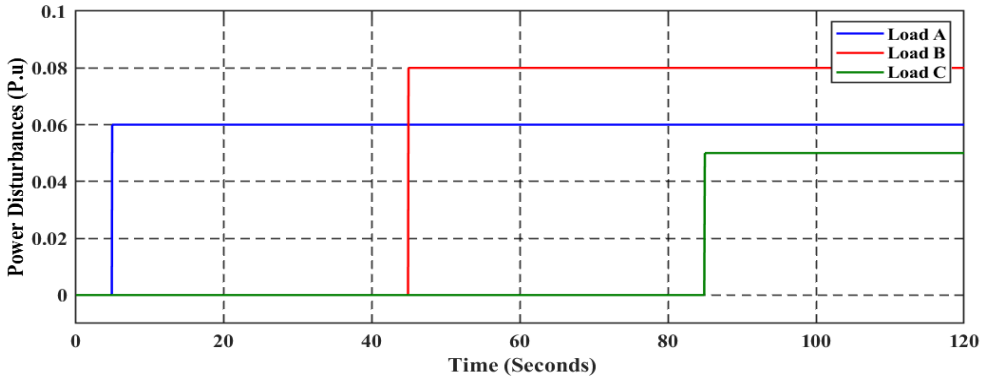

Figure III.18: Load disturbances.

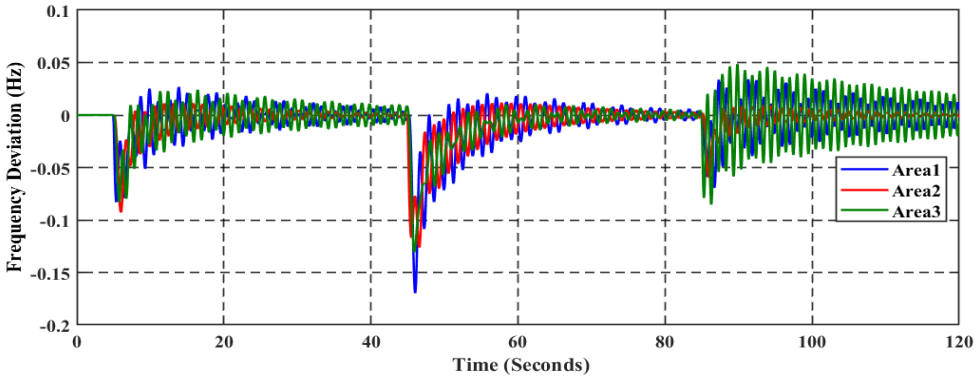

(a)

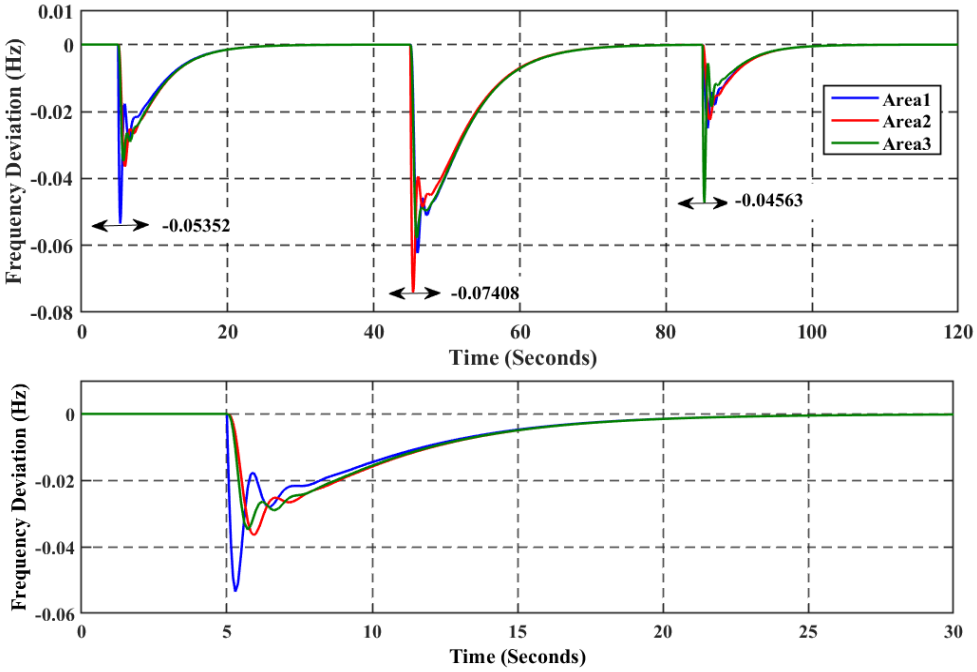

(b)

Figure III.19: Frequency response (a) without virtual inertia. (b) with virtual inertia.

power system. However, Figure III.19b demonstrates that with virtual inertia, the frequency deviations are much smaller (between -0.07 Hz and -0.04 Hz), and the system recovers quickly with reduced oscillations and improved stability (It is important to emphasise that the negative sign reflects the negative feedback mechanism

between the virtual inertia power and the frequency deviation).

In Figure III.20a, without virtual inertia, the thermal power shows significant oscillations and deviations among Areas 1, 2, and 3 following load changes, indicating poor stability and system response. In contrast, Figure III.20b shows that incorporating virtual inertia effectively reduces oscillations, stabilises thermal power transitions, and ensures a smoother response across all areas.

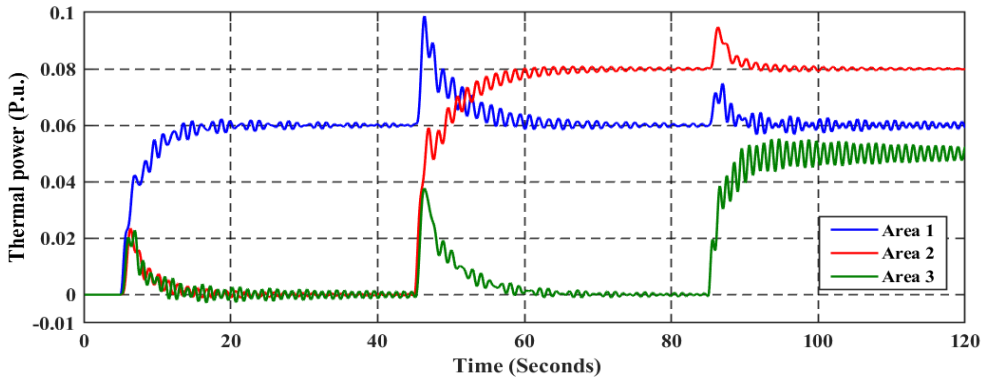

(a)

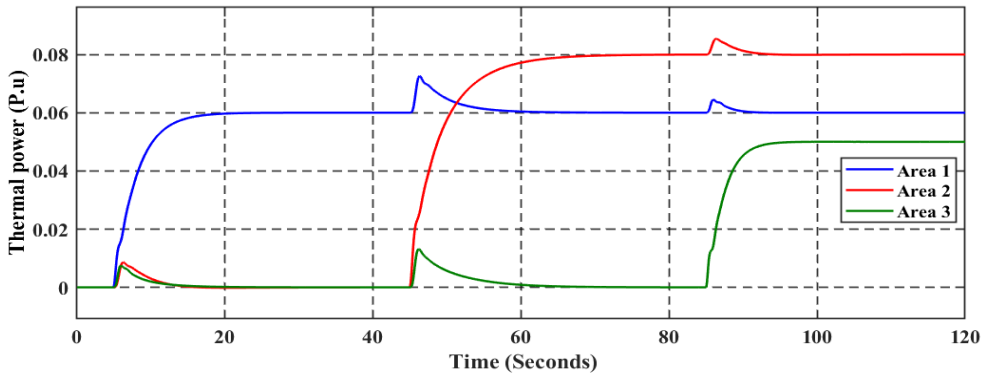

(b)

Figure III.20: Thermal power (a) without virtual inertia. (b) with virtual inertia.

The tie-line power response under load disturbances in an interconnected power system is illustrated in Figures III.21. Where the system response without virtual inertia exhibits large oscillations and instability in the tie-line power, particularly after disturbances, indicating a slower response and poor damping (see Figure III.21a). These oscillations persist for a longer duration before settling down. In contrast, Figure III.21b shows the system's behaviour with virtual inertia enabled. The tie-line power stabilises much faster, with significantly reduced oscillations after disturbances.

The virtual inertia power in all areas (Area 1, Area 2, and Area 3) quickly reacts to the disturbances, as illustrated in Figure III.22. This swift response helps absorb the sudden load changes and stabilizes the system. The power provided by the virtual inertia rapidly decreases right after each disturbance and then returns to near zero as the system stabilises, indicating that the virtual inertia helps smooth the frequency deviations and improve the overall system stability after disturbances.

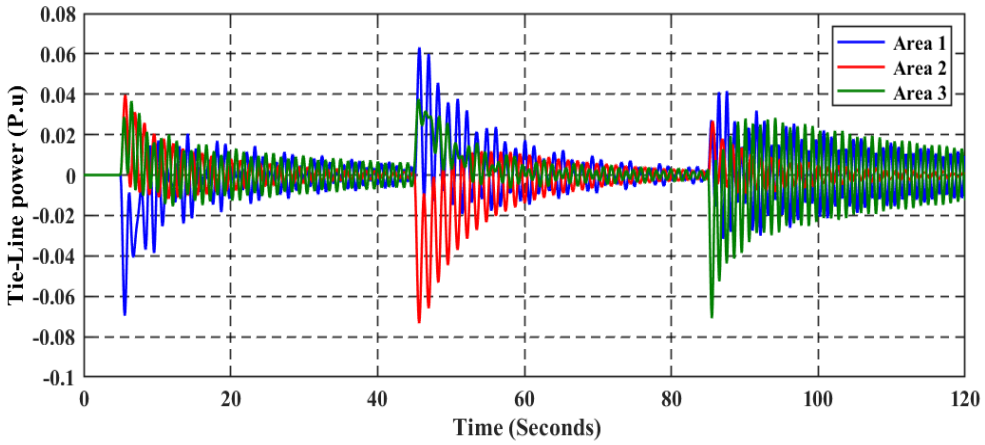

(a)

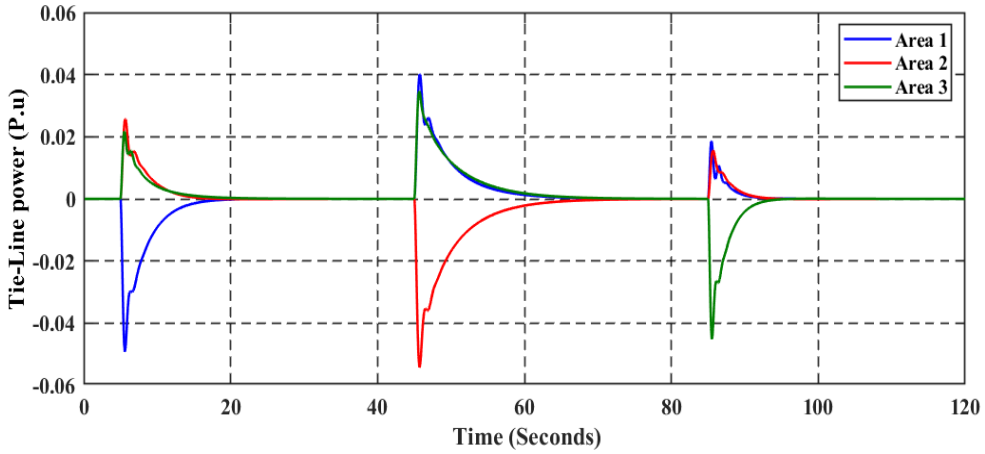

(b)

Figure III.21: Tie-line power (a) without virtual inertia. (b) with virtual inertia.

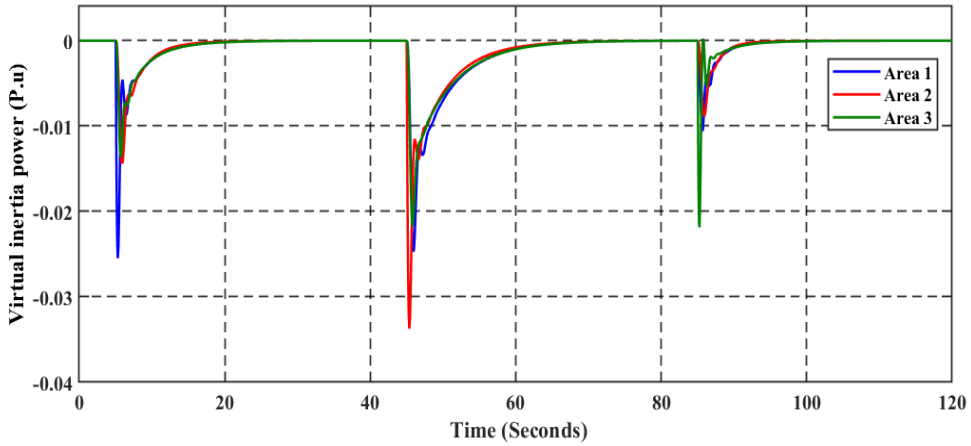

Figure III.22: Virtual inertia power of the interconnected system.

- **Load and generator disturbances**

To test the robustness of the multiple-virtual inertia control strategy, the power system is subjected to load and generator disturbances as illustrated in Figures III.23a and III.23b. In the case of the system without virtual inertia control, the frequency deviations are significantly larger, and oscillations persist over an extended period

for each area, as shown in Figure III.24. The system exhibits slower stabilisation due to the absence of sufficient inertia and damping mechanisms where excessive deviations in frequency can result in equipment damage, triggering protective mechanisms and leading to cascading failures or blackouts.

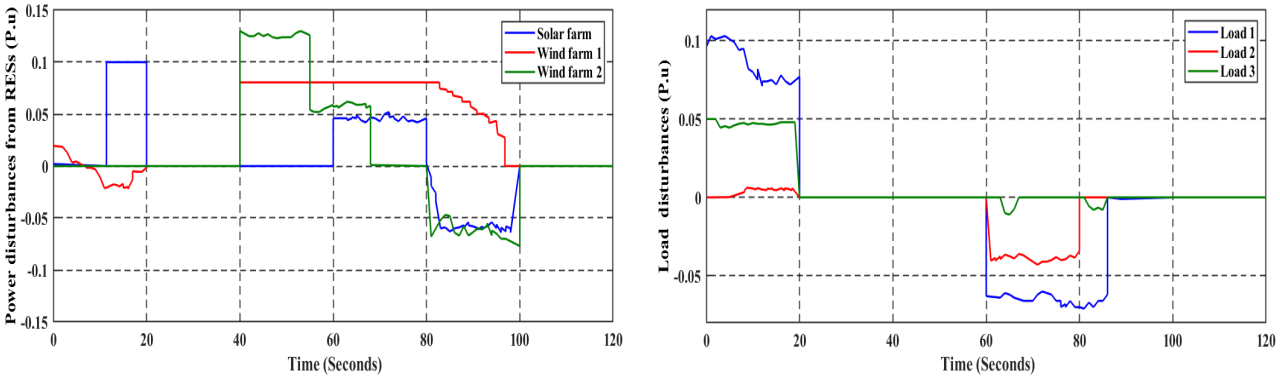

(a) (b)

Figure III.23: Power disturbance from (a) RES. (b) Load.

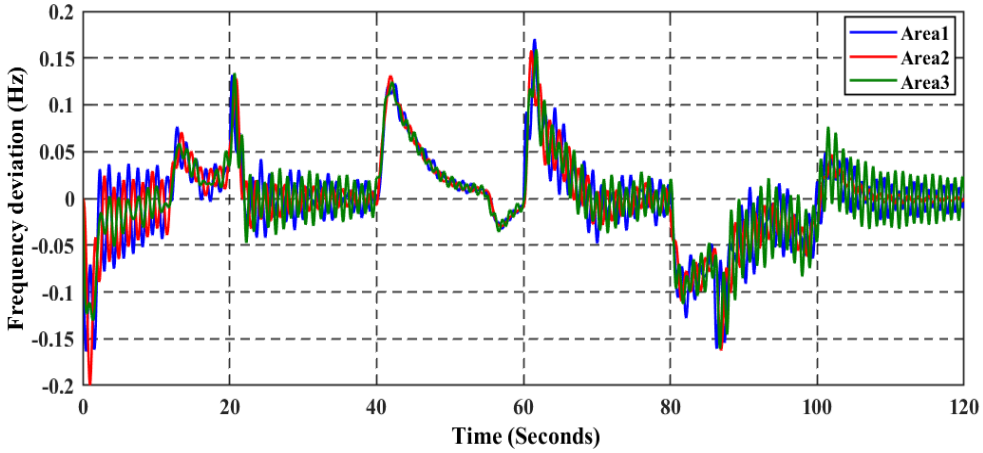

Figure III.24: Frequency response without virtual inertia.

By replicating the functionality of physical inertia, virtual inertia stabilises frequency dynamics, deviations are substantially reduced, and oscillations decay more rapidly (see Figure III.25). Virtual inertia control responds instantaneously to disturbances and supplies or absorbs power in real time to counteract frequency variations, enabling faster and smoother system recovery.

According to Figure III.26a, the tie line power is affected by insufficient inertia and damping proprieties where oscillations are pronounced, and exhibit prolonged undamped behaviour, indicating poor synchronisation between interconnected areas and a higher risk of inter-area oscillations. In the case of virtual inertia control (see Figure III.26b), the tie line power of each area is improved, and the oscillations are significantly damped and subside more quickly, reflecting enhanced coordination and stability across interconnected regions, indicating that the virtual inertia control improves synchronisation, providing enhanced damping to mitigate oscillations

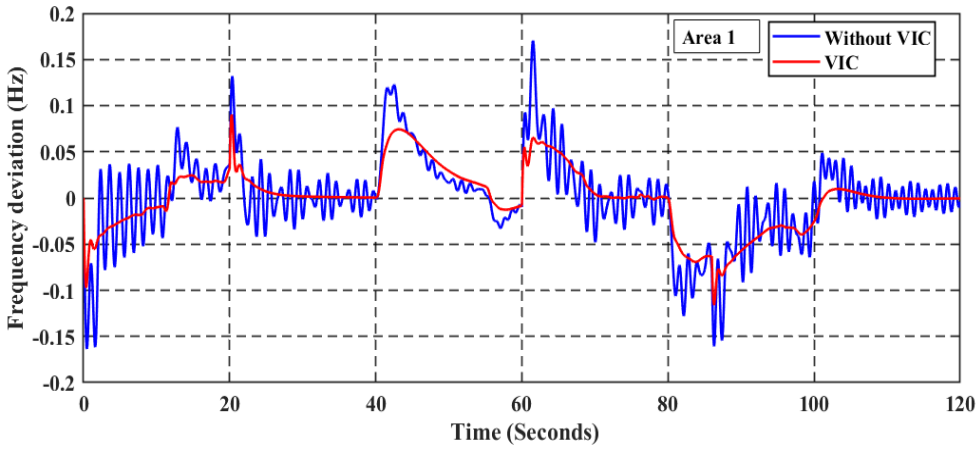

(a)

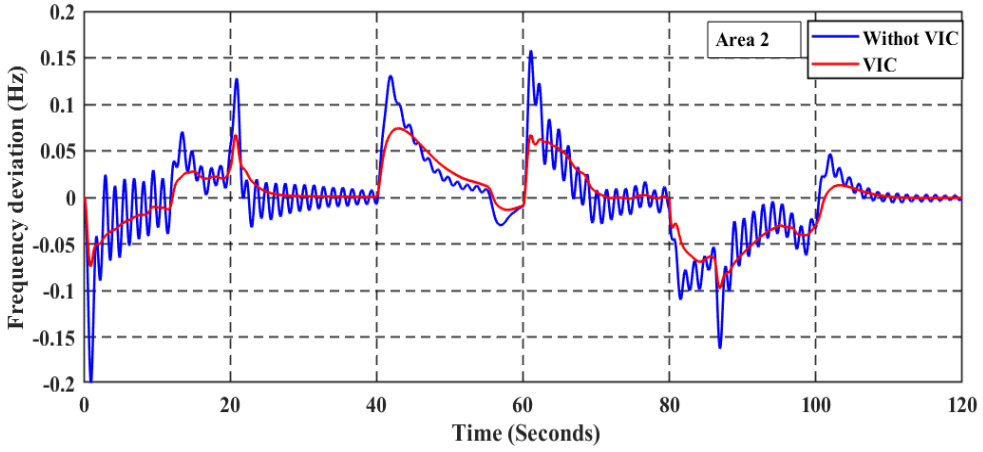

(b)

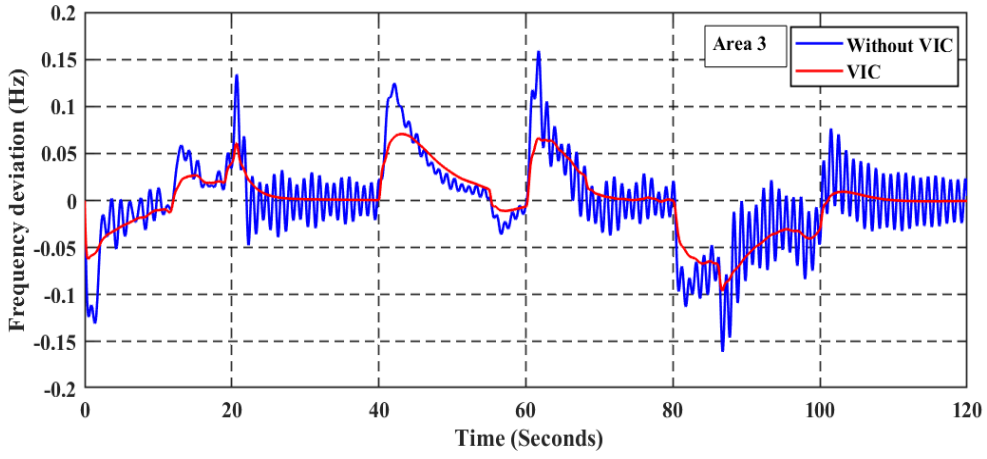

(c)

Figure III.25: Frequency response in (a) area 1. (b) area 3. (c)area 3.

effectively. Additionally, the contribution of virtual inertia power is illustrated in Figure III.27, which highlights the dynamic role of virtual inertia in stabilising the system under disturbances. Where the peaks represent the injection or absorption of power by virtual inertia in response to frequency fluctuations caused by transient events.

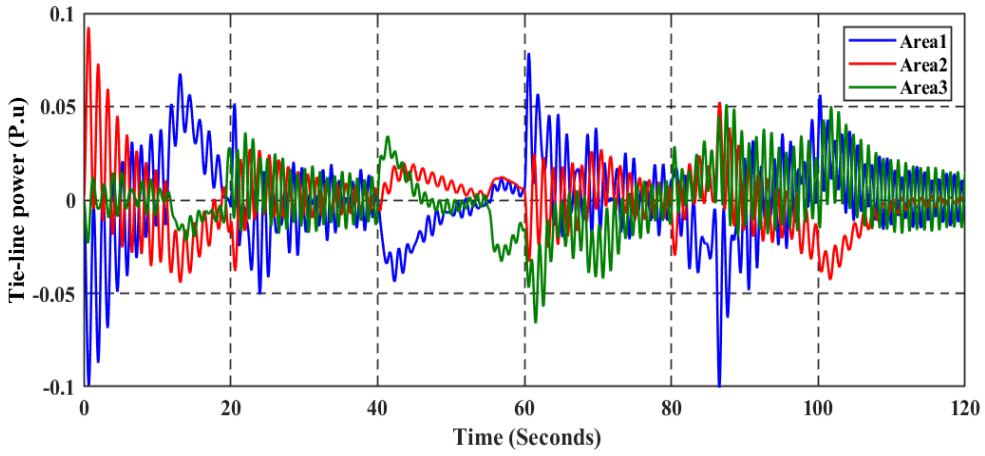

(a)

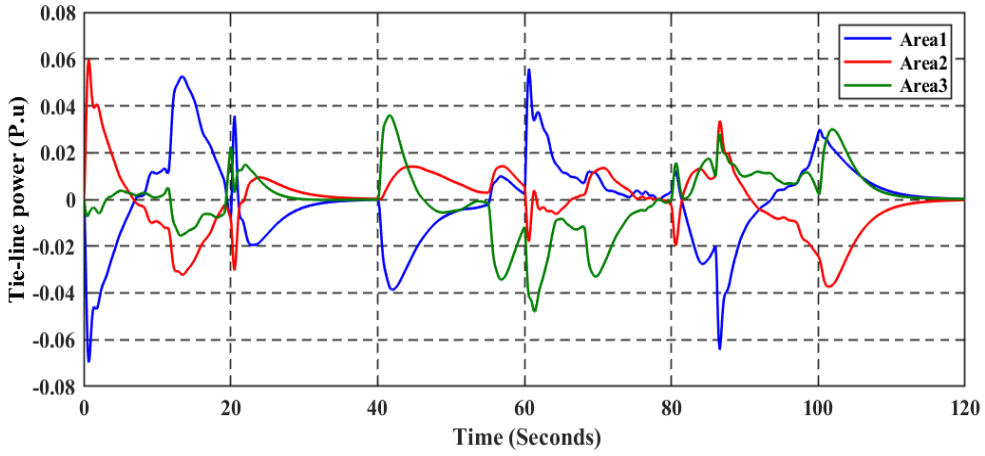

(b)

Figure III.26: Tie-line power (a) without virtual inertia. (b) with virtual inertia.

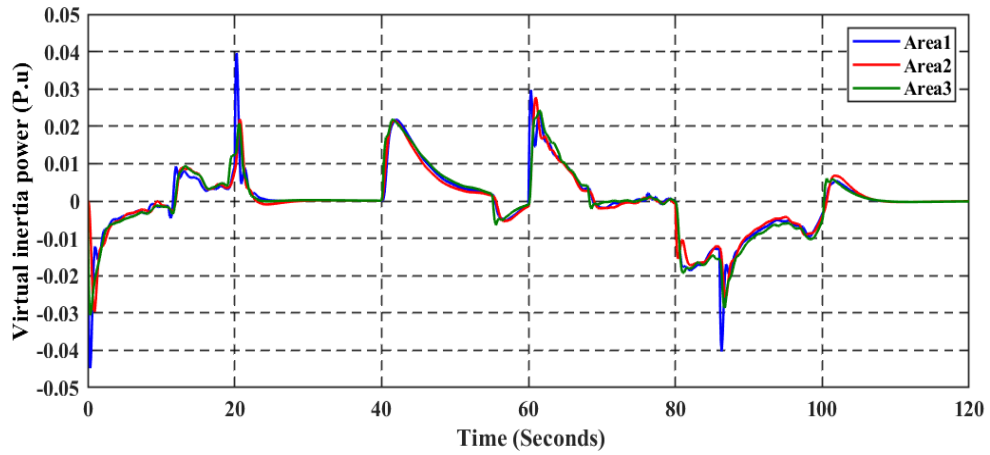

Figure III.27: Virtual inertia power under load and generator disturbances.

III.5 Conclusion

This chapter thoroughly analyses the modelling and design of interconnected *MGs* incorporating virtual inertia control. It begins with an introduction to frequency response modelling, detailing the primary and secondary frequency control loops and

their roles in maintaining system stability. The structure of frequency response, including physical constraints and the impact of renewable energy sources (RESs), is also examined, highlighting the challenges posed by modern low-inertia power systems.

The concept of virtual inertia control using *ESSs* was then introduced, along with its state-space modelling and practical design considerations. Both isolated and interconnected MGs were investigated to evaluate the performance of virtual inertia under different operational scenarios. For isolated systems, the effects of reduced inertia and varying virtual inertia control parameters were analysed, demonstrating their critical influence on system stability. In interconnected MGs, the efficacy of multiple virtual inertia controls was tested under disturbances, showcasing their ability to enhance the robustness and flexibility of modern power systems.

Overall, the chapter established the significance of virtual inertia control in addressing the challenges of frequency stability in low-inertia systems. By integrating advanced control strategies into both isolated and interconnected MGs, the chapter provides a foundation for the development of resilient and reliable power systems in the era of high renewable energy penetration.

Chapter IV

Fuzzy-virtual inertia control for multi-area power systems

IV.1 Introduction

Conventional systems are based mainly on rotating machines, where the frequency regulation is divided into four phases (inertia compensation, primary frequency control, secondary frequency control, and emergency control) based on the size of the frequency deviation and contingency. At the first milliseconds of disturbances, the inertia provided by *SGs* helps dampen the frequency deviations; this reaction is based mainly on the release or absorb the kinetic energy stored in rotating mass to reduce the frequency fluctuations and *RoCoF* [107, 108]. However, according to the studies focused on the assessment of the impact of RESs on the stability of power systems [109, 110], increasing the scale of penetration of PV units, wind turbines, and other RESs interfaced with systems by means of power electronic devices reduces the total MG-inertia and lack of dynamic grid support, resulting in a negative impact on the transient response of the system which makes it more susceptible to frequency instability leading to high overshoots and undershoots under normal and abnormal operations, especially with fast variability of RESs [51, 52, 107, 109, 111, 112]. Therefore, the absence of inertia compensation in modern power systems imposes challenges in frequency control in terms of *RoCoF*, recovery time, adaptability with variability of RESs and risk of load shedding. Without adequate frequency control, these challenges can impair system reliability, potentially leading to outages or damaged equipment, especially in the case of interconnected MGs, where the complexity of the system is increased, and the control is delicate. Therefore, there is a critical need for advanced frequency regulation techniques that can effectively emulate inertia in MGs and restore system stability.

Researchers have explored various virtual inertia controls (VIC) to overcome low-inertia issues in MGs. VIC techniques consist of releasing or absorbing virtual inertia power to compensate for the inertia of an SG to enhance the frequency stability [52, 54, 64, 106, 107, 113]. These VIC methods are implemented for inverter control via different modelling approaches, such as swing equations, ideal linear models, and phasor diagram-based impedance models of *SGs* [51, 111] [68, 82, 114]. All *VICs* aim to control the inverter's output to provide additional inertia to ensure power exchange similar to the mechanical behaviour of an SG [51, 111, 112].

The system's development via high integration and smart application of *RESs* made the basic model of VIC with constant virtual inertia and damping insufficient to deal with system changes [51], due to their inability to respond dynamically to load, generation, and system changes which lead to frequency instability, slower response times, oscillatory behaviour, and reduced effectiveness in interconnected MGs. To address these issues, researchers combined the VIC with classical and advanced approaches [99, 115, 116, 117, 118, 119, 120, 121]. The $PI-VIC$ developed in[115], for an MG under different rates of RES integration. In [116], a $GAPI-VIC$ (i.e., genetic algorithm) was proposed to achieve frequency stability. In [117], a

$PSO-PI-VIC$ was designed for an MG. However, these methods[115, 116, 117] still face limitations, such as a lack of flexibility in adapting to real-time conditions and potential instability under high RES variability in robustness and flexibility, especially when applied to interconnected MGs where the complexity of control is increased. In addition, the combination of a VIC with a PI controller needs to define the power system dynamics perfectly. [118] proposed an extended H_∞-VIC, where the uncertainties and disturbances of the system are considered, but voltage regulation suffers, with significant peaks. In [122], Model predictive control for VIC ($MPC-VIC$) is developed based on the first-order derivative transfer function with the virtual inertia gain with consideration of high penetration of RESs for MG. However, the proposed technique neglects the effect of the damping factor, which weakens the performance in case of high disturbances and interconnected MGs. Furthermore, $MPC-VIC$ and robust $MPC-VIC$-based $ESSs$ were proposed in [119] and [120], respectively, to provide predictive capabilities to anticipate instabilities in DGs. In [120], the time delay between DGs was also addressed, and both techniques [119] and [120] enhanced system performance but were difficult to implement due to the computational complexity, sensitivity to data quality, and need for real-time data acquisition, which may not always be feasible in practical MG systems.

Furthermore, [99] proposed a $FVIC$ for an MG based on frequency variation and the power change of RESs to adjust the virtual inertia and ignore the damping effect. Additionally, [121] proposed a $FVIC$ based on an ESS considering the state of charge of the battery (SOC), and both methods improved the system's stability compared to classical approaches. However, the $FVIC$ mentioned previously has numerous weaknesses, such as poor or missing data, implementation complexity, overshoots and nadirs, slow dynamic response, and study state errors in the context of high integration of RESs. Additionally, most methods optimise virtual inertia without considering damping factors, which have several negative effects on the power system with high penetration of $RESs$, such as greater frequency deviations and overshoots, increasing oscillations, prolonged recovery time after disturbances, in the case of interconnected MGs ignoring damping factor can cause oscillations to propagate or even amplify across regions [123, 124].

In previous studies, most research has focused on frequency regulation within islanded MG, often overlooking the complexities of interconnected or multi-area systems. However, as MGs become increasingly interlinked and reliant on $RESs$, disturbances in one area can affect others, making effective area coordination essential to prevent system instability. This chapter addresses this challenge by proposing a novel virtual inertia and damping control ($VIDC$) method based on fuzzy logic, tailored specifically for a connected system with three MG areas integrated with RESs. The fuzzy logic approach is chosen to deal with the complexity of control of interconnected MG due to its ability to handle non-linearity effectively and overcome

the problem of uncertainty of system parameters. It adapts to system changes and enhances dynamic performance under normal and abnormal conditions; it is well-suited for controlling non-linear systems. It can evaluate a wider range of conditions and make more nuanced decisions, so it is used in the optimisation tasks within the virtual inertia control to enhance their performances. Unlike the PID or $PSO-PID$, where control parameters are adjusted offline, the proposed $FVIDC$ is designed and tuned offline; however, it adaptively adjusts the inertia and damping factor to respond to system changes. The proposed tool is intended for offline study to evaluate the performances of $FVIDC$ under diverse conditions rigorously. This process ensures the robustness of control before real-time deployment in a practical system.

It compensates for low system inertia and enhances frequency regulation across interconnected MGs. By using fuzzy logic, the method adaptively manages power fluctuations and frequency changes, leading to robust, quick responses to disturbances. Unlike traditional VIC approaches, the proposed $FVIDC$ is designed to handle dynamic multi-area interactions, providing resilience even during area connection and disconnection events, as well as under varying load and generation conditions. The simulation results show a greater frequency regulation ability than that of the $PID-VIC$, $FVIC$, and $PID-VIDC$. The key contributions of this chapter are:

- This study specifically addresses the frequency problems in a connected system with three areas of integrated RESs rather than focusing on the frequency issues of multi-source MGs based on RESs.
- Enhance the adaptability of virtual inertia control with the variability of RESs.
- Unlike the existing method that fixed or neglected the damping factor in VIC, the proposed method optimises both the virtual inertia and the damping factor to minimise the effects of delayed time impact, reduce the frequency fluctuation and improve the system stability.
- The $FVIDC$ incorporates considerations for frequency deviation, $RoCoF$, and the power fluctuations from RESs into the control design to achieve precise control and better handling of the complexity and uncertainty of the system.
- Enhance the system performances where the simulation result demonstrates that the $FVIDC$ reduces the frequency deviation by approximately 50% and shortens the settling time under load and generator disturbances, outperforming the $FVIC$, $PID-VIC$, and $PID-VIDC$ methods.

IV.2 Principle of the PID-VIDC

For the control system, the PID controller has a crucial role in improving control performances due to its adaptability to system changes. It helps in minimising overshoots, undershoots, and settling time more effectively than classical approaches[125]. It is commonly used in control systems due to its simplicity. Their dynamic model-based proportional, integral, and derivative gains decrease the rise time, eliminate steady-state error (SSE) and improve system performance [126].

Researches have focused on the impact of VIC parameters on regulation [52, 69, 127, 128]. The VIC behaviour with fixed parameters affects the stability of the power system. The most common approach used to improve the VIC algorithm is the PI or PID controller. This approach is practicable and can be regulated when the dynamic performance is perfectly defined, as shown in Figure IV.1. The PID-VIDC obtains suitable amounts of virtual inertia and damping (constant coefficients in equation (III.20)) according to the system variation. Consequently, the PID-VIDC reaction given by:

$$\Delta P_{VI} = \left(\frac{1}{R_{VI}\left(1+s.T_{INV}\right)}\right)\left[\left(K_{Jp}+\frac{K_{Ji}}{s}+K_{Jd}s\right)\frac{d\Delta f}{dt}+\left(K_{Dp}+\frac{K_{Di}}{s}+K_{Dd}s\right)\Delta f\right] \tag{IV.1}$$

The proportional, integral and derivative gains are K_{Jp}, K_{Ji}, K_{Jd} respectively, for the virtual inertia parameter. The proportional, integral and derivative gains are K_{Dp}, K_{Di}, K_{Dd} respectively, for the virtual damping factor.

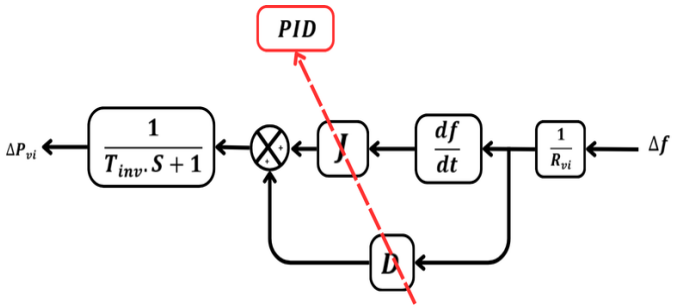

Figure IV.1: Schematic of the PID-VIDC.

The procedure for calculating the PID parameters is a very important and sensitive step. In [51],a PID- VIC is used for one-area systems where the PID parameters are calculated using the MATLAB PID tuning toolbox. The system response proved the utility of the PID-VIC for frequency control of signal MGs. Another research paper [129] proposed the PID-VIC for interconnected power systems where the PID parameters are calculated based on a heuristic search. Regardless of the ability of the PID-VIC to enhance the control system performance, it has several drawbacks, such as low robustness and system instability in cases of high disturbances. Additionally, the calculation of PID parameters plays a significant role in system regulation and

must be chosen carefully, which means that the classical PI-VIC or PID-VIC can only sometimes converge to the optimal virtual inertia power, which may introduce system instability.

IV.3 Fuzzy-virtual inertia and damping control design

To enhance the performance of *VIC* in connected MG systems, we integrate fuzzy logic into *VIC* to provide suitable virtual inertia and damping. The fuzzy logic approach can be adapted to system changes to enhance the performance of the system under diverse conditions [130]; it is well suited for controlling non-linear systems and overcoming the problem of uncertainty of system parameters, and it can be used in the optimisation tasks within the control system to adapt to system changes as disturbances.

In our proposition, we explore hybrid approaches that combine fuzzy logic with traditional *VIC* to achieve optimal performance. The proposed fuzzy-virtual inertia and damping control (*FVIDC*) is developed for each MG of the connected system as a decentralised control framework, as presented in Figure.IV.2. Where each MG is equipped with *FVIDC* and operates independently based on the local measurement of three inputs of the controller, which are the frequency deviation, the *RoCoF*, and the active power changes of the RESs, they are selected based on the system's performance to help achieve precise control and better handling of the complexity and uncertainty of the system. They are used to adjust the outputs of *VIC*, which are for the virtual inertia and damping parameters with system changes. The proposed method aims to provide adaptive virtual inertia and damping factors based on ESS with consideration of renewable power change to ensure sufficient virtual inertia power during system disturbances to improve the frequency response of each area by reducing the recovery time, frequency overshoot and nadirs, as well as ensuring a flexible reaction and better coordination between MGs during connection and disconnection of areas [125].

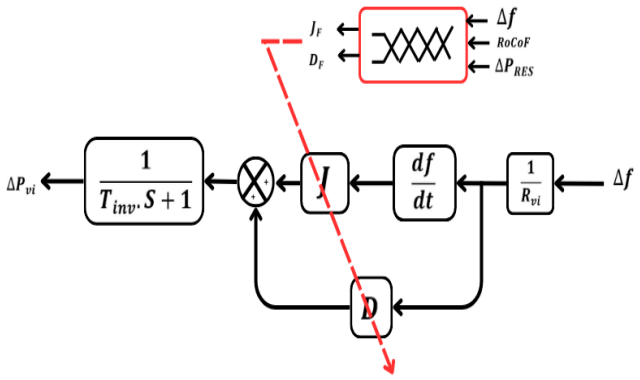

Figure IV.2: Structure of the proposed VIDC-based fuzzy logic approach.

The implementation of fuzzy logic can provide easy computing to control power systems [51]. The process of adding the fuzzy logic control to the VIC must be precise, where the inputs of the proposed $FVIDC$ are obtained from three actual inputs Δf, RoCoF, and $\triangle$PRES, then, the fuzzy outputs (i.e., virtual inertia and damping) are defined depending on the processing of fuzzy inputs according to established fuzzy rules. The real values of the outputs are determined through the defuzzification operation. Finally, the flow chart of the proposed $FVIDC$ is prepared in accordance with the above information as illustrated in Figure IV.3.

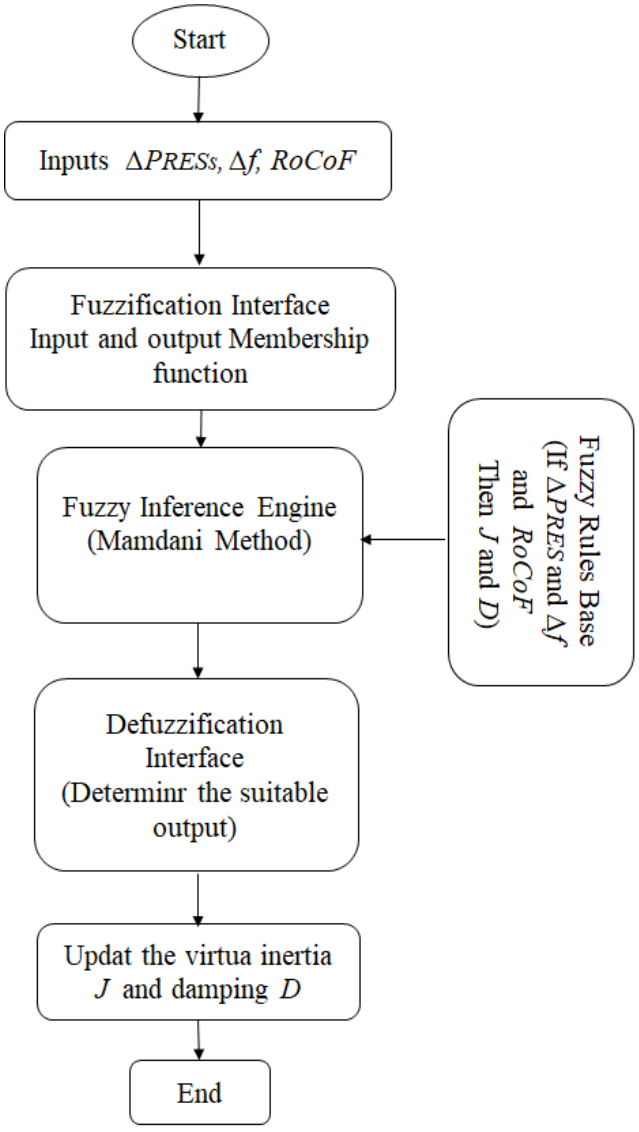

Figure IV.3: A flow chart of the proposed FVIDC.

After determining the inputs and outputs of fuzzy logic, it is necessary to define the range of each parameter to map them correctly and enable meaningful rule-based design.The ranges of the fuzzy inputs and outputs are : $\Delta f(Hz) = [-0.5\ 0.5]$; $\text{RoCoF}(\text{Hz/s}) = [-0.5\ 0.5]; \Delta \text{P}_{RES}\ (\text{P.u}) = [-1\ 1]; \quad J = [0\ 10]; D = [0\ 15]$. The next main step in the elaboration of fuzzy logic is the fuzzification phase, which is introduced to define the membership function of fuzzy variables based on the linguistic

variable where for $\Delta f, RoCoF, J$, and D are {Nl: Negatives Large, Ns: Negatives Small, ZO: Zero, Ps: Positives Small, Pl: Positives Large } and for ΔP_{RES} are $L: Low, M: Medium, H: High$. The defined membership functions of fuzzy variables are chosen to be triangular or trapezoidal as illustrated in Figures IV.4a and IV.4b; they represent the ability of fuzzy control to cope with knowledge.

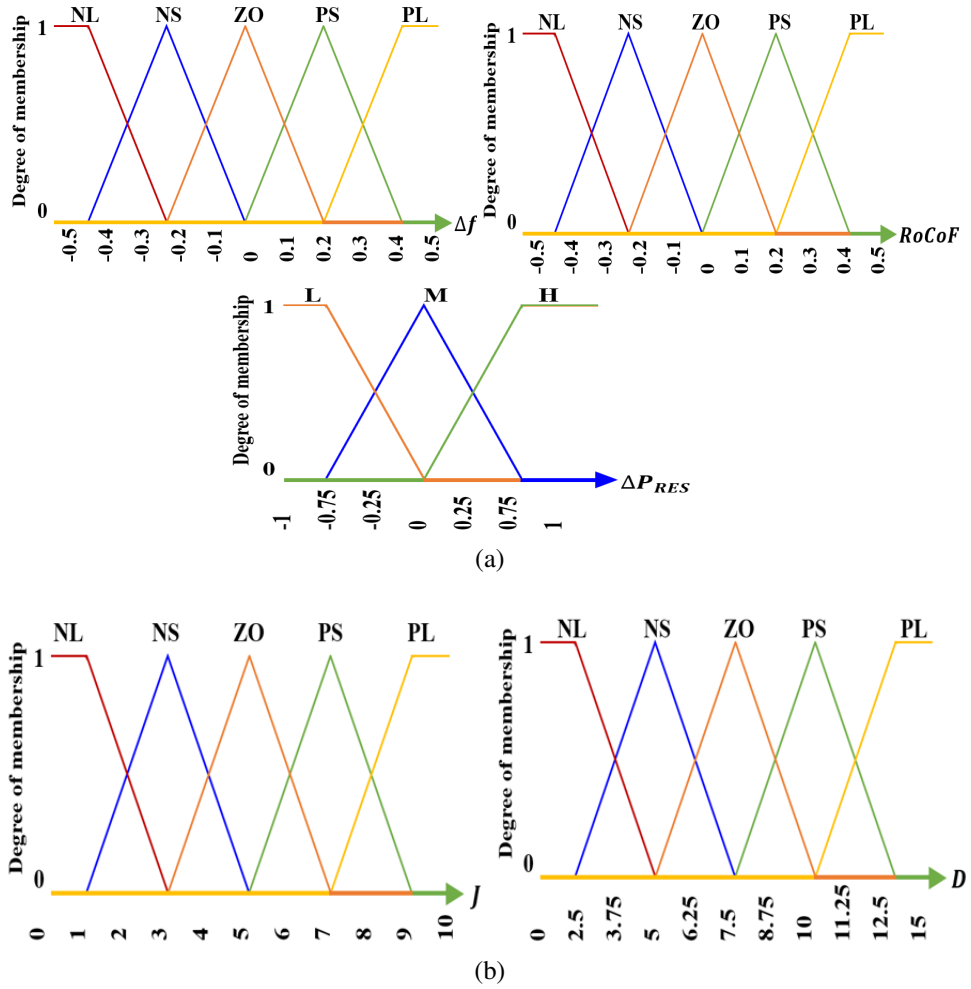

Figure IV.4: Membership functions for the proposed FVIDC. (a): input frequency deviations $\triangle f, RoCoF$ and renewable energy power changes ΔP_{RES}. (b): Outputs of virtual inertia J and virtual damping D.

The determination of fuzzy rules is based on understanding the system behaviour under different values of inertia and damping, defining the effects of inputs on frequency response and coordination of areas and understanding the relation between the inputs $(\Delta f, RoCoF, \Delta P_{RES})$, and the outputs (J, D) to ensure better performance of the fuzzy logic controller. The inertia power requirement of the system during frequency deviation sets the rules that govern the virtual inertia and damping values. Depending on the Δf, $RoCof$, and ΔP_{RES} signs, the response is divided into several

intervals as follows:

$$\Delta P_{RES} > 0 \text{ and } \begin{cases} \Delta f > 0 \text{ and } \frac{d\Delta f}{dt} < 0 \\ \Delta f > 0 \text{ and } \frac{d\Delta f}{dt} > 0 \\ \Delta f < 0 \text{ and } \frac{d\Delta f}{dt} < 0 \\ \Delta f < 0 \text{ and } \frac{d\Delta f}{dt} > 0 \end{cases}$$

$$\Delta P_{RES} < 0 \text{ and } \begin{cases} \Delta f > 0 \text{ and } \frac{d\Delta f}{dt} < 0 \\ \Delta f > 0 \text{ and } \frac{d\Delta f}{dt} > 0 \\ \Delta f < 0 \text{ and } \frac{d\Delta f}{dt} < 0 \\ \Delta f < 0 \text{ and } \frac{d\Delta f}{dt} > 0 \end{cases}$$

In the case of frequency deviation with a small *RoCoF* and low integration of RESs, the system needs a small amount of virtual inertia power. However, with high disturbances from RESs causing high-frequency deviation, the whole power system requires a large value of virtual inertia and a large damping factor. Consequently, depending on the Δf, $RoCof$, and ΔP_{RES} signs, 75 rules are defined for fuzzy control. The fuzzy rules for virtual inertia and damping of the proposed *FVIDC* are given in the tables IV.1,IV.2,andIV.3.

Table IV.1: Fuzzy rules for the proposed FVIDC in case of low ΔP_{RES} .

ΔP_{RES}	**Δf** / *RoCoF*	N L	N S	Z O	P S	P L
L	*NL*	N L	N S	N S	Z O	P L
	NS	N L	N L	N S	Z O	P L
	Z *O*	N L	N S	Z O	P S	P L
	PS	N L	N S	N S	Z O	P L
	PL	N L	Z O	N S	P S	P L

The inference mechanism used to process the inputs to adjust the output is the Mamdani method, where the activation strength α_i for each rule is determined as follows:

$$\alpha_i = min(\mu_{\Delta f}; \mu_{RoCoF}; \mu_{\Delta P_{RES}}) \tag{IV.2}$$

Where $\mu_{\Delta f}; \mu_{RoCoF}; \mu_{\Delta P_{RES}}$ are the membership degrees of inputs.

Table IV.2: Fuzzy rules for the proposed FVIDC in case of medium ΔP_{RES} .

ΔP_{RES}	**Δf** / *RoCoF*	N L	N S	Z O	P S	P L
M	*NL*	N S	Z O	Z O	P S	P L
	NS	N S	N S	Z O	P S	P L
	ZO	N L	N L	Z O	Z O	P L
	PS	N S	Z O	Z O	P S	P L
	PL	N L	P S	Z O	P L	P L

Table IV.3: Fuzzy rules for the proposed FVIDC in case of high ΔP_{RES} .

ΔP_{RES}	**Δf** / *RoCoF*	N L	N S	Z O	P S	P L
H	*NL*	Z O	P S	P S	P L	P L
	NS	N S	Z O	P S	P L	P L
	ZO	N L	N S	Z O	P S	P L
	PS	Z O	P S	P S	P L	P L
	PL	N S	Z O	P S	P L	P L

It represents the degree to which the antecedent of the rule is satisfied, and then the activated rules are combined to form the final fuzzy output for each output variable. The aggregation of this combination is formulated as follows:

$$\begin{cases} \mu'_J = max(\mu'_J; \alpha_i; \mu_J) \\ \mu'_D = max(\mu'_D; \alpha_i; \mu_D) \end{cases}$$

Where μ_J andμ_D are the membership degrees of outputs.

Finally, the defuzzification phase is introduced to convert the aggregated fuzzy output to crisp values of virtual inertia and damping factor. In this phase, the centroid of area method is used to transform the linguistic output to crisp values as follows:

$$\begin{cases} J_F = \frac{\sum_{j=1}^{n} y_j \cdot \mu(y_j)}{\sum_{j=1}^{n} \mu(y_j)} \\ D_F = \frac{\sum_{j=1}^{n} y_j \cdot \mu(y_j)}{\sum_{j=1}^{n} \mu(y_j)} \end{cases}$$

By applying the designed process of fuzzy logic for each area of the interconnected system, the virtual inertia and damping factor can adaptively adjust with the system changes and provide sufficient virtual inertia power with different levels of integration of RESs. In this case, the generated virtual inertia power can be written as follows:

$$\Delta P_{VI} = \frac{J_F.S + D_F}{1 + T_{inv}.S}\left(\frac{\Delta f(S)}{R_{VI}}\right) \tag{IV.3}$$

IV.4 Results and discussion

This chapter uses MATLAB-Simulink software to design the *FVIDC* and assess their performance for interconnected *MGs*. The simulation model of the studied system is created based on the state space model as developed in chapter 3, and it consists of three regions, each of which is powered by thermal generators, PV or wind power generation, and *ESSs*. Where renewable sources are considered disturbances due to their inherent variability and unpredictability, all regions are connected by tie-ling to facilitate the exchange of power between them, as illustrated in Figure IV.5.

The simulation parameters are outlined in Table IV.4 [131]. The proposed *FVIDC* is implemented in each region based on the ESS. The frequency regulation of the system utilising the proposed *FVIDC* is compared to $PID-VIC$ developed in [51], *FVIC* developed in [99] and $PID-VIDC$ presented in section 2 by incorporating the damping factor into *VIC* design, which aligns well with the objectives of the proposed *FVIDC*. Where the $PID-VIC$ is commonly used in MG control, it provides a standard point to show the effectiveness of the proposed *FVIDC*. On the other hand, the *FVIC* in [99] represents a more advanced approach to support frequency stability and handling of renewable power changes; it is introduced as a comprising benchmark to showcase the performance of the proposed *FVIDC*.

Additionally, comparing the proposed approach with the $PID-VIDC$ can emphasise the improvements in stability and frequency regulation of interconnected MGs achieved by optimizing the damping factor.

Four simulation cases are used to assess the effectiveness of the proposed control: first, load disturbances are accrued in all regions (scenario A), generation disturbances are introduced in each region through renewable power generation (scenario B), and simultaneous disturbances from loads and generations are introduced. Finally, the connection and disconnection of areas are introduced to analyse the behaviour of interconnected MG in coordination and regulation. The obtained results from each scenario are depicted and analysed in the following subsections.

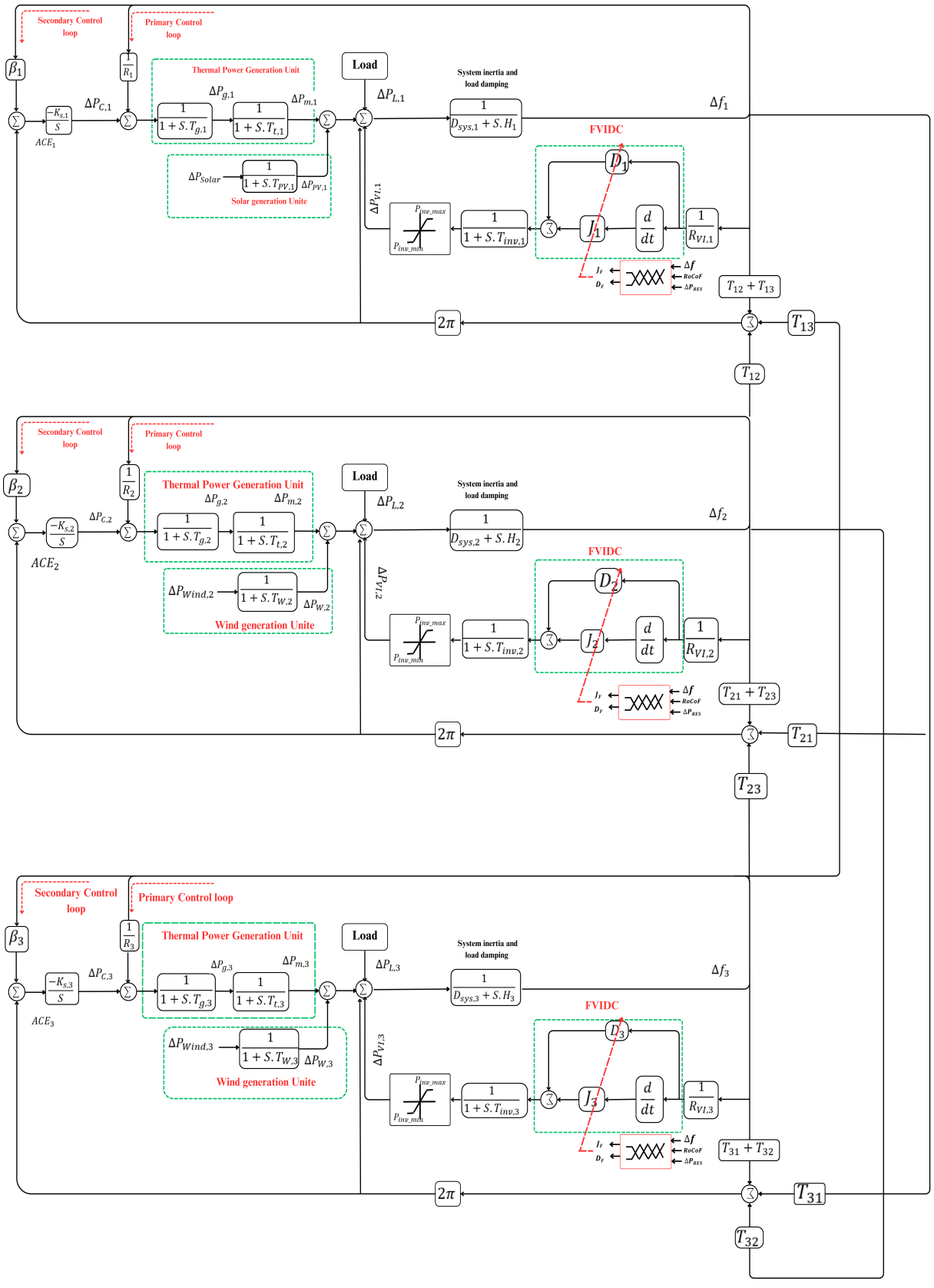

Figure IV.5: Simulation model of Interconnected MGs based FVIDC.

Table IV.4: Simulation parameters of interconnected MGs.

Parameters	Area 1	Area 2	Area 3
Active power of ESS (MW)	4	4	4
The active power of RESs (MW)	6	8	6
Generation active power (MW)	12	15	10
Active power of load (MW)	15	20	13
Integral controller gain K_s (s)	0.3	0.2	0.4
Governor time constant T_g(s)	0.08	0.07	0.06
Turbine time constant T_t (s)	0.39	0.46	0.35
Governor droop constant R (Hz/p.u.)	3.05	2.74	2.81
Bias factor β (p.u./Hz)	0.34	0.37	0.36
Virtual inertia constant J (p.u.s)	1.25	1.5	1.07
Virtual damping constant D (p.u./Hz)	0.5	0.5	0.5
Virtual inertia control droop R_{vi} (Hz/p.u.)	2.5	2.7	2.3
Inverter-based ESS time constant T_{inv} (s)	1	1.2	0.9
Wind turbine time constant T_{wt} (s)	-	1.5	1.2
Solar system time constant T_{pv} (s)	1.3	-	-
System inertia H (p.u. s)	0.083	0.1010	0.0623
System load damping (p.u./Hz)D_{sys}	0.015	0.016	0.014
Synchronizing coefficient (p.u.MW/Hz)	$T_{12} = 0.2$ $T_{13} = 0.25$	$T_{21} = 0.2$ $T_{23} = 0.12$	$T_{31} = 0.25$ $T_{32} = 0.25$

IV.4.1 Case A: load disturbances

To evaluate the effectiveness of the proposed *FVIDC*, load disturbances are introduced in each region during t = 300 s as illustrated in Figure.IV.6a. Firstly, in the region A at 5 s to 15 s with values around $0.18P.u$. Then, from t = 75 s to t = 95 s, the load changes are introduced in both regions A and B approximately equal to $0.3P.u$ and from $t = 160$ s to $t = 180$ s, the disturbances are introduced in all regions simultaneously, as shown in Figure.IV.6a.

Figures IV.6b,IV.6c,andIV.6d show the frequency deviation response of each region with different approaches. The resulting curves clearly show that disturbances in one region affect the frequency of all areas, demonstrating the complexity of the

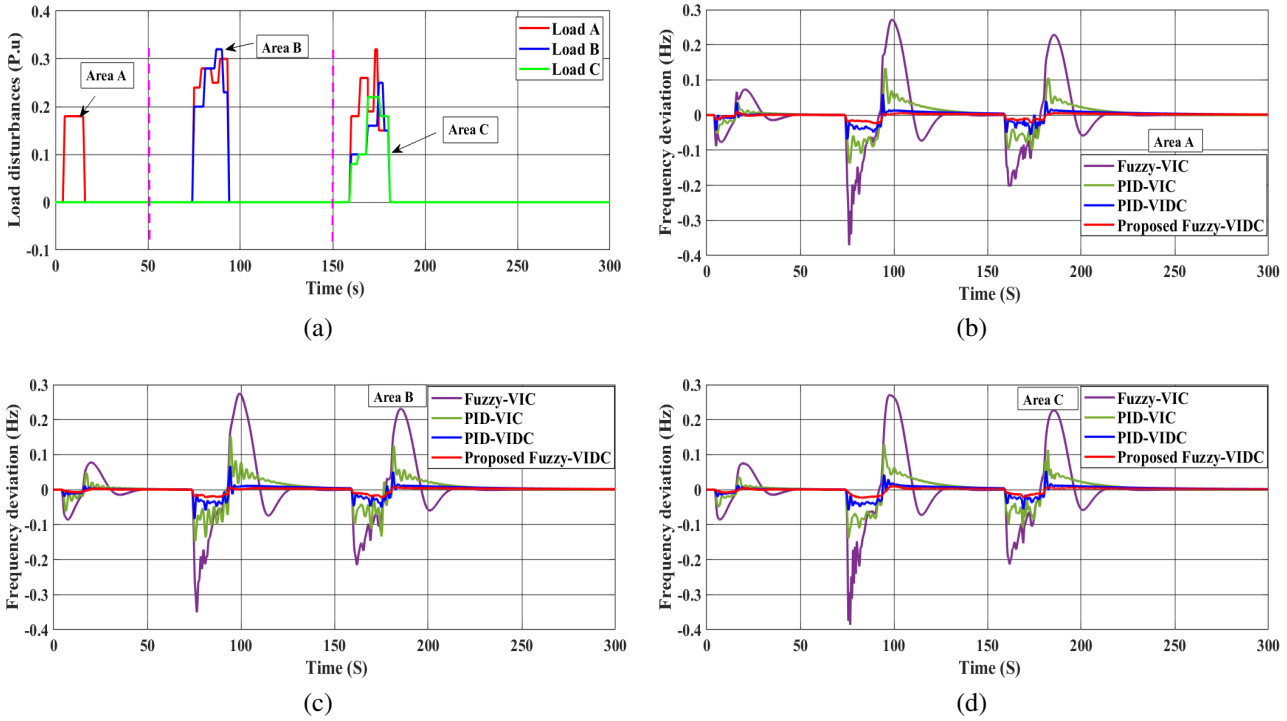

Figure IV.6: Frequency responses of the system under load disturbances. (a): Load disturbances. (b): Area A. (c): Area B. (d): Area C.

regulation processes in interconnected systems due to the coordination between areas. However, the frequency responses of the system controlled by the proposed $FVIDC$ exhibit better regulation with less fluctuation and excessively small overshoots and undershoots$\pm$0.015 Hz(with fast and smooth dynamic responses compared to $PID-VIC$, $FVIC$, and $PID-VIDC$, where the peaks are around $\pm$0.3 Hz ($FVIC$), $\pm$0.15 Hz ($PID-VIC$), $\pm$0.08 Hz ($PID-VIDC$).

IV.4.2 Case B: generation disturbances

In this case, the studied system is tested under renewable power generation changes as illustrated in Figure IV.7a to assess and analyse the behaviour of the proposed $FVIDC$ in the frequency regulation of interconnected systems. At $t = 5$ s until t = 15 s, the disturbance is introduced from the solar farm in region A, then at t = 75 s to t = 95 s the power changes are introduced in the solar farm and the wind farm in regions A and B, respectively, and from $t = 160$ s to t = 180 s, the disturbances are introduced in all regions from the RES frames.

As shown in Figures.IV.7b,IV.7c, and IV.7d, from the curves of each region, it notes that the fluctuations are increasingly increased with the disturbances and the frequency response presents high overshoes and nadirs, where the system under $FVIC$ without damping factor presents high overshoots and nadirs (+75 Hz and -0.5 Hz) which is unsuitable and over the limit. Furthermore, the frequency response of the system under $PID-VIC$ presents a long settling time with peaks

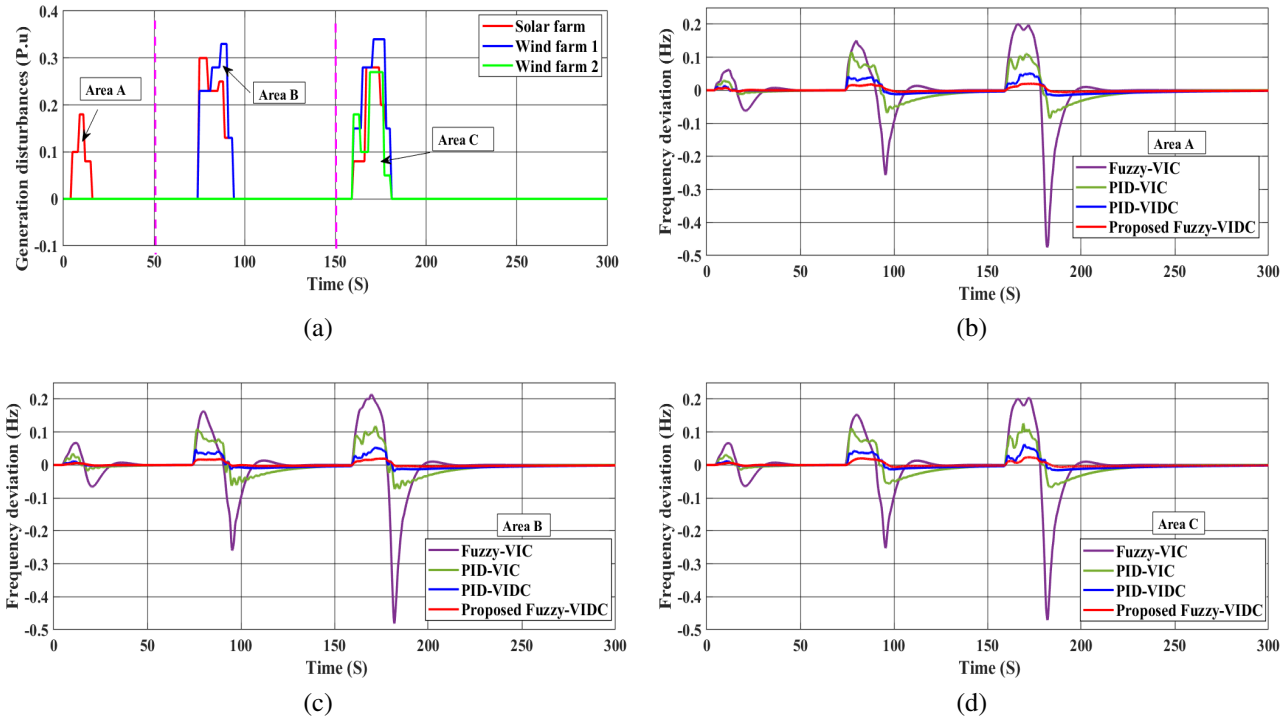

Figure IV.7: Frequency responses of the system under renewable power changes. (a): Generation disturbances. (b): Area A. (c): Area B. (d): Area C.

around ± 0.1 Hz and more fluctuations than the response of $PID-VIDC$ where peaks are around ± 0.05 Hz. However, the proposed technique overcomes these issues with better frequency dynamics than the other approaches; it presents good coordination between regions where the injected virtual inertia power is effectively faced with the system changes. The fluctuations are almost unremarkable in all areas, and the recovery time is shorter than other techniques, which proves the efficiency of the proposed $FVIDC$ under disturbances from RESs in the case of interconnected MGs

IV.4.3 Case C: load and generation disturbances

Both previous disturbances are considered and introduced in all regions for 120 s simultaneously, where renewable power changers around $\pm 0.25 P.u$ as illustrated in Figure IV.8a, and the load disturbances are introduced with values between $\pm 0.2 P.u$ as illustrated in Figures IV.8b. The frequency response of each region from the connected system is depicted in Figures IV.9a,IV.9b, and IV.9c, respectively.

The improvement of response based on the proposed $FVIDC$ is presented, where the overshoots and undershoots are reduced by approximately 50% with too few fluctuations and better settling time compared to $FVIC$ and other techniques where the frequency response is more stressed, which highlights the impact of virtual damping in the design and optimisation of VIC. Table IV.5 presents the evaluation of performances of proposed $FVIDC$ through a comparison of various time domain

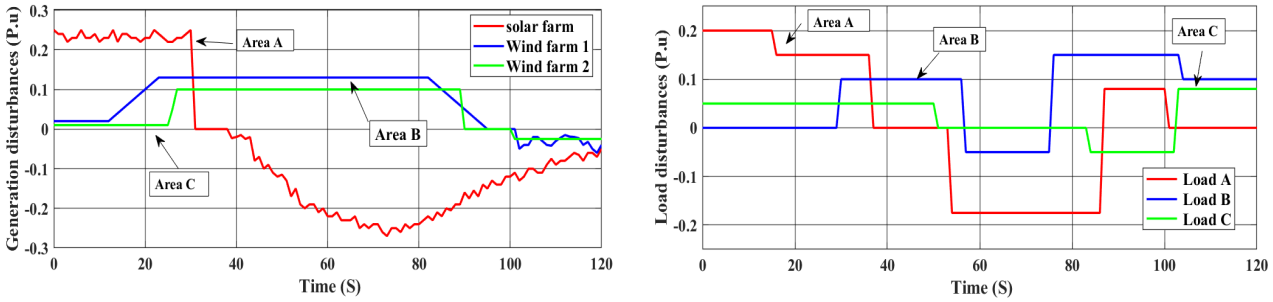

(a) (b)

Figure IV.8: Power disturbances from (a) RESs (b) load.

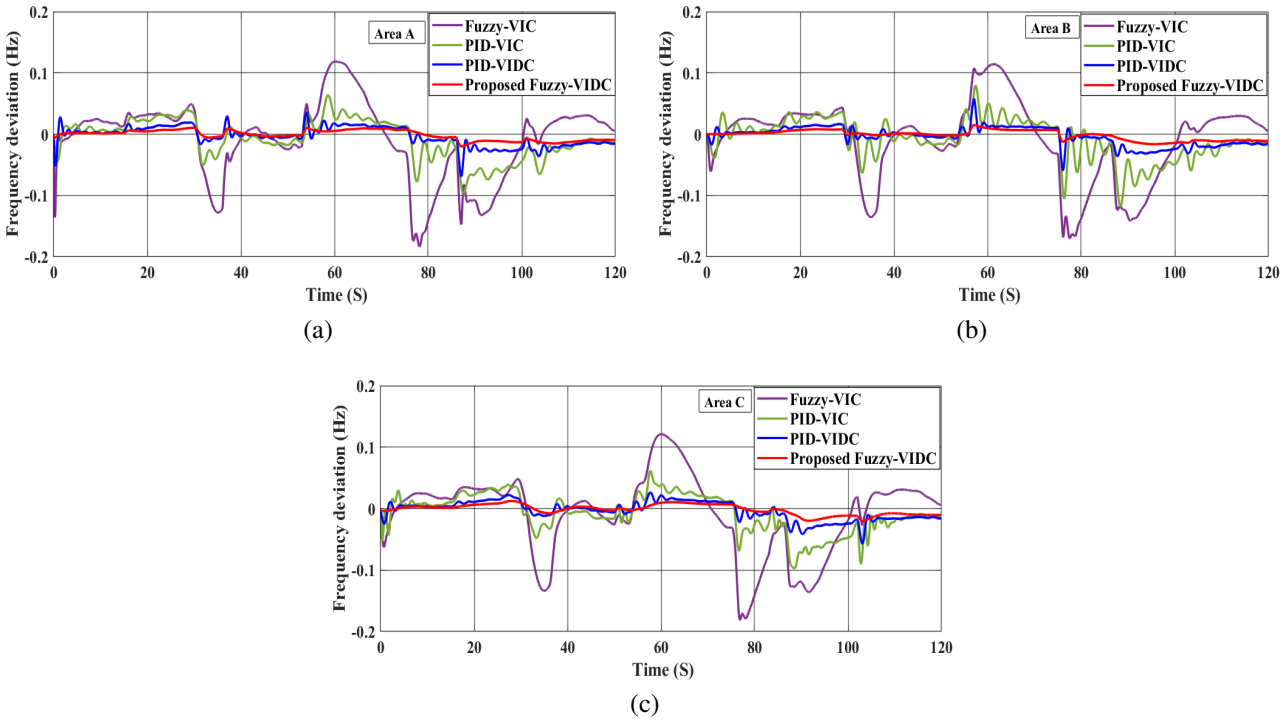

(a) (b)

(c)

Figure IV.9: Frequency responses of the system under load/generator disturbances. (a): Generation disturbances. (b): Load disturbances. (c): Area A. (d): Area B. (e): Area C.

specifications, where the overshoot of *RoCoF* is approximately 0.007 Hz/s, and the undershoot -0.009 Hz/s, which is aligned with standers and proved the efficiency and compatibility of the designed control with the interconnected power system.

IV.4.4 Case D: plug and play test

To evaluate the coordination between regions in the case of the connection and disconnection of areas. First, area C is connected to the system from 0 s to 40 s under load/generation disturbances, as shown in the figures. IV.8a,IV.8b. At $t = 40s$, the third area is disconnected until $t = 80s$, then, at 80 s to 120 s, area C is reconnected to the system. According to Figures IV.10a,IV.10b, and IV.10c, in the case of the proposed *FVIDC*, the frequency response of each area quickly compensates for the

deviations with a better dynamic response compared with the other methods.

Additionally, in the case of disconnecting area C from the system, it is still under load and generation disturbances. Remarkably, compared with the $FVIC$,$PID-VIC$ and $PID-VIDC$, the frequency response from the proposed $FVIDC$ presents a smooth curve that exhibits a fast dynamic response without overshoots or undershoots. Therefore, the $FVIDC$ is based on the optimisation of virtual inertia and damping factors through frequency deviation,$RoCoF$, and proved its ability in frequency regulation through inertia compensation for connected or islanded power systems.

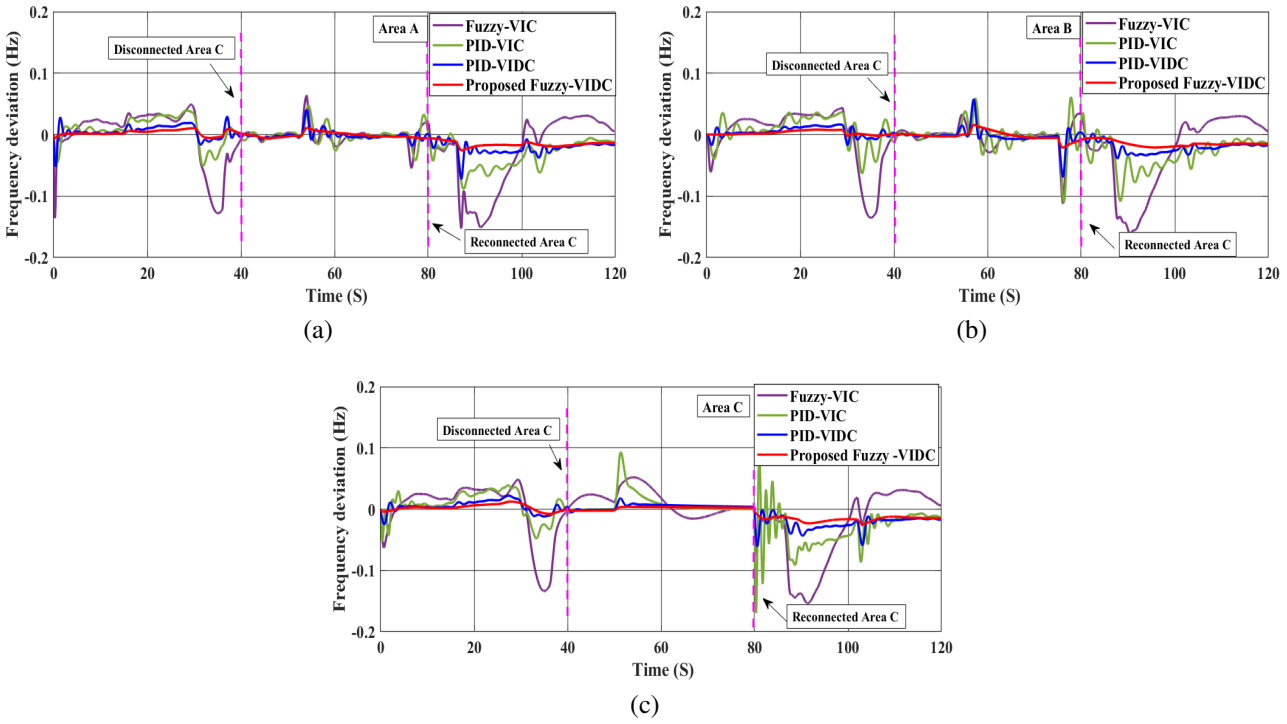

Figure IV.10: Frequency responses of the connected - system for the plug-and-play test. (a): Area A. (b): Area B. (c): Area C.

The scenarios applied to the system present the main characteristics of the enhanced $VIDC$ represented in the frequency responses in terms of deviation, and $RoCoF$ with a fast dynamic response are compared with those of the $FVIC$, $PID-VIC$, and $PID-VIDC$ where the system has a slow dynamic reaction with more fluctuations and low flexibility, as summarised in Table IV.5.

In addition, the effectiveness of the suggested controller is assessed through the time domain specification in the table below, where the settling time of the whole system is decreased by approximately 30% to 50% under different scenarios. On the other hand, the frequency deviations of the overshoots and nadirs decrease from ± 0.3 Hz to ± 0.02 Hz within the standard limits, which enhances the frequency deviation performance of the multi-area system Moreover, the $RoCoF$ is improved when the maximum number of overshoots is approximately 0.01 Hz/s and the minimum

undershoots around -0.01 Hz/s, which is less than 0.6 Hz/s, which proves the effectiveness of the proposed *FVIDC*.

Table IV.5: Evaluation of performances of proposed technique through a comparison of various time domain specifications.

Factors	Parameters	Method	Load Disturbances	Generation Disturbances	Load and Generation Disturbances
frequency deviation	overshoot	*FVIC*	0.2749	0.2201	0.05201
		PID − VIC	0.1513	0.1210	0.0721
		PID − VIDC	0.06751	0.06259	0.05793
		FVIDC	**0.01045**	**0.02307**	**0.0158**
	Nadir	*FVIC*	-0.3801	-0.4827	0.1862
		PID − VIC	-0.1527	-0.0756	-0.1201
		PID − VIDC	-0.08378	-0.01978	-0.06947
		FVIDC	**-0.02358**	**-0.00684**	**-0.02128**
	Settling time	*FVIC*	30 s	35 s	High
		PID − VIC	30 s	37 s	medium
		PID − VIDC	12 s	13 s	low
		FVIDC	7 s	7 s	**Very low**
RoCoF	Overshoot	*FVIC*	0.1531	0.0606	0.14591
		PID − VIC	0.05218	0.02623	0.06081
		PID − VIDC	0.04778	0.01812	0.05181
		FVIDC	**0.01049**	**0.004969**	**0.006811**
	Nadir	*FVIC*	-0.1140	-0.05261	-0.09986
		PID − VIC	-0.04263	-0.02182	-0.03811
		PID − VIDC	-0.03916	-0.01892	-0.03371
		FVIDC	**-0.01032**	**-0.004019**	**-0.009614**

IV.5 Conclusion

This chapter aims to overcome low inertia and stability problems in interconnected systems to ensure better coordination between *MGs*. It highlights the important im-

pact of the damping factor in virtual inertia control designed for frequency regulation. The $FVIDC$ is proposed as a solution for the frequency regulation of an interconnected system based on three MGs where the complexity of control is increased. The proposed $FVIDC$ is based on the frequency deviation, $RoCoF$, and renewable energy changes to adapt the virtual inertia and damping factor with system changes. The illustrated results show that the frequency responses of each MG are improved in different scenarios. It provides control with high performance and flexible response compared with other control topologies. According to the simulation results, the proposed method offers a fast dynamic response with fewer overshoots and undershoots under load/generation disturbances and a lower SSE than the $FVIC$, $PID-VIC$, and $PID-VIDC$ controllers In all areas, the frequency deviation, $RoCoF$, and recovery time are greatly improved The proposed technique enhances the stability and resiliency of interconnected power systems with better coordination It is concluded that the introduction of $FVIDC$ over PID or conventional VIC in connected systems is beneficial While the simulation results confirm the robustness and reliability of the proposed approach.

Chapter V

Adaptive virtual inertia control for multi-area power system

V.1 Introduction

To provide a practical solution for conventional production issues, international energy organisations and scientific researchers are paying close attention to trends in total energy production from renewable sources. Most of the current energy production architecture is an interconnected power system based on multiple *MGs*, where each *MG* produces its energy to fulfil the load demand, and they are interconnected with tie lines to ensure the power management and stability of the system under various operating conditions [132, 133, 134]. On the other hand, this novel *MG* architecture presents new challenges in terms of regulation and control, where the complexity of the system increases with the integration of *RESs* and the number of connected areas [132]. The most important aspect of controlling an interconnected power system is frequency stabilisation in each area. This significantly contributes to the power management of the whole system, and each area must ensure its local frequency stability and fulfil its power demand in the case of disconnection from the interconnected power system [134] and [135].

Most *RESs* are integrated into existing power systems via power electronic equipment to ensure power exchange in *MGs* [52]. However, the major drawback of this process is the low or no inertia property (in the case of *PV* farms), which makes the system more sensitive to small disturbances [52, 136, 137] and [59]. As a result, power systems with high penetration of *RESs* suffer from low inertia and damping characteristics, which affect frequency regulation and endanger the stability and reliability of the system [52, 51]. To overcome these critical issues, *VIC* knows *VSG* is an effective method for compensating for the lack of inertia in islands and interconnected *MGs* [73] and [138]. Generally, the selection of virtual inertia and damping is based on the comparison between the power size of a modern system and that of a *SG*, then selecting the *VIC* parameter similarly to those of the corresponding *SG*. In other words, the inertia of the system is dictated by the size and the dimensions of the *SG*, which aligns with the active power of the distributed generators [51].

Additionally, in other studies, the essential parameters of *VIC* are determined depending on the integration rate of RESs and the available power reserve. In [119], it depends on the system's response under several values of inertia and damping to choose the appropriate and accurate values. However, these criteria are insufficient for a precise selection of *VIC* parameters following the dynamics of modern systems due to the frequent occurrence of system-wide issues, especially with the increase in *RESs* in the system. Very few studies have investigated the control of multi-area systems powered by RESs, considering frequency responses [139, 140]. Reference [141] used an efficient algorithm to calculate the stability delay margin (*SDM*) to examine the effect of virtual inertia and damping control (*VIDC*) on the SDMs of two connected areas, taking into account the time delay. Authors in [142] investigated the dynamic behaviour of multiple *VIC* in an interconnected power system; the results

proved the weakness of basic VIC in the frequency regulation, which necessitates the improvement of VIC to be compatible with modern power system architecture.

Furthermore, an optimal robust VIC method based on the coefficient diagram method (CDM) was developed in [143] considering the frequency measurement effects to enhance the frequency stability of two-area interconnected. Reference [106] proposed a derivative control technique based on the second-order characteristic of VIC to ensure the frequency stability of two areas connected via a tie lien. However, the designed control is based on fixed virtual inertia without considering damping effects, where the high integration of RESs and load disturbance could affect the frequency stability of the whole system. To enhance the transient stability in an interconnected system, the authors of [144] proposed a multi-objective VIC for RESs to provide variable virtual inertia based on the transient process of the rotor angle after disturbances to introduce additional accelerating and decelerating energy for rotor angle variation whereas considering the damping factor in the control design could enhance frequency stability. In [145], a novel bidirectional VIC strategy has been designed for interconnected hybrid systems (AC and DC MGs) to be more flexible, ensure inertia transfer between areas, and improve the ability of the system to respond to power fluctuations. The designed technique is based on the established inertia equation in both the AC and DC areas of the hybrid system. However, more tests may be necessary to evaluate the performance of the proposed strategy fully.

The $PI-VSG$ and $PID-VSG$ are proposed in several pieces of literature to benefit from the PI characteristics in regulation by enhancing the performance of VSG control. The $PI-VSG$ and $PID-VSG$ are used in [126] for islanded MG based on the derivative technique to generate the suitable virtual inertia power under a wide range of $RESs$ and load penetration where the PI and PID parameters are tuned by the IMC tuning method. However, the conventional tuning methods of PI/PID controllers could not perform satisfactorily. The fractional order PID ($FOPID-VIC$) is proposed in [146] to deal with the high integration of RESs. It is employed to adjust the virtual inertia gain, to ensure fast response, and to absorb oscillating frequencies for the MG. The parameters of PI coupled with VIC in [117] are determined based on the PSO algorithm. In another study for an interconnected power system based on two regions, the VIC is combined with PSO-optimized fractional-order proportional integral ($FOPI$) controller-based superconducting magnetic energy storage ($SMES$) approach in [147].

Furthermore, the $MPC-VSG$ proposed in [119] aims to enhance system voltage and frequency dynamic characteristics by providing inertia support during transient states and calculating the necessary active and reactive power increments. However, the virtual inertia and damping factor selection are classically based on applying values that differ from the suitable values corresponding to the better response selected. This approach is proposed in [122] with consideration of high penetration of RESs

for MG. It is based on the first-order derivative transfer function with the virtual inertia gain and time delay without considering the damping effect. The authors in [148] used the African Vultures Optimization Algorithm ($AVOA$) for the optimisation of $MPC-VIC$ to enhance the inertia response of islanded MG. On the other hand, the robust-$MPC-VSG$ ($RMPC-VSG$) approach is developed in [120] where the VSG based only on virtual inertia propriety to address time delays in MG by modelling system uncertainty using polytopic models and Sedumi solvers. However, its computational complexity increases significantly in large-scale or real-time applications, making it less practical for systems with high variability in renewable energy inputs.

The authors in [149] proposed $H_\infty-VSG$ to enhance MG performance and stability by considering high RES penetration, ensuring robust performance despite disturbances and parametric uncertainties. The selection of virtual inertia gain considering frequency deviation and the power change from RESs is proposed in [99] based on the FL approach under different levels of integration of RESs. The $FL-VIC$ is used in [121] to determine the suitable inertia and damping based on frequency deviation and $RoCoF$ with consideration of SOC for ESS. The $FL-VIC$ approach used in [150] to adaptively adjust the virtual inertia and damping factor where the differential evolution (DE) optimisation algorithm is used to train the FL for optimal frequency performance, aiming to minimise deviation, $RoCoF$, and settling time. Another strategy for compensating for the lack of inertia in modern power systems, a $ANFIS-VSG$ [151, 152, 153], is proposed in [151] for a PV system; it aims to provide suitable inertia power based on frequency deviation and $RoCoF$ as inputs to determine the fuzzy rules. However, the major drawbacks of the most proposed $FL-VSG$ are the difficulty of determining the rules and the time calculation, especially in critical situations where the response must be very fast to avoid damage. Additionally, it often lacks precision in handling fast dynamics, particularly when confronted with rapidly changing renewable energy sources. Furthermore, the virtual inertia in [129] is introduced for interconnected MGs based on an artificial neural network ($ANN-VIC$) to adapt the virtual inertia with the system changes and ensure the coordination between regions. The focus was solely on optimising the virtual inertia factor without taking into account the influence of damping parameters and the effect of power changes from RESs in the optimisation process, where the designed control is based on the frequency deviation as a dataset and the virtual inertia parameter as output.

However, a significant portion of the research published in this field neglects the virtual damping effect in the design of VIC, which could lead to several important effects [154]. The system may experience increased oscillations as virtual inertia stabilises frequency but, without damping, lacks a mechanism to dissipate energy, causing oscillations to persist, resulting in a longer transient response, with the system taking more time to settle into a steady state after disturbances. In the most severe

cases, this can result in instability, where oscillations increase rather than decrease, potentially causing the system to become unbalanced. Moreover, the system's energy efficiency decreases due to the energy loss caused by continuous oscillations, which increase the risk of resonances, where oscillations match the natural frequency of system components, potentially leading to large, damaging oscillations. Hence, although virtual inertia improves stability, proper damping is crucial to prevent these adverse effects and maintain overall system performance [154, 155].

Additionally, a large portion of published papers is based on the optimisation of VIC in island MG without taking into account the dynamic of the interconnected power system, which is closer to the reality architecture of the power system where the coordination of the control system is necessary and must be robust, flexible and faster. On the other hand, the most designed VIC relies either on frequency deviation with $RoCoF$ or frequency deviation with the power change from RESs to provide the virtual inertia to the power system. Table V.1 compares the literary works and the approach proposed in this chapter.

Ref	[156]	[129]	[99]	[149]	[157]	[158]	[151]	[148]	proposed
Studied system	MG	Multi-MGs	MG	MG	Multi-MGs	Multi-MGs	MG	MG	Multi-MG
Model	simplify	simplify	simplify	simplify	simplify	simplify	detail	simplify	simplify
VIC technique	MPC	ANN	FL	H_∞	VI-Selector	FL	ANFIS	MPC	ANN
Inertia propriety	Yes	Yes	Yes	Yes	Yes	Yes	Yes	Yes	Yes
Damping propriety	Yes	No	No	No	No	No	cst	No	Yes
Control design based on	Δf	Δf	Δf, $\Delta PRESs$	Δf	RoC of rotor angle of turbine	Δf, $\Delta PRESs$	Δf, $RoCoF$	Δf	Δf, $RoCoF$, $\Delta PRESs$

Table V.1: Comparison between the literary works and the proposed approach.

Inspired by the studies above, this chapter aims to enhance the dynamic performance of interconnected power systems by introducing a novel intelligent VIDC framework based on an ANN approach. Our proposed method generates optimal virtual inertia and damping parameters that dynamically respond to changes in RESs, thereby improving the system's stability and response time. The primary contri-

bution of this work lies in designing a robust control system for multiarea power systems that compensates for the lack of inertia, with a particular emphasis on the rapid fluctuations associated with renewable energy integration.

The proposed control method considers not only the virtual inertia but also the damping factor, ensuring enhanced frequency stability and a significant reduction in settling time, especially in high-disturbance scenarios. To achieve greater precision and adaptability, the ANN-based $VIDC$ continuously monitors key indicators such as frequency deviation, $RoCoF$, and variations in RES power. This allows the system to intelligently and adaptively adjust the virtual inertia and damping for each area, even under disturbances and area disconnections or re-connections. Furthermore, our approach ensures improved coordination between multiple $VIDCs$ across interconnected regions. The results obtained from the simulation of the multiarea power system, controlled by the proposed $ANN-VIDC$, are compared with the existing $FLC-VIC$ from [99] and the $MPC-VIDC$ from [156]. These comparisons clearly demonstrate the superior performance of the $ANN-VIDC$ in terms of frequency stability, response time, and overall robustness, underscoring the effectiveness of our approach.

V.1.1 The proposed ANN-virtual inertia and damping control

Due to the complexity and the dynamic interaction between the multi-MGs system, defining the range for virtual inertia and damping gains becomes more critical. These gains must be carefully selected and tuned to ensure the efficiency of virtual inertia control. Based on the studied interconnected MGs characteristics, the virtual inertia and damping range is from 0 to 15. This range is defined through simulation testing to ensure the stability of the power system. However, the adaptive control strategy is required to fine-tune these parameters according to the system changes and to improve the performance of $VIDC$ in connected MG systems.

This chapter proposes the integration of an artificial neural network (ANN) to adapt $VIDC$ to provide suitable virtual inertia and damping factors (virtual inertia power) for each MG against system variations that manage the complexities introduced by inverters-based RES, especially in the case of interconnected power system, it is designed to address the complexities related on the interactions between MGs such power oscillations and frequency instability through simplification and adaptability. The ANN approach can adjust and learn from system data to enhance the dynamic performance of a system under normal and abnormal operating conditions [159, 160]. It is well suited for controlling non-linear systems and overcoming the problem of uncertainty in system parameters. It can be used in optimisation tasks within a control system to adapt to system changes such as disturbances. The main proposition is to explore hybrid approaches that combine the ANN with traditional

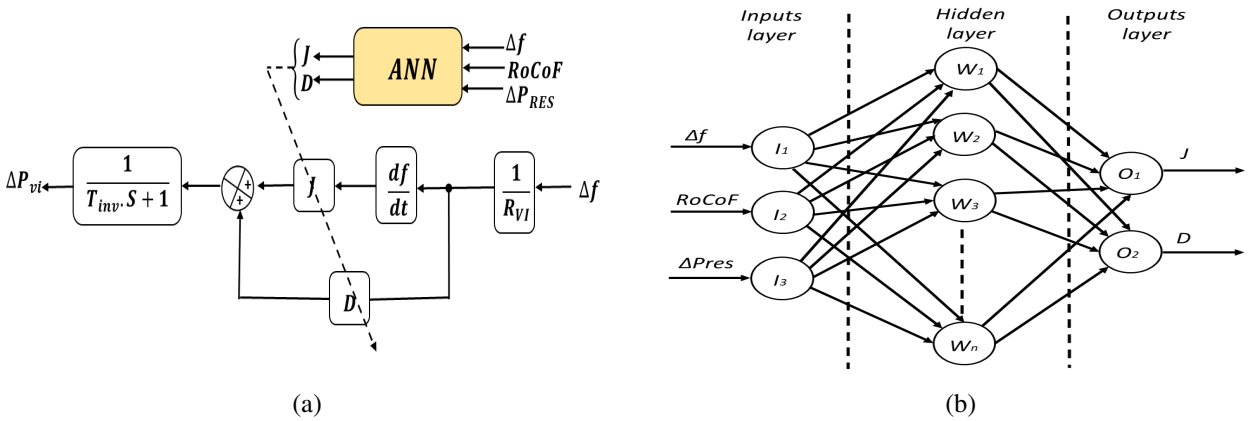

(a) (b)

Figure V.1: (a) Diagram of ANN-VIDC (b) ANN controller block diagrams.

virtual inertia and damping control to achieve optimal performance. The proposed $ANN-VIDC$ presented in Figure V.1a is developed for each MG of the connected system.

The architecture of the *ANN* controller consists of three layers (inputs, hidden, and outputs), where the connections between layers are guaranteed through neurons (nodes). First, the *ANN* controller outputs are based on two main levels: training the dataset (inputs and outputs) and learning to map the inputs to the desired outputs. Then, the *ANN* controller adapts and adjusts its behaviour to achieve the control strategy objectives. Figure V.1b presents the *ANN* controller associated inputs (Δf, $RoCoF$,and ΔP_{RES}) and outputs (J and$D$). The core strength of the proposed *ANN*-based approach lies in its ability to learn from system dynamics. The artificial neural network continuously processes input data (Δf, $RoCoF$, and ΔP_{RES}). This real-time learning capability allows the *ANN* to identify and adapt to the dynamic behaviours of the system, making it capable of rapidly generating optimal virtual inertia and damping parameters. In other words, it ensures an accurate and fast estimation of $VIDC$ parameters according to the system dynamics.

The construction of the ANN model of each MG is carried out using MATLAB/Simulink as illustrated in Figure V.2, which provides a feedforward neural network (NN) model consisting of three neurons in the input layer, ten neurons in the hidden layer and two neurons in the output layer. This structure is kept lightweight; it enables the system to make quick decisions with minimal delay, which is crucial for real-time implementation. Furthermore, the computational training of the ANN is performed offline, ensuring the efficiency of the online implementation. The collection of input and output data based on the simulation was trained using the Levenberg–Marquardt algorithm, which efficiently deals with problems with many parameters; it combines the Gauss-Newton method and the gradient descent to ensure fast and stable convergence to optimal solutions. The training process uses the main squared errors, minimising the overall error between the observed and predicted values of the ANN output model.

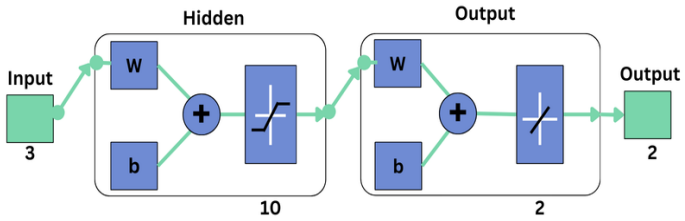

Figure V.2: The ANN Controller Architecture.

Figure V.3 shows the training performance curve where the mean squared error is $3.3287e-06$ after 1000 epochs.

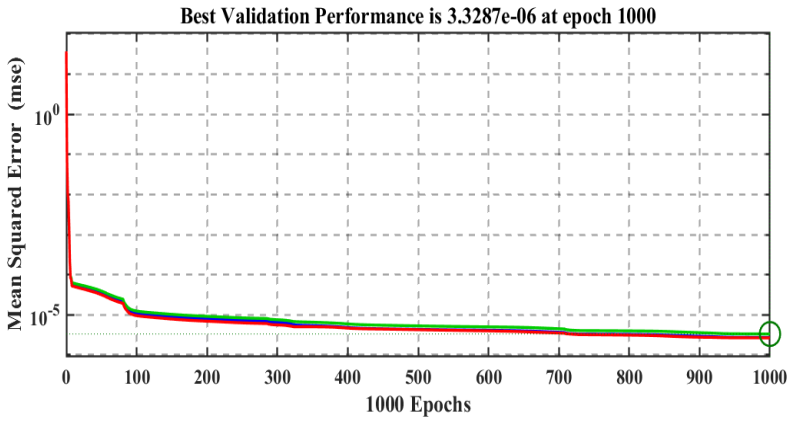

Figure V.3: Performance of the ANN controller.

V.2 Simulation results and discussion

V.2.1 Case of islanded *MG*

To examine the performance of the suggested $ANN-VIDC$. Firstly, it is used for an islanded MG consisting of a thermal generator, wind, and solar farms, an ESS, and loads, as shown in Figure V.4. The simulation parameters used for the islanded MG are the same as those in reference [51, 156] and are given in Table V.2. The studied MG is tested under load and generation disturbances, and the obtained results are compared to those of $FLC-VIC$ developed in [99] and $MPC-VIDC$ developed in [156] to evaluate the frequency stability.

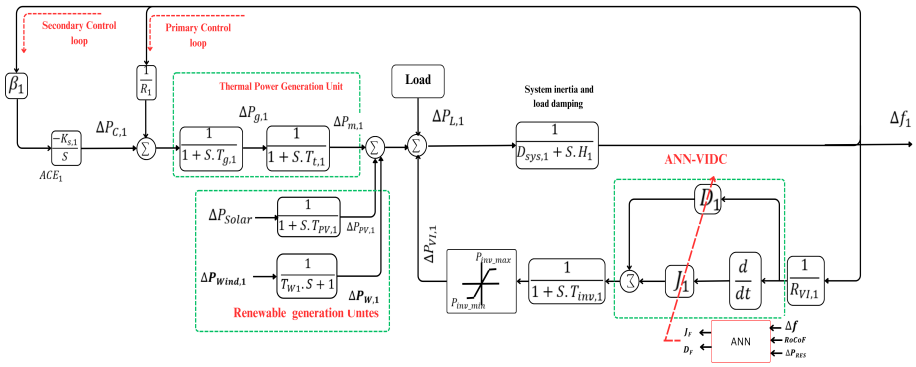

Figure V.4: Diagram of an MG based on ANN-VIDC strategy.

Table V.2: Simulation Parameters of Island System

Parameters	**Values**
Gain of Integral controller K_s(s)	0.1
Governor time constant T_g(s)	0.07
Turbine time constant T_t(s)	0.37
Governor droop constant R(Hz/p.u)	2.6
Bias factor β (p.u/Hz)	0.98
Virtual inertia constant J (p.u.s)	0.6
Virtual damping constant D (P.u/Hz)	0.3
Virtual inertia control droop R_{vi}(Hz/p.u)	2.7
Time constant of inverter-based ESS T_{inv} (s)	1.0
Time constant of wind turbine T_{wt} (s)	1.4
Time constant of solar system T_{pv} (s)	1.9
System inertia H (p.u.s)	0.0830
System load damping D_{sys} (p.u./Hz)	0.0160

Random signals with varying first- and second-order sampling times are used to represent the simulated dynamics of loads and *RES* for the islanded MG, as illustrated in Figures V.5a and V.5b. First, a load change occurs in the MG during 1200 s, as shown in Figure V.5a. Then, at 100 s, the studied signal area is perturbed through a solar farm (see Figure V.5). Finally, a power disturbance from a wind farm is introduced at 300 s, as shown in Figure V.5b. The system response based on the proposed approach and those developed in [99]and [156] is illustrated in Figure V.5c through the frequency deviation. To analyse the robustness of the proposed $ANN-VIDC$, the mean square error (MSE), the root mean square error (RMSE), and the mean absolute error (MAE) are calculated for $FLC-VIC$,$MPC-VIDC$, and the proposed

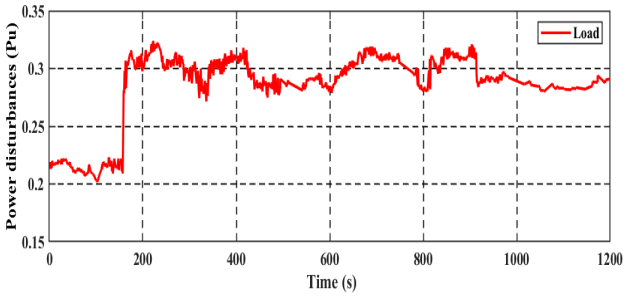

(a)

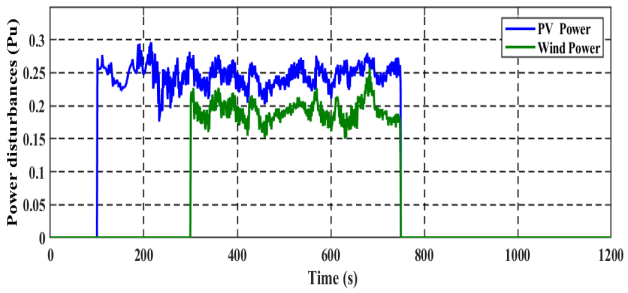

(b)

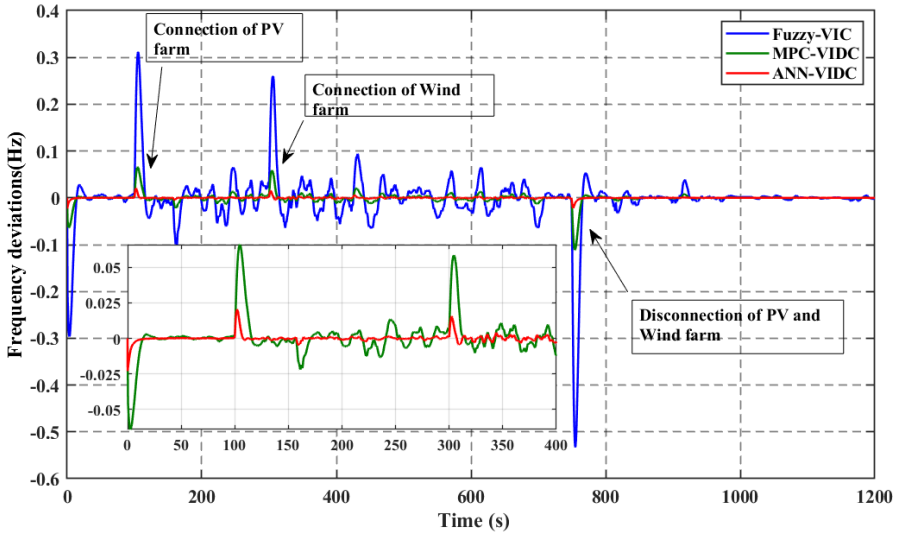

(c)

Figure V.5: Frequency deviation of the islanded MG (a) load disturbances (b) generation disturbances (c) frequency deviations.

$ANN-VIDC$ as presented in Table V.3.

Table V.3: Performances of the proposed ANN-VIDC for an islanded MG.

	Performance analysis		
Method	MSE	RMSE	MAE
FL-VIC	0.004	0.0623	0.0278
MPC-VIDC	0.0002	0.0128	0.0054
ANN-VIDC	**0**	**0.0023**	**0.0009**

The calculated metrics (MSE, $RMSE$, and MAE) show that the proposed $ANN-VIDC$ performs better than the system based on $FLC-VIC$ and $MPC-VIDC$. A decrease in peak values is presented with less oscillation and a fast time response, demonstrating the better performance of the proposed control. As displayed in Figure V.5c, at the moment of introducing the RESs disturbances, the frequency response presents an overshoot equal to $0.3Hz$ in the case of $FLC-VIC$ and equal

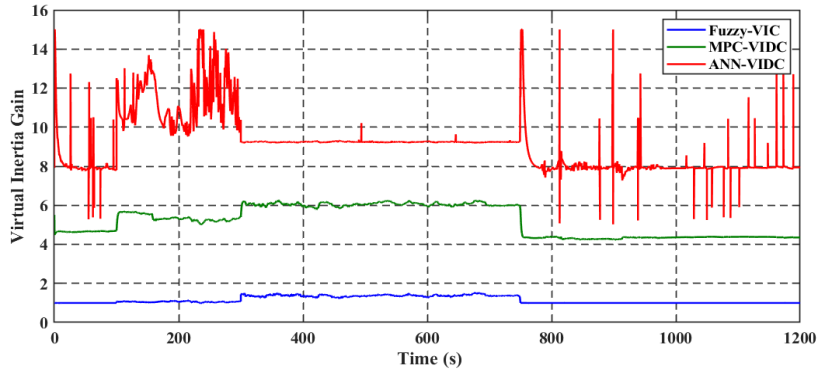

(a)

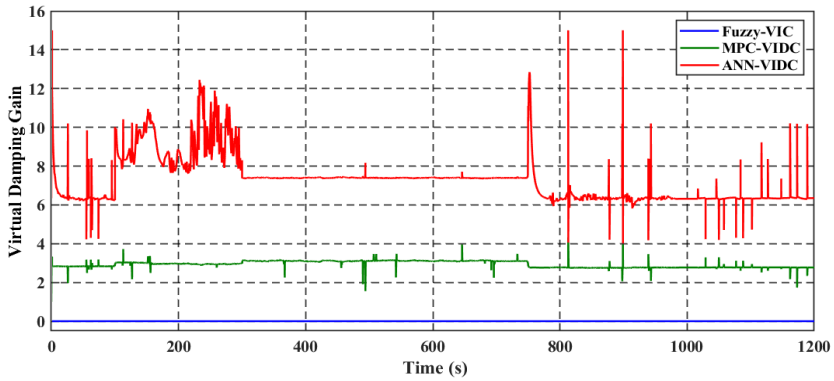

(b)

Figure V.6: Evolution of virtual inertia and damping (a) Virtual inertia gain (b) Virtual Damping gain.

to $0.05Hz$ in the case of the $MPC-VIDC$. However, the overshoots and the undershoots are well decreased in the case of $ANN-VIDC$, and the results present a better dynamic performance of the studied MG, which proves the efficiency of the proposed strategy in the compensation of the lack of inertia, the regulation, and control of the MG under sudden loads and generation changes.

Figure V.6 shows the online estimation of virtual inertia and damping gains over time for the three methods. It illustrates the variation of these gains (virtual inertia and damping figure V.6a and figureV.6b respectively) with the variation of load and renewable power sources where the estimated gains from the proposed $ANN-VIDC$ are increased and decreased to ensure sufficient inertia and damping to deal with the frequency changes which improve the frequency response compared with $MPC-VIC$ and $FLC-VIC$ where the damping factor is changed between 1.5 to 5 for the $MPC-VIDC$ and it is for $FLC-VIDC$, while the virtual inertia does not exceed 6.5 in the case of $MPC-VIDC$ and 1.8 in the case $FLC-VIC$.

V.2.2 Case of interconnected MGs

The proposed $ANN-VIDC$ is introduced for three areas of interconnected power systems, as presented in Figure V.7. The simulation parameters used for the interconnected MG are primarily based on those provided in references [51, 129, 131], and

are detailed in Table V.4; however, small but significant modifications were made to tailor the parameters to the specific dynamics and operational conditions of the studied system.

Table V.4: Simulation parameters of the interconnected MGs.

Parameters	Area 1	Area 2	Area 3
Gain of Integral controller K_s (s)	0.3	0.2	0.4
Governor time constant (s)T_g	0.08	0.07	0.06
Turbine time constant (s)T_t	0.39	0.46	0.35
Governor droop constant R (Hz/p.u)	3.05	2.74	2.81
Bias factor β (p.u/Hz)	0.34	0.37	0.36
Virtual inertia control droop R_{vi} (p.u.s)	2.5	2.7	2.3
Time constant of inverter-based ESS T_{inv} (s)	1	1.2	0.9
Time constant of wind turbine T_{wt} (s)	1.4	1.5	1.2
Time constant of solar system T_{pv} (s)	1.3	1.9	1.5
System inertia H (p.u.s)	0.083	0.01010	0.0623
System load damping D_{sys} p.u./Hz)	0.15	0.16	0.14
Synchronizing coefficient (p.u.MW/Hz)	$T_{12} = 0.2$	$T_{21} = 0.2$	$T_{31} = 0.25$
Synchronizing coefficient (p.u.MW/Hz)	$T_{13} = 0.25$	$T_{22} = 0.12$	$T_{32} = 0.25$

The studied system is tested under high and low disturbances from renewable generation and loads, continuous and discontinuous disturbances, as well as connection and disconnection of areas, to examine the performance of the designed ANN-VIDC compared with $FLC-VIC$ and $MPC-VIDC$ developed in [99] and [156] respectively. It must be noted that the simulated dynamics of loads and wind and PV system for each MG shown in Figures V.8 and V.11 are generated as random signals with varying first- and second-order sampling times.

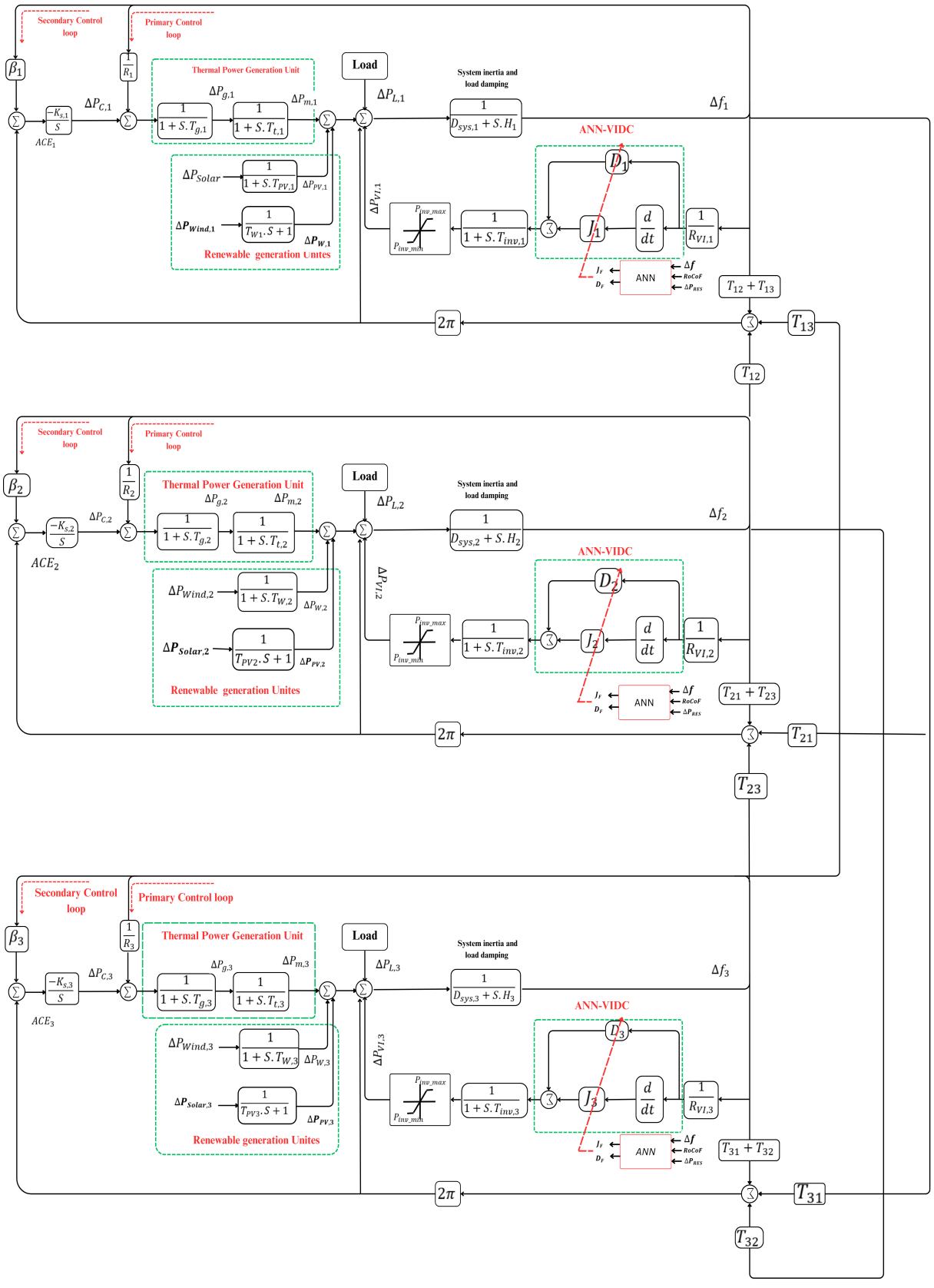

Figure V.7: Structure of interconnected MGs based on ANN-VIDC

V.2.2.1 Under continuous and discontinuous load disturbances

The three areas connected to the system are tested under constant and discontinuous load disturbances, as shown in Figure V.8a. On the other hand, the applied PV and Wind power disturbance are illustrated in Figures V.8b and V.8c to evaluate the performance of the proposed $ANN-VIDC$.

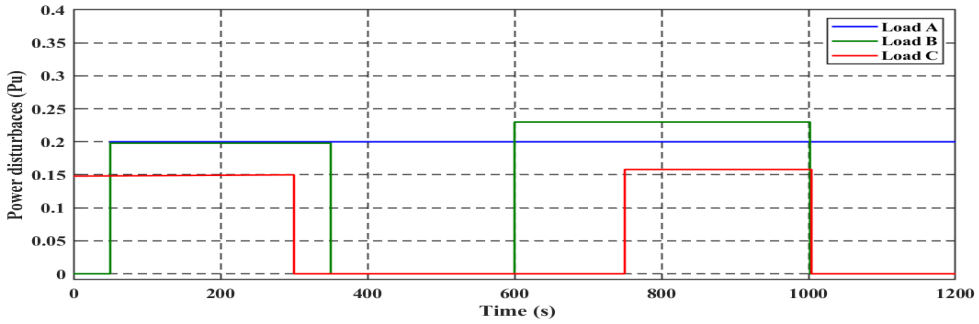

(a)

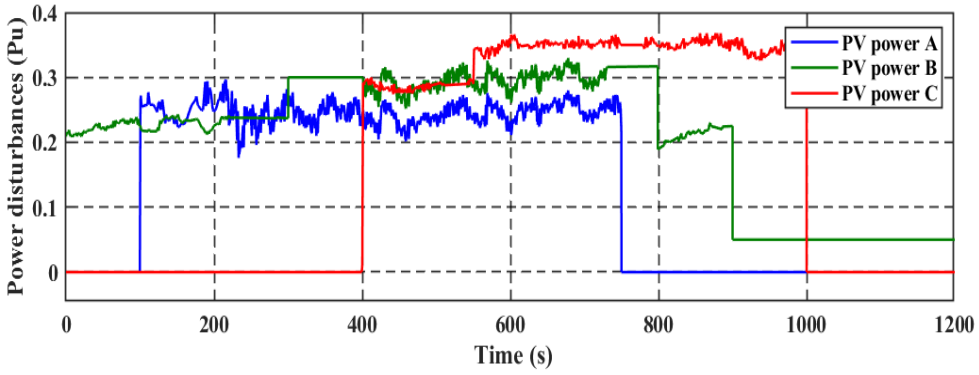

(b)

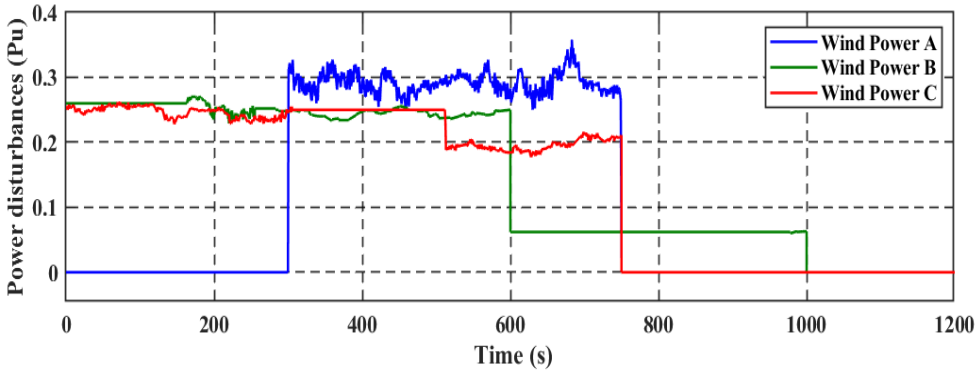

(c)

Figure V.8: (a) load disturbances, (b) PV power disturbances, (c) Wind power disturbances.

Figures V.9a, V.9b, and V.9c present the evolution of frequency deviation during the applied disturbances. For each sudden change in load and renewable power in each area (see Figure V.8), the frequency response present overshoots around $0.4Hz$ and nadirs around -0.25 in the case of $FLC-VIC$, which are bigger than those presented from the system under $MPC-VIDC$ and $ANN-VIDC$. However, the proposed $ANN-VIDC$ performs better than $FLC-VIC$ and $MPC-VIDC$, where

the overshoots, nadirs and fluctuation are too small in all areas, as shown in Figure V.9. The evolution of virtual inertia power-based *ESS* is illustrated in Figure V.10 (V.10a, V.10b, and V.10c) where the proposed control provided more power to deal with changes compared with the $FLC-VIC$ and $MPC-VIDC$.

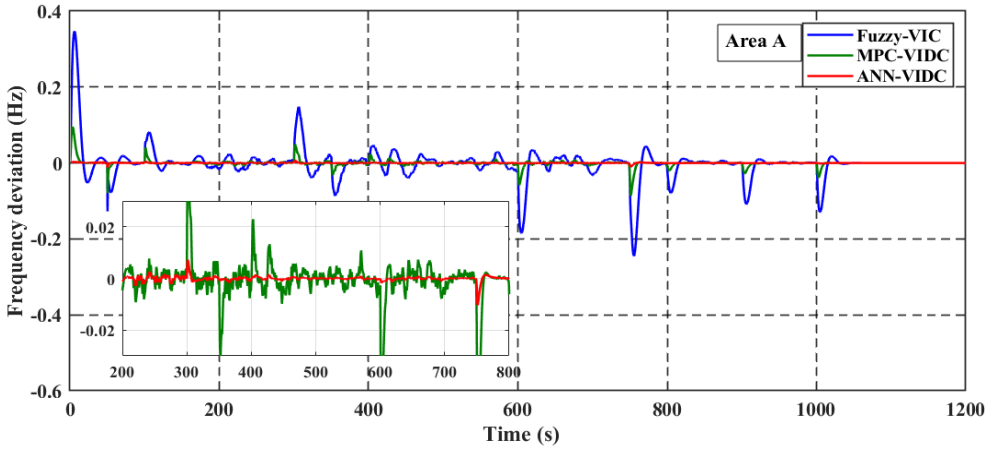

(a)

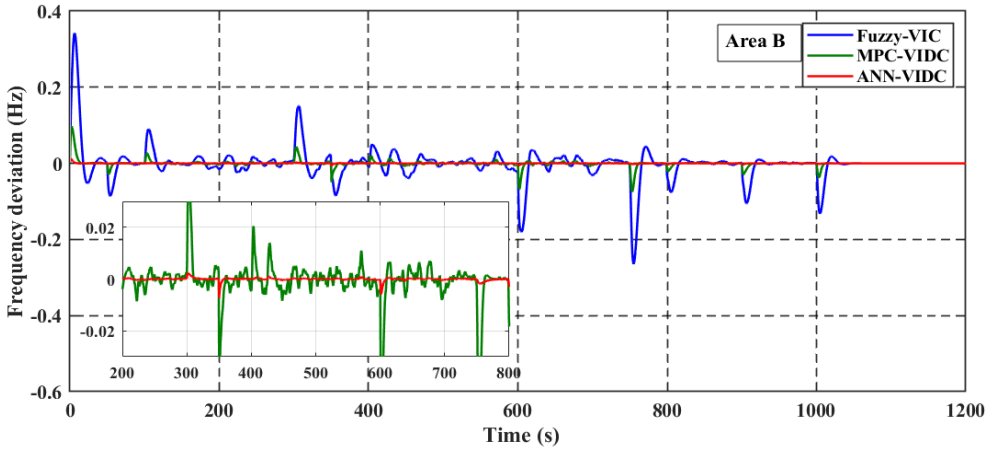

(b)

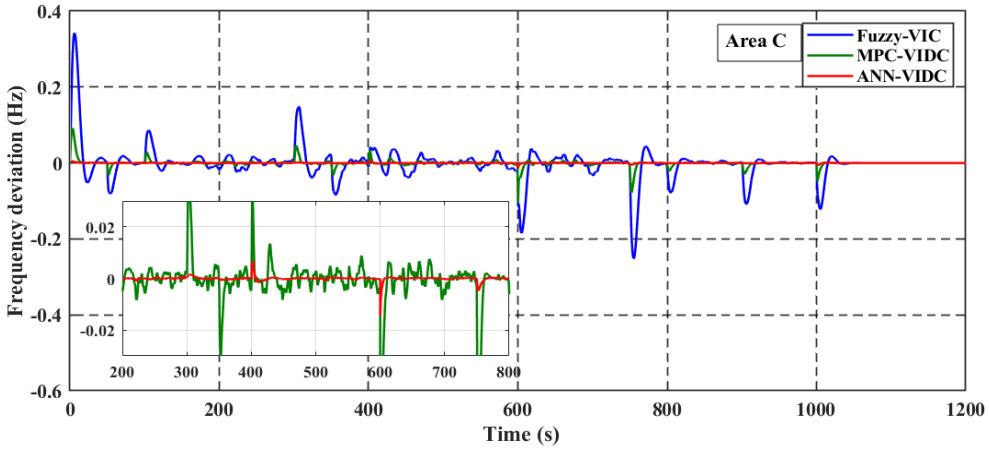

(c)

Figure V.9: Frequency response of the interconnected MGs: (a) from area A, (c) from area B, and (d) from area C.

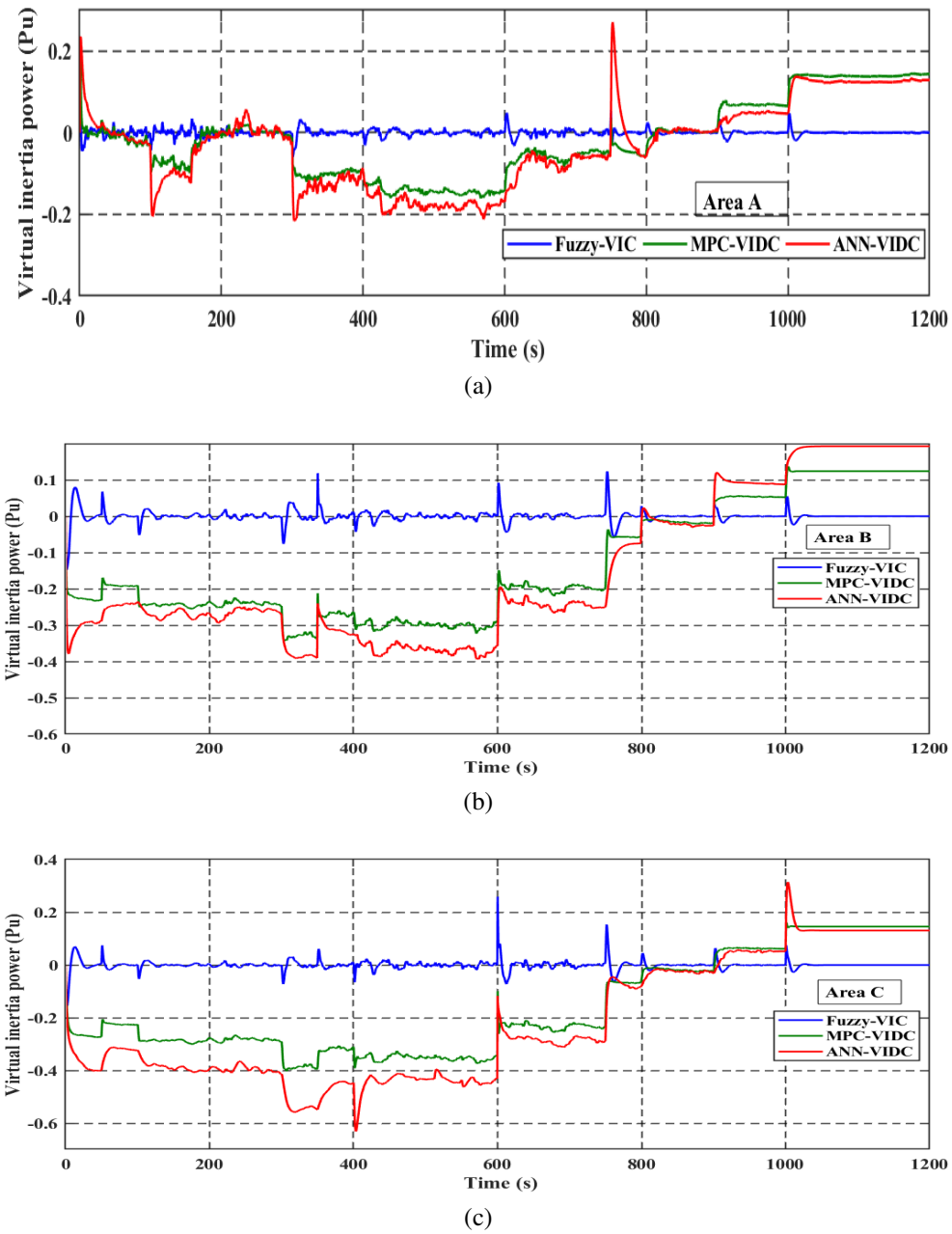

Figure V.10: Virtual inertia power changes: (a) from area A, (b) from area B, and (c) from area C.

V.2.2.2 Under load and generation disturbances

The regulation performance of the $ANN-VIDC$ used for the three areas of the connected system is tested under loads and generation disturbances, which are introduced in all regions during the $1200s$, where the disturbance from the PV and wind farm introduced in each region are depicted in Figures V.8b and V.8c and the load disturbance in areas A, B, and C are between $0.05P.u$ and $0.6P.u$ as illustrated in Figure V.11. The frequency deviation curve (see Figures V.12a, V.12b, and V.12c) of each area presents a smooth response without undesirable peaks where the highest one is $0.01Hz$ observed in area A in the case of $ANN-VIDC$ instead of $FLC-VIC$ and $MPC-VIDC$ present peaks roughly equal to $0.15Hz$ and $0.05Hz$ respectively and nadirs around $-0.2Hz$ and $0.05Hz$ respectively which means that the frequency

deviations are decreased around 75% compared with $MPC - VIDC$.

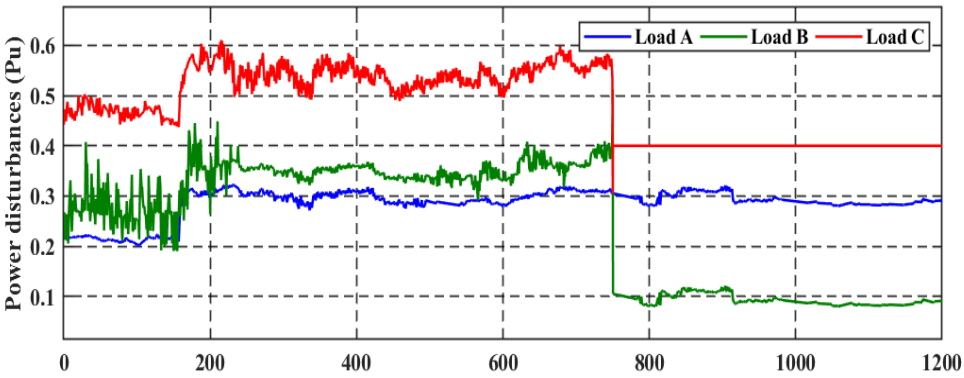

Figure V.11: Load disturbances in areas A, B, and C.

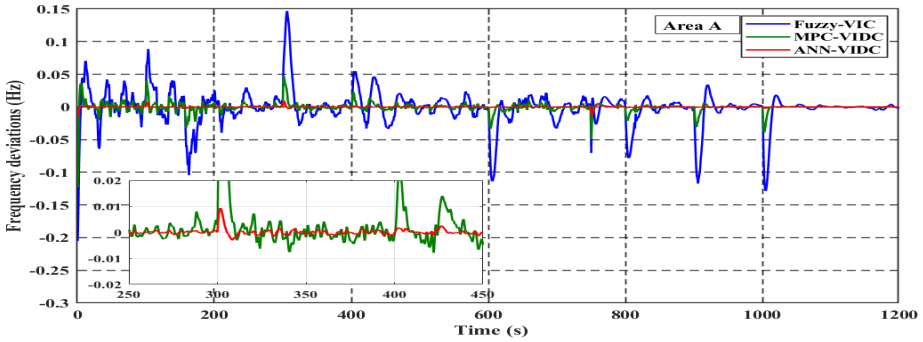

(a)

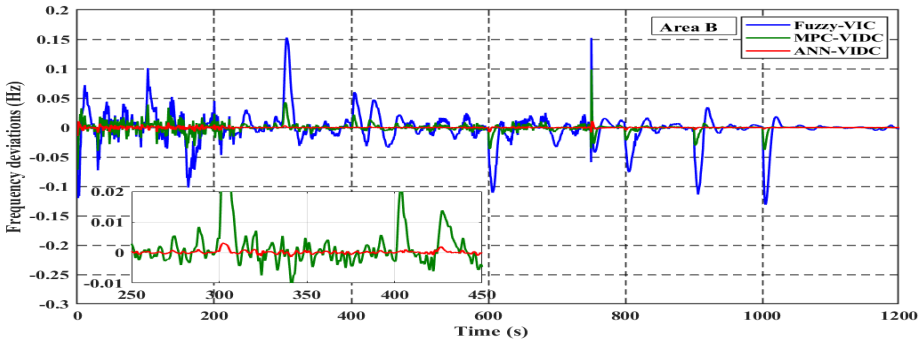

(b)

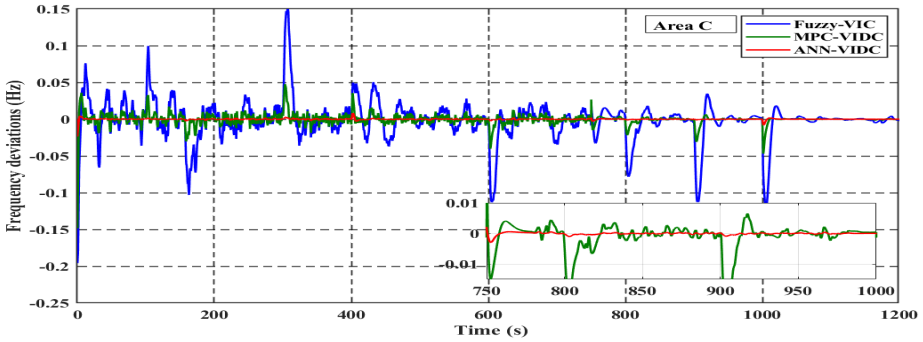

(c)

Figure V.12: Frequency response of the interconnected MGs: (a) from area A, (b) from area B, and (c) from area C.

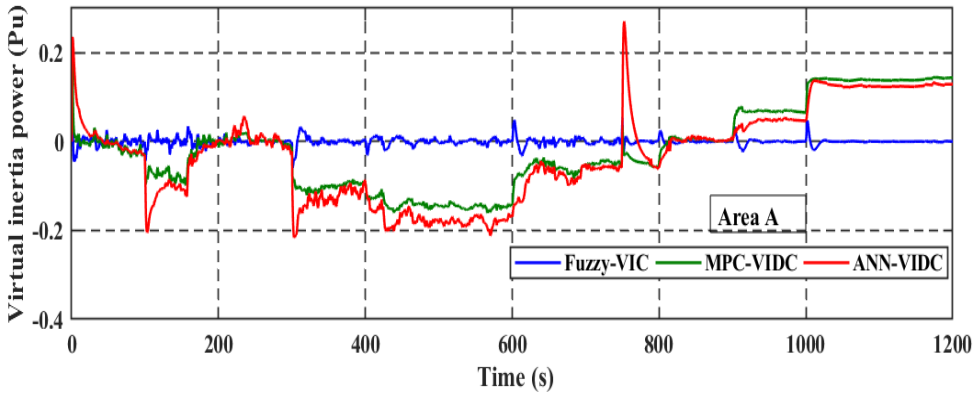

(a)

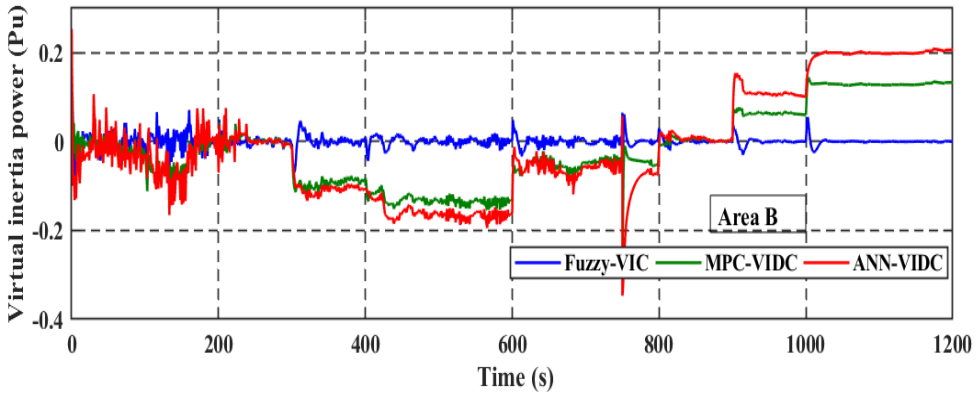

(b)

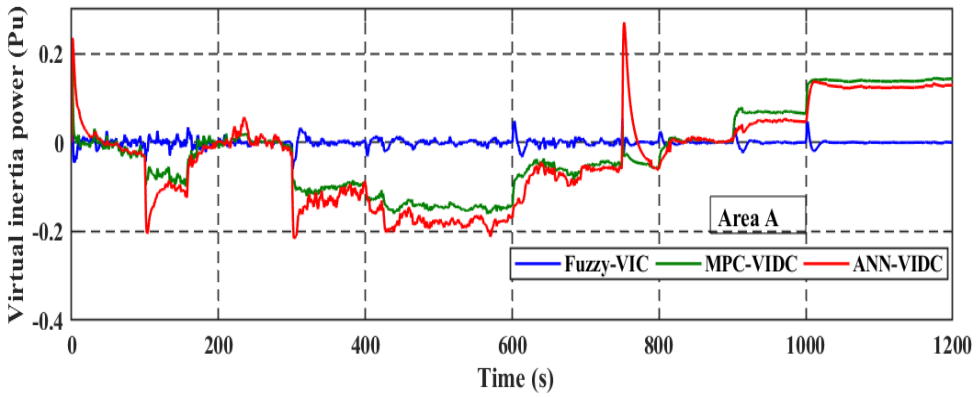

(c)

Figure V.13: Virtual inertia power changes: (a) from area A, (b) from area B, and (c) from area C.

Figures V.13a, V.13b, and V.13c display the virtual inertia power provided in each region. According to the variation of loads and *RES*, the virtual inertia power generated based on the estimated virtual inertia and damping values via the *ANN* approach is increased or decreased to provide sufficient power support to maintain frequency stability smoothly with peaks and nadirs smaller than the $FLC-VIC$ and $MPC-VIDC$ where the provided virtual inertia is lower.

In general, the performance of the connected system presents better coordination between areas ensured by the $ANN-VIDC$ compared to other approaches, as shown in Figures V.12 and V.13 and summarised in Table V.5 where the calculated values

of MSE, $RMSE$, and MAE for each region and each applied approach shows the robustness of the proposed $ANN-VIDC$ in frequency regulation and the coordination between areas which highlight the ability of the $ANN-VIDC$ to properly adapted with the power system changes.

Table V.5: Performances of the proposed ANN-VIDC for interconnected MGs under disturbances.

	Strategy	Performance analysis		
		MSE	RMSE	MAE
Area A	FL	0.0008	0.0275	0.0152
	MPC	0.0001	0.0081	0.0040
	ANN	**0**	**0.0008**	**0.0004**
Area B	FL	0.0080	0.0276	0.0153
	MPC	0.0001	0.0276	0.0045
	ANN	**0**	**0.0008**	**0.0004**
Area C	FL	0.0080	0.0277	0.0155
	MPC	0.0001	0.0085	0.0046
	ANN	**0**	**0.0008**	**0.0004**

V.2.2.3 Plug and play test

To test the resilience of areas under sudden changes, the connection and disconnection of areas are introduced to analyse the robustness and regulation performance of the designed control strategy. First, all areas are connected and subjected to load and generation disturbances, as illustrated in Figures V.8b, V.8c, and V.11. At 100 s, the third area is disconnected, the second area is disconnected at 200 s, and area A is disconnected at 300 s. Each area based on $ANN-VIDC$ presents less fluctuation and peaks of approximately ± 0.01 Hz compared to the other approaches, where in the case of $FL-VIC$, the fluctuations are stronger with high overshoots (around 0.35 Hz in area B and C) and nadirs around $-0.6Hz$ in the first region at $75Os$ the moment where the PV and wind from the first and second region are discontinuous respectively (see Figures V.14a, V.14b, and V.14c).

Additionally, the provided virtual inertia power from the ESS for each area and each approach is illustrated in Figures V.15a, V.15b, and V.15c. All areas operate in the islanded mode from $400s$ to $800s$. It is observed that the frequency deviation based on the proposed $ANN-VIDC$ presents a better performance in terms of peaks and fluctuations compared to $FLC-VIC$ and $MPC-VIDC$.

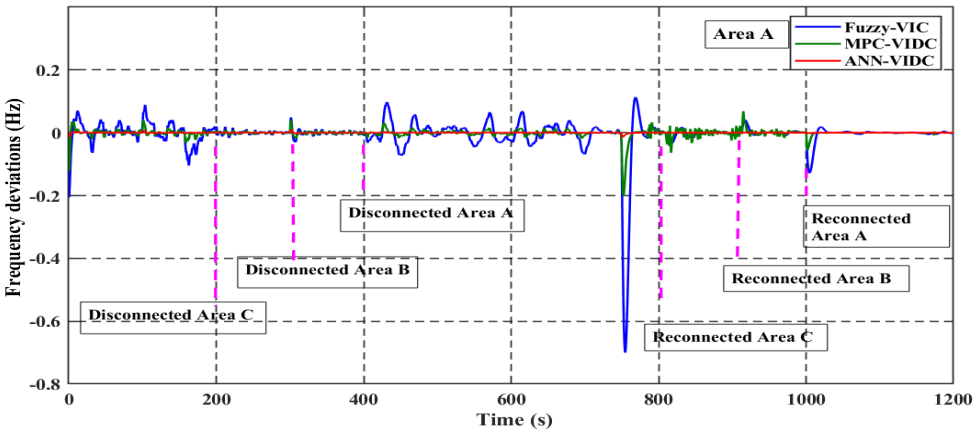

(a)

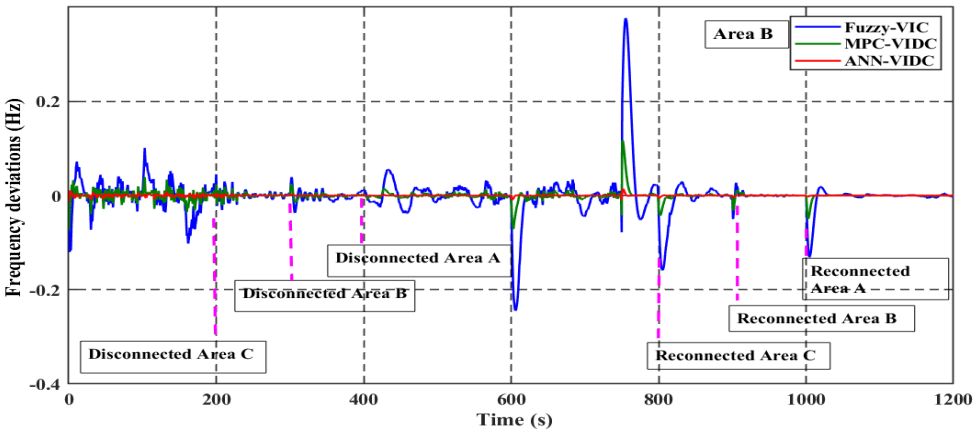

(b)

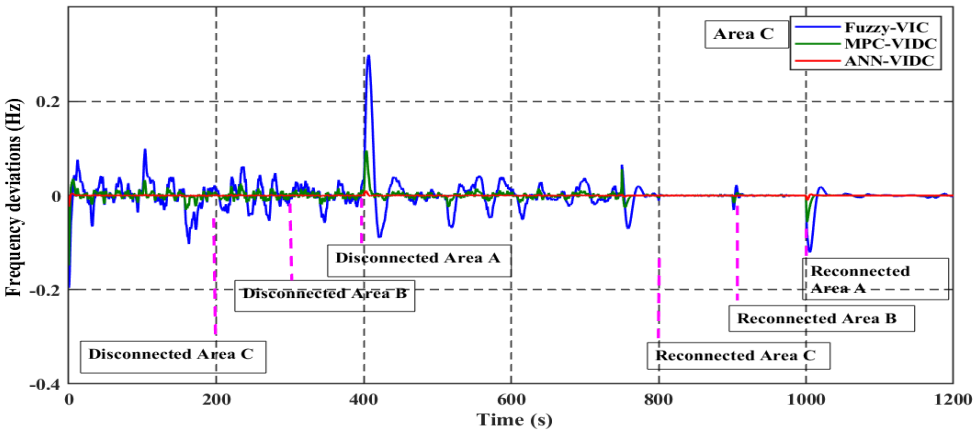

(c)

Figure V.14: Frequency response of the interconnected MGs: (a) from area A, (b) from area B, and (d) from area C.

The results obtained, as presented in FigureV.14 and Table V.6, demonstrate the dynamic responses of each area in terms of frequency. The response-based $ANN-VIDC$ presents a smooth curve compared to the other approaches, with better coordination between areas. The calculated MSE, $RMSE$, and MAE of each region, as shown in Table V.6, effectively prove the efficiency and robustness of the proposed control method.

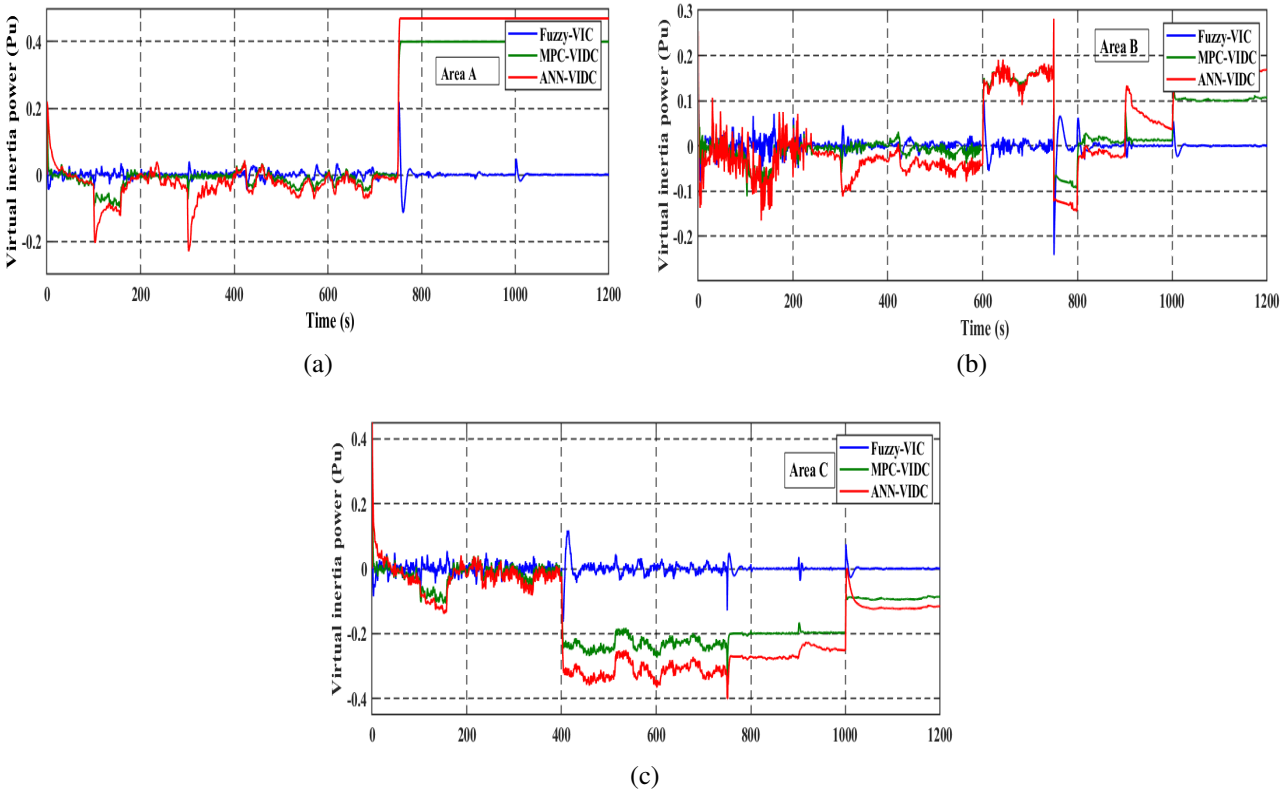

Figure V.15: Virtual inertia power changes: (a) from area A, (b) from area B, and (c) from area C.

Table V.6: Performances of the proposed ANN-VIDC for Interconnected MGs under disturbances, connection and disconnection of MGs.

	Method	Performances analysis		
		MSE	RMSE	MAE
Area A	FL	0.0012	0.0362	0.0213
	MPC	0.0001	0.0106	0.0051
	ANN	**0**	**0.0013**	**0.0007**
Area B	FL	0.0019	0.0368	0.0217
	MPC	0.001	0.0109	0.0053
	ANN	**0**	**0.0014**	**0.0007**
Area C	FL	0.0017	0.0365	0.0215
	MPC	0.0001	0.0107	0.0052
	ANN	**0**	**0.0012**	**0.0006**

V.3 Conclusion

A novel topology of *VIDC* based on the *ANN* approach is proposed in this chapter for an interconnected power system based on three areas with high integration of *RESs*. It aims to enhance the frequency response and ensure better coordina-

tion between regions in cases of high disturbances in load and generation, as well as in the case of connection and disconnection of areas. The designed control considers the frequency deviation, $RoCoF$, and power changes from *RESs* to highlight the impact of high penetration of *RESs* in the power system and ensure accuracy during the online estimation of virtual inertia and damping factors according to the system requirement. The effectiveness of the elaborated $ANN-VIDC$ is proven via comparative analysis with $PID-VIC$ and $FLC-VIC$ applied to islanded MGs and connected MG systems based on three areas powered via thermal generators, wind farms and solar farms. The studied system is tested under load and generation disturbances and connection and disconnection of areas. From the obtained curves of frequency deviation and the robustness analysis based on the calculation of the MSE,$RMSE$ and MAE, the system-based $ANN-VIDC$ provides better performances with smooth responses, less fluctuation and small overshoots and nadirs compared with the system-based $MPC-VIDC$ and $FLC-VIC$.

General Conclusion

The evolution of modern power systems, driven by integrating *RES* and reducing reliance on conventional *SG*, has presented significant challenges in ensuring system stability and frequency regulation. This thesis explored virtual inertia control as a transformative solution to address these challenges, emphasizing its potential to emulate the inertial response of SGs and adapt to the dynamic demands of modern, low-inertia systems.

The investigation began by analysing the fundamentals of inertia in power systems and the adverse effects of reduced physical inertia on system stability. Virtual inertia emerged as a pivotal concept, employing advanced control strategies and power electronics to bridge the gap between traditional and modern grid paradigms. Various VIC topologies, including synchronverter-based models, swing equation-based designs, and frequency-power response approaches, were examined. Emerging strategies such as virtual oscillator control and inducverters were also highlighted, showcasing ongoing innovation in the field.

The research delved into interconnected *MGs* to evaluate the effectiveness of VIC in addressing frequency regulation under diverse scenarios. The frequency response modelling of primary and secondary control loops revealed the influence of physical constraints and *RES* penetration on system stability. Using energy storage systems (*ESSs*) as part of virtual inertia control demonstrated significant improvements in isolated and interconnected MGs, showcasing their ability to enhance system flexibility and robustness under load and generation disturbances.

Two advanced control methodologies were introduced to refine the performance of VIC. The first, Fuzzy-Virtual Inertia and Damping Control (FVIC), was designed to adaptively adjust virtual inertia and damping factors based on system changes such as frequency deviation, *RoCoF*, and variations in *RES* output. Simulation results demonstrated that *FVIC* significantly improved frequency responses, reduced steady-state errors, and achieved faster recovery times than traditional controllers. The second methodology, Artificial Neural Network-Based Virtual Inertia and Damping Control ($ANN-VIDC$), proposed a novel topology to enhance coordination and frequency stability in interconnected systems. Using machine learning techniques,$ANN-VIDC$ exhibited improved robustness and adaptability, delivering smoother responses,

reduced overshoots, and lower nadirs during system disturbances. Comparative analyses further highlighted its superiority over traditional and fuzzy logic-based controllers, showcasing its potential for modern low-inertia power systems.

Looking ahead, the outlined perspectives for virtual inertia control (VIC) focus on integrating advanced algorithms like AI and machine learning for improved optimization in complex systems. Real-time implementation through hardware-in-the-loop testing and pilot projects is critical for practical deployment. *VIC*'s role in hybrid systems combining multiple *RESs* and *ESSs* could enhance grid resilience, while addressing cybersecurity and communication vulnerabilities is essential. Ensuring compliance with evolving grid codes and improving scalability and cost-efficiency will facilitate broader adoption. Finally, *VIC* should support the energy transition by complementing demand-side management, storage innovations, and market mechanisms to drive sustainable power systems

Bibliography

[1] Arka360. Solar energy: Global transition. *Arka360*, 2024. [Online]. Available: https://arka360.com/ros/solar-energy-global-transition/.

[2] Climate Investment Funds. Renewable energy integration. *Climate Investment Funds*, 2024. [Online]. Available: https://www.cif.org/topics/renewable-energy-integration.

[3] World Economic Forum. Electricity generation from renewables set to break records, says iea. *World Economic Forum*, 2023. [Online]. Available: https://www.weforum.org/stories/2023/03/electricity-generation-renewables-power-iea/.

[4] International Renewable Energy Agency (IRENA). World energy transitions outlook 2023. *International Renewable Energy Agency*, 2023. [Online]. Available: https://www.irena.org/Digital-Report/World-Energy-Transitions-Outlook-2023.

[5] Faist Group. Global renewable energy outlook. *Faist Group*, 2024. [Online]. Available: https://www.faistgroup.com/news/global-renewable-energy-outlook/.

[6] BS Hartono, Yan Budiyanto, and Rudy Setiabudy. Review of microgrid technology. In *2013 international conference on QiR*, pages 127–132. IEEE, 2013.

[7] Muhammad Hammad Saeed, Wang Fangzong, Basheer Ahmed Kalwar, and Sajid Iqbal. A review on microgrids' challenges & perspectives. *IEEE Access*, 9:166502–166517, 2021.

[8] Gnana Swathika OV and S Hemamalini. Review on microgrid and its protection strategies. *International Journal of Renewable Energy Research (IJRER)*, 6(4):1574–1587, 2016.

[9] Robert H Lasseter. Microgrids. In *2002 IEEE power engineering society winter meeting. Conference proceedings (Cat. No. 02CH37309)*, volume 1, pages 305–308. IEEE, 2002.

[10] Magdi Sadek Mahmoud, S Azher Hussain, and Mohammad A Abido. Modeling and control of microgrid: An overview. *Journal of the Franklin Institute*, 351(5):2822–2859, 2014.

[11] Dan T Ton and Merrill A Smith. The us department of energy's microgrid initiative. *The Electricity Journal*, 25(8):84–94, 2012.

[12] Pranita Singh, Priyanka Paliwal, and Anoop Arya. A review on challenges and techniques for secondary control of microgrid. In *IOP conference series: Materials science and engineering*, volume 561, page 012075. IOP Publishing, 2019.

[13] Annu Dagar, Pankaj Gupta, and Vandana Niranjan. Microgrid protection: A comprehensive review. *Renewable and Sustainable Energy Reviews*, 149:111401, 2021.

[14] Filipe Bandeiras, Mário Gomes, Paulo Coelho, José Fernandes, Antonio Camacho, and Miguel Castilla. Microgrid architecture evaluation for small and medium size industries. *International Journal of Emerging Electric Power Systems*, 19(2):20170174, 2018.

[15] Abinash Singh and Balwinder Singh Surjan. Microgrid: A review. *International Journal of Research in Engineering and Technology*, 3(2):185–198, 2014.

[16] Maysam Abbasi, Ehsan Abbasi, Li Li, Ricardo P Aguilera, Dylan Lu, and Fei Wang. Review on the microgrid concept, structures, components, communication systems, and control methods. *Energies*, 16(1):484, 2023.

[17] Luis Fernando Grisales-Noreña, Bonie Johana Restrepo-Cuestas, Brandon Cortés-Caicedo, Jhon Montano, Andrés Alfonso Rosales-Muñoz, and Marco Rivera. Optimal location and sizing of distributed generators and energy storage systems in microgrids: A review. *Energies*, 16(1):106, 2022.

[18] Axèle Giroud. World investment report 2023: Investing in sustainable energy for all: United nations conference on trade and development, geneva and new york, 2023, 205 pp., 2024.

[19] Global microgrid market size, share, growth, trends, and forecast (2024 - 2031). https://www.predain.com/energy/global-microgrid-market-size Accessed: 2024-08-06.

[20] Vinayak Bali. Microgrid market report 2024 (global edition). https://www.cognitivemarketresearch.com/microgrid-market-report, March 2024. Accessed: 2024-08-06.

[21] Microgrid market size, share, and trends 2024 to 2033. https://www.precedenceresearch.com/microgrid-market, June 2024. Accessed: 2024-08-06.

[22] Abdelkader Harrouz, Meriem Abbes, Ilhami Colak, and Korhan Kayisli. Smart grid and renewable energy in algeria. In *2017 IEEE 6th International Conference on Renewable Energy Research and Applications (ICRERA)*, pages 1166–1171. IEEE, 2017.

[23] Mohammed Bouznit, María del P Pablo-Romero, and Antonio Sánchez-Braza. Measures to promote renewable energy for electricity generation in algeria. *Sustainability*, 12(4):1468, 2020.

[24] Sid Ahmed Tadjer, Abdelhakim Idir, and Fathia Chekired. Comparative performance evaluation of four photovoltaic technologies in saharan climates of algeria: Ghardaïa pilot station. *Indonesian Journal of Electrical Engineering and Computer Science (IJEECS)*, 18(2):586–598, 2020.

[25] Mounir Khiat, Sid Ahmed Khiat, Mohamed Mankour, and Leila Ghomri. Microgrid application in algeria saharian remote areas. In *Micro-grids-Applications, Operation, Control and Protection*. IntechOpen, 2019.

[26] Lubna Mariam, Malabika Basu, and Michael F Conlon. A review of existing microgrid architectures. *Journal of engineering*, 2013(1):937614, 2013.

[27] Moslem Uddin, Huadong Mo, Daoyi Dong, Sondoss Elsawah, Jianguo Zhu, and Josep M Guerrero. Microgrids: A review, outstanding issues and future trends. *Energy Strategy Reviews*, 49:101127, 2023.

[28] Adam Hirsch, Yael Parag, and Josep Guerrero. Microgrids: A review of technologies, key drivers, and outstanding issues. *Renewable and sustainable Energy reviews*, 90:402–411, 2018.

[29] Saif Jamal, Nadia ML Tan, and Jagadeesh Pasupuleti. A review of energy management and power management systems for microgrid and nanogrid applications. *Sustainability*, 13(18):10331, 2021.

[30] Ramy Georgious, Rovan Refaat, Jorge Garcia, and Ahmed A Daoud. Review on energy storage systems in microgrids. *Electronics*, 10(17):2134, 2021.

[31] Longlong Zhang and Ming Sun. Research on the type of load of accessing to microgrid based on reliability. In *2015 2nd International Conference on Electrical, Computer Engineering and Electronics*, pages 1665–1670. Atlantis Press, 2015.

[32] Yuqi Wang. A review of microgrid research. In *AIP Conference Proceedings*, volume 1971. AIP Publishing, 2018.

[33] Monika Yadav, Nitai Pal, and Devender Kumar Saini. Microgrid control, storage, and communication strategies to enhance resiliency for survival of critical load. *IEEE Access*, 8:169047–169069, 2020.

[34] Bilal M Eid, Nasrudin Abd Rahim, Jeyraj Selvaraj, and Ahmad Elkhateb. Control methods and objectives for electronically coupled distributed energy resources in microgrids: A review. *IEEE systems journal*, 10(2):446–458, 2014.

[35] Paul K Olulope, Oyinlolu A Odetoye, and Matthew O Olanrewaju. A review of emerging design concepts in applied microgrid technology. *AIMS Energy*, 10(4):776–800, 2022.

[36] Ritu Kandari, Neeraj Neeraj, and Alexander Micallef. Review on recent strategies for integrating energy storage systems in microgrids. *Energies*, 16(1):317, 2022.

[37] TB Seane, R Samikannu, and T Bader. A review of modeling and simulation tools for microgrids based on solar photovoltaics. *Frontiers in Energy Research*, 10:772561, 2022.

[38] Anand Abhishek, Aashish Ranjan, Sachin Devassy, Brijendra Kumar Verma, Subhash Kumar Ram, and Ajeet Kr Dhakar. Review of hierarchical control strategies for dc microgrid. *IET Renewable Power Generation*, 14(10):1631–1640, 2020.

[39] Xiong Liu, Tianyang Zhao, Hui Deng, Peng Wang, Jizhen Liu, and Frede Blaabjerg. Microgrid energy management with energy storage systems: A review. *CSEE Journal of Power and Energy Systems*, 9(2):483–504, 2022.

[40] Ali Aillane. *Développement d'approches de commande d'un onduleur photovoltaïque fonctionnant en mode connecté au réseau et en mode isolé*. PhD thesis, École Nationale d'Ingénieurs de Sfax (ENIS), Sfax, Tunisia, December 2023. Doctoral dissertation.

[41] Necmi Altin and Süleyman Emre Eyimaya. A review of microgrid control strategies. In *2021 10th International Conference on Renewable Energy Research and Application (ICRERA)*, pages 412–417. IEEE, 2021.

[42] Saad Ahmad, Md Shafiullah, Chokri Belhaj Ahmed, and Maad Alowaifeer. A review of microgrid energy management and control strategies. *IEEE Access*, 11:21729–21757, 2023.

[43] Trinadh Pamulapati, Muhammed Cavus, Ishioma Odigwe, Adib Allahham, Sara Walker, and Damian Giaouris. A review of microgrid energy management strategies from the energy trilemma perspective. *Energies*, 16(1):289, 2022.

[44] Aiman J Albarakati, Younes Boujoudar, Mohamed Azeroual, Lahcen Eliysaouy, Hossam Kotb, Ayman Aljarbouh, Hend Khalid Alkahtani, Samih M Mostafa, Asifa Tassaddiq, and Alexander Pupkov. Microgrid energy management and monitoring systems: A comprehensive review. *Frontiers in Energy Research*, 10:1097858, 2022.

[45] Maruf A Aminu. Review of microgrids and associated protective systems. *Archives of Current Research International*, 18(2):1–11, 2019.

[46] Mushtaq N Ahmed, Mojgan Hojabri, Ali Mahmood Humada, Hamdan Bin Daniyal, and H Fahad Frayyeh. An overview on microgrid control strategies. *International Journal of Engineering and Advanced Technology (IJEAT)*, 4(5):93–98, 2015.

[47] Daniela Yassuda Yamashita, Ionel Vechiu, and Jean-Paul Gaubert. A review of hierarchical control for building microgrids. *Renewable and Sustainable Energy Reviews*, 118:109523, 2020.

[48] Khurram Hashmi, Rizwan Ali, Muhammad Hanan, Waseem Aslam, Abubakar Siddique, and MUHAMMAD KHAN. Reactive power sharing and voltage restoration in islanded ac microgrids. *Turkish Journal of Electrical Engineering and Computer Sciences*, 30(3):818–838, 2022.

[49] Sonam Shrivastava and Bidyadhar Subudhi. Comprehensive review on hierarchical control of cyber-physical microgrid system. *IET Generation, Transmission & Distribution*, 14(26):6397–6416, 2020.

[50] Ilyas Bennia, Abdelghani Harrag, and Yacine Dailia. Small-signal modelling and stability analysis of island mode microgrid paralleled inverters. *Journal of Renewable Energies*, 24(1):105–120, 2021.

[51] Thongchart Kerdphol, Fathin Saifur Rahman, Masayuki Watanabe, and Yasunori Mitani. *Virtual inertia synthesis and control*. Springer, 2021.

[52] Djaraf Nourelhouda, Yacine Daili, and Abdelghani Harrag. A review of recent control trchniques of virtual synchronous machine for renewable energy. *The Scientific Bulletin of Electrical Engineering Faculty*, 23(2):20–32, 2024.

[53] Khalid Mehmood Cheema. A comprehensive review of virtual synchronous generator. *International journal of electrical power & energy systems*, 120:106006, 2020.

[54] OO Mohammed, AO Otuoze, S Salisu, O Ibrahim, and NA Rufa'i. Virtual synchronous generator: an overview. *Nigerian Journal of Technology*, 38(1):153–164, 2019.

[55] Jingyang Fang, Hongchang Li, Yi Tang, and Frede Blaabjerg. On the inertia of future more-electronics power systems. *IEEE Journal of Emerging and Selected Topics in Power Electronics*, 7(4):2130–2146, 2018.

[56] Meiyi Li, Wentao Huang, Nengling Tai, and Dongliang Duan. Virtual inertia control of the virtual synchronous generator: A review. *arXiv preprint arXiv:2109.07590*, 2021.

[57] Md Nahid Haque Shazon, Atik Jawad, et al. Frequency control challenges and potential countermeasures in future low-inertia power systems: A review. *Energy Reports*, 8:6191–6219, 2022.

[58] Kamala Sarojini Ratnam, K Palanisamy, and Guangya Yang. Future low-inertia power systems: Requirements, issues, and solutions-a review. *Renewable and Sustainable Energy Reviews*, 124:109773, 2020.

[59] Kumar Prabhakar, Sachin K Jain, and Prabin Kumar Padhy. Inertia estimation in modern power system: A comprehensive review. *Electric Power Systems Research*, 211:108222, 2022.

[60] Hassan Bevrani, Hêmin Golpîra, Arturo Román Messina, Nikos Hatziargyriou, Federico Milano, and Toshifumi Ise. Power system frequency control: An updated review of current solutions and new challenges. *Electric Power Systems Research*, 194:107114, 2021.

[61] Peter Christensen, Gert Karmisholt Andersen, Matthias Seidel, Sigrid Bolik, Sönke Engelken, Thyge Knueppel, Athanasios Krontiris, Klaus Wuerflinger, Thorsten Bülo, Jörg Jahn, et al. High penetration of power electronic interfaced power sources and the potential contribution of grid forming converters. 2020.

[62] Hans-Peter Beck and Ralf Hesse. Virtual synchronous machine. In *2007 9th international conference on electrical power quality and utilisation*, pages 1–6. IEEE, 2007.

[63] Expert group: Advanced capabilities for grids with a high share of power park modules report version 1.00, June 2023.

[64] Ujjwol Tamrakar, Dipesh Shrestha, Manisha Maharjan, Bishnu P Bhattarai, Timothy M Hansen, and Reinaldo Tonkoski. Virtual inertia: Current trends and future directions. *Applied sciences*, 7(7):654, 2017.

[65] Md Asaduzzaman Shobug, Nafis Ahmed Chowdhury, Md Alamgir Hossain, Mohammad J Sanjari, Junwei Lu, and Fuwen Yang. Virtual inertia control for power electronics-integrated power systems: Challenges and prospects. *Energies*, 17(11):2737, 2024.

[66] Johan Driesen and Klaas Visscher. Virtual synchronous generators. In *2008 IEEE power and energy society general meeting-conversion and delivery of electrical energy in the 21st century*, pages 1–3. IEEE, 2008.

[67] Salvatore D'Arco, Jon Are Suul, and Olav B Fosso. Small-signal modeling and parametric sensitivity of a virtual synchronous machine in islanded operation. *International Journal of Electrical Power & Energy Systems*, 72:3–15, 2015.

[68] Qing-Chang Zhong and George Weiss. Synchronverters: Inverters that mimic synchronous generators. *IEEE transactions on industrial electronics*, 58(4):1259–1267, 2010.

[69] Xiangwu Yan, Sara YA Mohamed, Dongxue Li, and Abuzaid S Gadalla. Parallel operation of virtual synchronous generators and synchronous generators in a microgrid. *The Journal of Engineering*, 2019(16):2635–2642, 2019.

[70] Xiaorong Zhu, Yi Wang, Lie Xu, Xiangyu Zhang, and Heming Li. Virtual inertia control of dfig-based wind turbines for dynamic grid frequency support. 2011.

[71] Jianhui Meng, Xinchun Shi, Yi Wang, and Chao Fu. A virtual synchronous generator control strategy for distributed generation. In *2014 China International Conference on Electricity Distribution (CICED)*, pages 495–498. IEEE, 2014.

[72] Zheng Zeng, Rongxiang Zhao, Huan Yang, Chong Cheng, and Shengqing Tang. Single-phase virtual synchronous generator for distributed energy sources. In *2013 International Conference on Electrical Machines and Systems (ICEMS)*, pages 190–195. IEEE, 2013.

[73] Adrián Criollo, Luis I Minchala-Avila, Dario Benavides, Paul Arévalo, Marcos Tostado-Véliz, Daniel Sánchez-Lozano, and Francisco Jurado. Enhancing virtual inertia control in microgrids: A novel frequency response model based on storage systems. *Batteries*, 10(1):18, 2024.

[74] Shuan Dong and Yu Christine Chen. Adjusting synchronverter dynamic response speed via damping correction loop. *IEEE Transactions on Energy Conversion*, 32(2):608–619, 2016.

[75] Qing-Chang Zhong, Phi-Long Nguyen, Zhenyu Ma, and Wanxing Sheng. Self-synchronized synchronverters: Inverters without a dedicated synchronization unit. *IEEE Transactions on power electronics*, 29(2):617–630, 2013.

[76] Tiancong Shao, Trillion Q Zheng, Hong Li, and Xiaochao Zhang. Parameter design and hot seamless transfer of single-phase synchronverter. *Electric Power Systems Research*, 160:63–70, 2018.

[77] Zhenyu Ma, Qing-Chang Zhong, and Joseph D Yan. Synchronverter-based control strategies for three-phase pwm rectifiers. In *2012 7th IEEE conference on industrial electronics and applications (ICIEA)*, pages 225–230. IEEE, 2012.

[78] Toshifumi Ise and Hassan Bevrani. Virtual synchronous generators and their applications in microgrids. In *Integration of Distributed Energy Resources in Power Systems*, pages 282–294. Elsevier, 2016.

[79] Yong Chen, Ralf Hesse, Dirk Turschner, Hans-Peter Beck, et al. Dynamic properties of the virtual synchronous machine (visma). *Proc. Icrepq*, 11:755–759, 2011.

[80] Liang Lu and Nicolaos A Cutululis. Virtual synchronous machine control for wind turbines: a review. In *Journal of Physics: Conference Series*, volume 1356, page 012028. IOP Publishing, 2019.

[81] Yong Chen, Ralf Hesse, Dirk Turschner, Hans-Peter Beck, et al. Comparison of methods for implementing virtual synchronous machine on inverters. *RE&PQJ*, 10(6), 2012.

[82] Yuko Hirase, Kazuhiro Abe, Kazushige Sugimoto, and Yuji Shindo. A grid-connected inverter with virtual synchronous generator model of algebraic type. *Electrical Engineering in Japan*, 184(4):10–21, 2013.

[83] K Sakimoto, Y Miura, and T Ise. Stabilization of a power system with a distributed generator by a virtual synchronous generator function. In *8th International Conference on Power Electronics-ECCE Asia*, pages 1498–1505. IEEE, 2011.

[84] E Barklund, Nagaraju Pogaku, Milan Prodanovic, C Hernandez-Aramburo, and Tim C Green. Energy management in autonomous microgrid using stability-constrained droop control of inverters. *IEEE Transactions on Power Electronics*, 23(5):2346–2352, 2008.

[85] Weiyi Zhang, Antoni Mir Cantarellas, Joan Rocabert, Alvaro Luna, and Pedro Rodriguez. Synchronous power controller with flexible droop characteristics

for renewable power generation systems. *IEEE Transactions on Sustainable Energy*, 7(4):1572–1582, 2016.

[86] Weiyi Zhang, Daniel Remon, and Pedro Rodriguez. Frequency support characteristics of grid-interactive power converters based on the synchronous power controller. *IET Renewable Power Generation*, 11(4):470–479, 2017.

[87] Pedro Rodriguez, Costantino Citro, J Ignacio Candela, Joan Rocabert, and Alvaro Luna. Flexible grid connection and islanding of spc-based pv power converters. *IEEE Transactions on Industry Applications*, 54(3):2690–2702, 2018.

[88] Andrés Tarrasó, Cristian Verdugo, Ngoc Bao Lai, Jose Ignacio Candela, and Pedro Rodriguez. Synchronous power controller for distributed generation units. In *2019 IEEE Energy Conversion Congress and Exposition (ECCE)*, pages 4660–4664. IEEE, 2019.

[89] Josep M Guerrero, L Garcia De Vicuna, José Matas, Miguel Castilla, and Jaume Miret. A wireless controller to enhance dynamic performance of parallel inverters in distributed generation systems. *IEEE Transactions on power electronics*, 19(5):1205–1213, 2004.

[90] Salvatore D'Arco and Jon Are Suul. Virtual synchronous machines—classification of implementations and analysis of equivalence to droop controllers for microgrids. In *2013 IEEE Grenoble Conference*, pages 1–7. IEEE, 2013.

[91] Brian B Johnson, Sairaj V Dhople, Abdullah O Hamadeh, and Philip T Krein. Synchronization of parallel single-phase inverters with virtual oscillator control. *IEEE Transactions on Power Electronics*, 29(11):6124–6138, 2013.

[92] Brian B Johnson, Sairaj V Dhople, James L Cale, Abdullah O Hamadeh, and Philip T Krein. Oscillator-based inverter control for islanded three-phase microgrids. *IEEE Journal of Photovoltaics*, 4(1):387–395, 2013.

[93] Mahdi Ashabani, Francisco D Freijedo, Saeed Golestan, and Josep M Guerrero. Inducverters: Pll-less converters with auto-synchronization and emulated inertia capability. *IEEE Transactions on Smart Grid*, 7(3):1660–1674, 2015.

[94] Viktoriia Kryvda, Maksym Maksymov, Viktor Zubak, Andrii Ivaneiev, and Ruslan Ryaboshapka. Development of the model and improvement of the method of automated control of steam turbine parameters to minimize the power imbalance in the energy system to increase its efficiency. *Technology audit and production reserves*, 5(1 (79)):19–29, 2024.

[95] Changhong Zhao, Ufuk Topcu, and Steven H Low. Frequency-based load control in power systems. In *2012 American Control Conference (ACC)*, pages 4423–4430. IEEE, 2012.

[96] Binh-Minh Nguyen, Ngoc Tran-Huynh, Michihiro Kawanishi, and Tatsuo Narikiyo. A discussion on stabilization of frequency control for power systems. *arXiv preprint arXiv:2010.05389*, 2020.

[97] Naresh Kumari and AN Jha. Effect of generation rate constraint on load frequency control of multi area interconnected thermal systems. *Journal of Electrical and Electronics Engineering Research*, 5(3):44–49, 2013.

[98] Javad Morsali, Kazem Zare, and M Tarafdar Hagh. Appropriate generation rate constraint (grc) modeling method for reheat thermal units to obtain optimal load frequency controller (lfc). In *2014 5th Conference on Thermal Power Plants (CTPP)*, pages 29–34. IEEE, 2014.

[99] Thongchart Kerdphol, Masayuki Watanabe, Komsan Hongesombut, and Yasunori Mitani. Self-adaptive virtual inertia control-based fuzzy logic to improve frequency stability of microgrid with high renewable penetration. *IEEE Access*, 7:76071–76083, 2019.

[100] Elyas Rakhshani, Daniel Remon, Antoni Mir Cantarellas, and Pedro Rodriguez. Analysis of derivative control based virtual inertia in multi-area high-voltage direct current interconnected power systems. *IET Generation, Transmission & Distribution*, 10(6):1458–1469, 2016.

[101] Elyas Rakhshani, Daniel Remon, Antoni Mir Cantarellas, Jorge Martinez Garcia, and Pedro Rodriguez. Virtual synchronous power strategy for multiple hvdc interconnections of multi-area agc power systems. *IEEE Transactions on Power Systems*, 32(3):1665–1677, 2016.

[102] Prabha Kundur. Power system stability. *Power system stability and control*, 10:7–1, 2007.

[103] Manoj Datta and Tomonobu Senjyu. Fuzzy control of distributed pv inverters/energy storage systems/electric vehicles for frequency regulation in a large power system. *IEEE Transactions on Smart Grid*, 4(1):479–488, 2013.

[104] Yavuz Güler, Mustafa NALBANTOĞLU, and Ibrahim Kaya. Cascade controller design via controller synthesis for load frequency control of electrical power systems. *Turkish Journal of Electrical Engineering and Computer Sciences*, 32(2):285–304, 2024.

[105] Ilyas Bennia, Abdelghani Harrag, Yacine Daili, Allal Bouzid, and Josep M Guerrero. Decentralized secondary control for frequency regulation based on fuzzy logic control in islanded microgrid. *Indonesian Journal of Electrical Engineering and Computer Science*, 29(1):85–100, 2023.

[106] Thongchart Kerdphol, Fathin Saifur Rahman, and Yasunori Mitani. Virtual inertia control application to enhance frequency stability of interconnected power systems with high renewable energy penetration. *Energies*, 11(4):981, 2018.

[107] Jesus C Hernández, Pedro G Bueno, and Francisco Sanchez-Sutil. Enhanced utility-scale photovoltaic units with frequency support functions and dynamic grid support for transmission systems. *IET Renewable Power Generation*, 11(3):361–372, 2017.

[108] Jesus C Hernández, F Sanchez-Sutil, PG Vidal, and CJIJoEP Rus-Casas. Primary frequency control and dynamic grid support for vehicle-to-grid in transmission systems. *International Journal of Electrical Power & Energy Systems*, 100:152–166, 2018.

[109] Pedro G Bueno, Jesus C Hernández, and Francisco J Ruiz-Rodriguez. Stability assessment for transmission systems with large utility-scale photovoltaic units. *IET Renewable Power Generation*, 10(5):584–597, 2016.

[110] Tianfeng Chu, Miao Xu, Yu Xie, Shunjiang Wang, Dianyang Li, and Gang Liu. Small-signal stability analysis of the power system based on active support of renewable energy vscs. *Frontiers in Energy Research*, 10:907790, 2022.

[111] Pengbang Wei and Weidong Chen. Microgrid in china: A review in the perspective of application. *Energy Procedia*, 158:6601–6606, 2019.

[112] Suud Ademnur Hasen, ŞAHİN SÖNMEZ, and Saffet Ayasun. Enhancement of stability delay margins by virtual inertia control for microgrids with time delay. *Turkish Journal of Electrical Engineering and Computer Sciences*, 30(6):2221–2236, 2022.

[113] Ana Fernández-Guillamón, Emilio Gómez-Lázaro, Eduard Muljadi, and Ángel Molina-Garcia. A review of virtual inertia techniques for renewable energy-based generators. *Renewable Energy–Technologies and Applications*, 2021.

[114] Ralf Hesse, Dirk Turschner, Hans-Peter Beck, et al. Micro grid stabilization using the virtual synchronous machine (visma). *Renew. Energy Power Qual. J*, 1(07):676–681, 2009.

[115] Pranjal Saxena, Navdeep Singh, and Ashok Kumar Pandey. Enhancing the transient performance and dynamic stability of microgrid using pi inertia injection controller. *International Journal of Electrical Power & Energy Systems*, 134:107334, 2022.

[116] Rajasi Mandal and Kalyan Chatterjee. Virtual inertia emulation and rocof control of a microgrid with high renewable power penetration. *Electric Power Systems Research*, 194:107093, 2021.

[117] Gaber Magdy, G Shabib, Adel A Elbaset, and Yasunori Mitani. A novel coordination scheme of virtual inertia control and digital protection for microgrid dynamic security considering high renewable energy penetration. *IET Renewable Power Generation*, 13(3):462–474, 2019.

[118] Abdulwahab Fathi, Qobad Shafiee, and Hassan Bevrani. Robust frequency control of microgrids using an extended virtual synchronous generator. *IEEE Transactions on Power Systems*, 33(6):6289–6297, 2018.

[119] Bo Long, Yong Liao, Kil To Chong, José Rodríguez, and Josep M Guerrero. Mpc-controlled virtual synchronous generator to enhance frequency and voltage dynamic performance in islanded microgrids. *IEEE Transactions on Smart Grid*, 12(2):953–964, 2020.

[120] Mohammad Hassan Moradi and Farhad Amiri. Virtual inertia control in islanded microgrid by using robust model predictive control (rmpc) with considering the time delay. *Soft Computing*, 25:6653–6663, 2021.

[121] Xiaoyi Zhang, Dacheng Li, Zhaoxiang Yang, Lin Tian, Jianhui Meng, Yuan Liu, and Chao Fu. Fuzzy adaptive virtual inertia control of energy storage systems considering soc constraints. *Energy Reports*, 9:2431–2439, 2023.

[122] Thongchart Kerdphol, Fathin S Rahman, Yasunori Mitani, Komsan Hongesombut, and Sinan Küfeoğlu. Virtual inertia control-based model predictive control for microgrid frequency stabilization considering high renewable energy integration. *Sustainability*, 9(5):773, 2017.

[123] Prateek Utkarsha, NK Swami Naidu, Batta Sivaprasad, and Kumar Abhishek Singh. A flexible virtual inertia and damping control strategy for virtual synchronous generator for effective utilization of energy storage. *IEEE Access*, 2023.

[124] Aleksey Suvorov, Alisher Askarov, Nikolay Ruban, Vladimir Rudnik, Pavel Radko, Andrey Achitaev, and Konstantin Suslov. An adaptive inertia and damping control strategy based on enhanced virtual synchronous generator model. *Mathematics*, 11(18):3938, 2023.

[125] Vjatseslav Skiparev, Ram Machlev, Nilanjan Roy Chowdhury, Yoash Levron, Eduard Petlenkov, and Juri Belikov. Virtual inertia control methods in islanded microgrids. *Energies*, 14(6):1562, 2021.

[126] Thongchart Kerdphol, Fathin Saifur Rahman, Masayuki Watanabe, Yasunori Mitani, Thongchart Kerdphol, Fathin Saifur Rahman, Masayuki Watanabe, and Yasunori Mitani. Application of pi/pid control for virtual inertia synthesis. *Virtual Inertia Synthesis and Control*, pages 111–140, 2021.

[127] David Arricibita, Pablo Sanchis, and Luis Marroyo. Virtual synchronous generators classification and common trends. In *IECON 2016-42nd Annual Conference of the IEEE Industrial Electronics Society*, pages 2433–2438. IEEE, 2016.

[128] Ren Wang, Laijun Chen, Tianwen Zheng, and Shengwei Mei. Vsg-based adaptive droop control for frequency and active power regulation in the mtdc system. *CSEE Journal of Power and Energy Systems*, 3(3):260–268, 2017.

[129] Vjatseslav Skiparev, Komeil Nosrati, Eduard Petlenkov, and Juri Belikov. Reinforcement learning based virtual inertia control of multi-area microgrids. *Available at SSRN 4449057*, 2023.

[130] Özgür Aslan, Aytaç Altan, and Rıfat Hacıoğlu. Level control of blast furnace gas cleaning tank system with fuzzy based gain regulation for model reference adaptive controller. *Processes*, 10(12):2503, 2022.

[131] Nourelhouda Djaraf, Yacine Daili, and Abdelghani Harrag. A multiple-areas based on pid-virtual inertia control strategy for inverters. In *International Conference on Electrical Engineering and Control Applications*, pages 151–162. Springer, 2022.

[132] Ipeleng L Machele, Adeiza J Onumanyi, Adnan M Abu-Mahfouz, and Anish M Kurien. Interconnected smart transactive microgrids—a survey on trading, energy management systems, and optimisation approaches. *Journal of Sensor and Actuator Networks*, 13(2):20, 2024.

[133] Nian Liu and Jie Wang. Energy sharing for interconnected microgrids with a battery storage system and renewable energy sources based on the alternating direction method of multipliers. *Applied Sciences*, 8(4):590, 2018.

[134] Mahmoud Elshenawy, Ashraf Fahmy, Adel Elsamahy, Shaimaa A Kandil, and Helmy M El Zoghby. Optimal power management of interconnected microgrids using virtual inertia control technique. *Energies*, 15(19):7026, 2022.

[135] Shreya Vishnoi, Srete Nikolovski, More Raju, Mukesh Kumar Kirar, Ankur Singh Rana, and Pawan Kumar. Frequency stabilization in an interconnected micro-grid using smell agent optimization algorithm-tuned classical controllers considering electric vehicles and wind turbines. *Energies*, 16(6):2913, 2023.

[136] Andreas Ulbig, Theodor S Borsche, and Göran Andersson. Impact of low rotational inertia on power system stability and operation. *IFAC Proceedings Volumes*, 47(3):7290–7297, 2014.

[137] Peter Makolo, Ramon Zamora, Uvini Perera, and Tek Tjing Lie. Flexible synthetic inertia optimization in modern power systems. *Inventions*, 9(1):18, 2024.

[138] Thongchart Kerdphol, Fathin Saifur Rahman, Masayuki Watanabe, Yasunori Mitani, Dirk Turschner, and Hans-Peter Beck. Enhanced virtual inertia control based on derivative technique to emulate simultaneous inertia and damping properties for microgrid frequency regulation. *IEEE access*, 7:14422–14433, 2019.

[139] Amira Hassan, Mokhtar Aly, Ahmed Elmelegi, Loai Nasrat, Masayuki Watanabe, and Emad A Mohamed. Optimal frequency control of multi-area hybrid power system using new cascaded tid-pi λ d μ n controller incorporating electric vehicles. *Fractal and Fractional*, 6(10):548, 2022.

[140] Yu-Qing Bao, Yang Li, Beibei Wang, Minqiang Hu, and Peipei Chen. Demand response for frequency control of multi-area power system. *Journal of Modern Power Systems and Clean Energy*, 5(1):20–29, 2017.

[141] Suud Ademnur Hasen, Ömer Aydın, Saffet Ayasun, and Şahin Sönmez. Impact of virtual inertia and damping control on stability delay margins of load frequency control systems with renewable energy sources. *Electrical Engineering*, 106(1):323–341, 2024.

[142] Kathrin Susanne Skinder, Thongchart Kerdphol, Yasunori Mitani, and Dirk Turschner. Frequency stability assessment of multiple virtual synchronous generators for interconnected power system. *IEEE Transactions on Industry Applications*, 58(1):91–101, 2021.

[143] Hossam Ali, Gaber Magdy, and Dianguo Xu. A new optimal robust controller for frequency stability of interconnected hybrid microgrids considering non-inertia sources and uncertainties. *International Journal of Electrical Power & Energy Systems*, 128:106651, 2021.

[144] Xiangyu Zhang, Zhengzhen Zhu, Yuan Fu, and Wenqi Shen. Multi-objective virtual inertia control of renewable power generator for transient stability improvement in interconnected power system. *International Journal of Electrical Power & Energy Systems*, 117:105641, 2020.

[145] Jie Wang, Wentao Huang, Nengling Tai, Moduo Yu, Ran Li, and Yong Zhang. A bidirectional virtual inertia control strategy for the interconnected converter of standalone ac/dc hybrid microgrids. *IEEE Transactions on Power Systems*, 39(1):745–754, 2023.

[146] Komsan Hongesombut and Ruangyos Keteruksa. Fractional order based on a flower pollination algorithm pid controller and virtual inertia control for microgrid frequency stabilization. *Electric Power Systems Research*, 220:109381, 2023.

[147] Md Shafiul Alam, Fahad Saleh Al-Ismail, and Mohammad Ali Abido. Pv/wind-integrated low-inertia system frequency control: Pso-optimized fractional-order pi-based smes approach. *Sustainability*, 13(14):7622, 2021.

[148] Amr Saleh, Hany M Hasanien, Rania A. Turky, Balgynbek Turdybek, Mohammed Alharbi, Francisco Jurado, and Walid A Omran. Optimal model predictive control for virtual inertia control of autonomous microgrids. *Sustainability*, 15(6):5009, 2023.

[149] Thongchart Kerdphol, Fathin Saifur Rahman, Yasunori Mitani, Masayuki Watanabe, and Sinan Küfeo Küfeoğlu. Robust virtual inertia control of an islanded microgrid considering high penetration of renewable energy. *IEEE Access*, 6:625–636, 2017.

[150] Youssef Awda and Maad Alowaifeer. Adaptive optimization of virtual synchronous generator based on fuzzy logic control and differential evolution. *Ain Shams Engineering Journal*, 15(4):102606, 2024.

[151] Dina SM Osheba, SM Osheba, Abdallah Nazih, and Arafa S Mansour. Performance enhancement of pv system using vsg with anfis controller. *Electrical Engineering*, 105(5):2523–2537, 2023.

[152] Abdul Waheed Kumar, Mairaj Ud din Mufti, and Mubashar Yaqoob Zargar. Fuzzy based virtual inertia emulation in a multi-area wind penetrated power system using adaptive predictive control based flywheel storage. *Sustainable Energy Technologies and Assessments*, 53:102515, 2022.

[153] Akbar Karimipouya, Shahram Karimi, and Hamdi Abdi. Microgrid frequency control using the virtual inertia and anfis-based controller. *International Journal of Industrial Electronics Control and Optimization*, 2(2):145–154, 2019.

[154] Changwei Gao, Wei Wang, Chongyang Huang, and Weiqiang Zheng. An improved vsg control strategy based on transient electromagnetic power compensation. *Scientific Reports*, 13(1):15045, 2023.

[155] Sue Wang and Yuxin Xie. Virtual synchronous generator (vsg) control strategy based on improved damping and angular frequency deviation feedforward. *Energies*, 16(15):5635, 2023.

[156] Asmaa Fawzy, Abualkasim Bakeer, Gaber Magdy, Ibrahem E Atawi, and Mohamed Roshdy. Adaptive virtual inertia-damping system based on model predictive control for low-inertia microgrids. *IEEE Access*, 9:109718–109731, 2021.

[157] Xiangyu Zhang, Zhengzhen Zhu, Yuan Fu, and Lingfei Li. Optimized virtual inertia of wind turbine for rotor angle stability in interconnected power systems. *Electric power systems Research*, 180:106157, 2020.

[158] Li Yang and Zhijian Hu. Coordination of generators and energy storage to smooth power fluctuations for multi-area microgrid clusters: A robust decentralized approach. *IEEE Access*, 9:12506–12520, 2021.

[159] Salma Benchikh, Tarik Jarou, Mohamed Khalifa Boutahir, Elmehdi Nasri, and Roa Lamrani. Design of artificial neural network controller for photovoltaic system. In *The International Conference on Artificial Intelligence and Smart Environment*, pages 559–565. Springer, 2023.

[160] Abdellah El kharki, Zakaria Boulghasoul, Lamyae Et-taaj, and Abdelhadi Elbacha. Utilizing neural networks for dynamic performance improvement of induction motor drive: a fresh approach with the novel ip-self-tuning controller. *Electrical Engineering*, 106(1):553–565, 2024.

Contribution to the modelling and control of an AC micro grid integrating decentralised renewable energy

الملخص: تتناول هذه الأطروحة التحدي المتمثل في الحفاظ على استقرار أنظمةتتناول هذه الدراسة مشكلة انخفاض العطالة الناتج عن الاندماج المتزايد لمصادر الطاقة المتجددة، وتركّز على تصميم وتنفيذ استراتيجيات متقدمة للتحكم في العطالة الافتراضية بهدف ضمان التشغيل الموثوق والمرن والفعّال للشبكات المصغّرة المترابطة تحت ظروف ديناميكية متنوعة. تبدأ الدراسة بمراجعة شاملة لأنماط تشغيل الشبكات المصغّرة وهياكل التحكم الخاصة بها، بما في ذلك الأنظمة المعزولة وتلك المتصلة بالشبكة، مع التركيز على البنية الهرمية للتحكم وتعقيدات تنظيم التردد في الأنظمة التي تعاني من انخفاض كبير في العطالة الفيزيائية نتيجة ارتفاع نسبة دمج مصادر الطاقة المتجددة. تمثّل إحدى المساهمات الرئيسة لهذه الأطروحة في تطوير نماذج استجابة ترددية لكل من الشبكات المصغّرة المعزولة والمترابطة، مما يوفّر رؤى حاسمة حول سلوك النظام ويشكّل أساسًا لتصميم حلول فعّالة تضمن استقرار التردد. كما تقترح الأطروحة منهجيات تحكم متقدمة تشمل المنطق الضبابي والتحكم التكيفي القائم على الشبكات العصبية الاصطناعية، حيث تتيح هذه الأساليب تعديل قيم العطالة الافتراضية ديناميكيًا لتحقيق أداء موثوق واستجابة سلسة للتغيرات في ظروف التشغيل.
الكلمات المفتاحية: العطالة الافتراضية، الشبكات المصغرة، الطاقة المتجددة، التحكم التكيفي، تنظيم التردد.

Résumé : Cette thèse aborde le défi de la stabilité des systèmes électriques à faible inertie, causée par l'intégration croissante des sources d'énergie renouvelable (SER). Elle se concentre sur le développement de stratégies avancées de contrôle de l'inertie virtuelle (VIC) pour assurer un fonctionnement fiable et efficace des micro-réseaux (MG) interconnectés dans des conditions dynamiques variées. Une revue détaillée des modes de fonctionnement et des structures de contrôle des MG est d'abord réalisée, avec un accent particulier sur le contrôle hiérarchique et les défis de la régulation de fréquence dus à la diminution de l'inertie physique. Une contribution majeure réside dans l'élaboration de modèles de réponse en fréquence pour les MG en mode isolé et connecté, servant de base pour concevoir des solutions efficaces en matière de stabilité de fréquence. La thèse propose également des méthodes de contrôle avancées, telles que la logique floue et le contrôle adaptatif basé sur les réseaux de neurones, permettant une adaptation dynamique aux variations du système et assurant une performance robuste.
Mots-clés : Inertie virtuelle, Micro-réseaux, Énergie renouvelable, Contrôle adaptatif, Régulation de fréquence.

Abstract : This dissertation addresses the challenge of maintaining stability in low-inertia power systems due to the increasing integration of renewable energy sources (RES). It focuses on developing advanced virtual inertia control (VIC) strategies to ensure the reliable and efficient operation of interconnected microgrids (MGs) under dynamic conditions. The study begins with a comprehensive review of MG control architectures and operational modes, highlighting hierarchical control and frequency regulation challenges caused by reduced physical inertia. A key contribution of this research is the development of frequency response models for both isolated and grid-connected MGs. These models provide critical insights into system behavior and serve as a foundation for designing effective frequency stability solutions. The thesis introduces advanced control approaches such as fuzzy logic and neural network-based adaptive control of virtual inertia and damping, enabling dynamic adjustments and robust performance in RES-dense environments.
Keywords : Virtual inertia, Microgrids, Renewable energy, Adaptive control, Frequency regulation.